Topological Methods in

Shape Reconstruction and Comparison

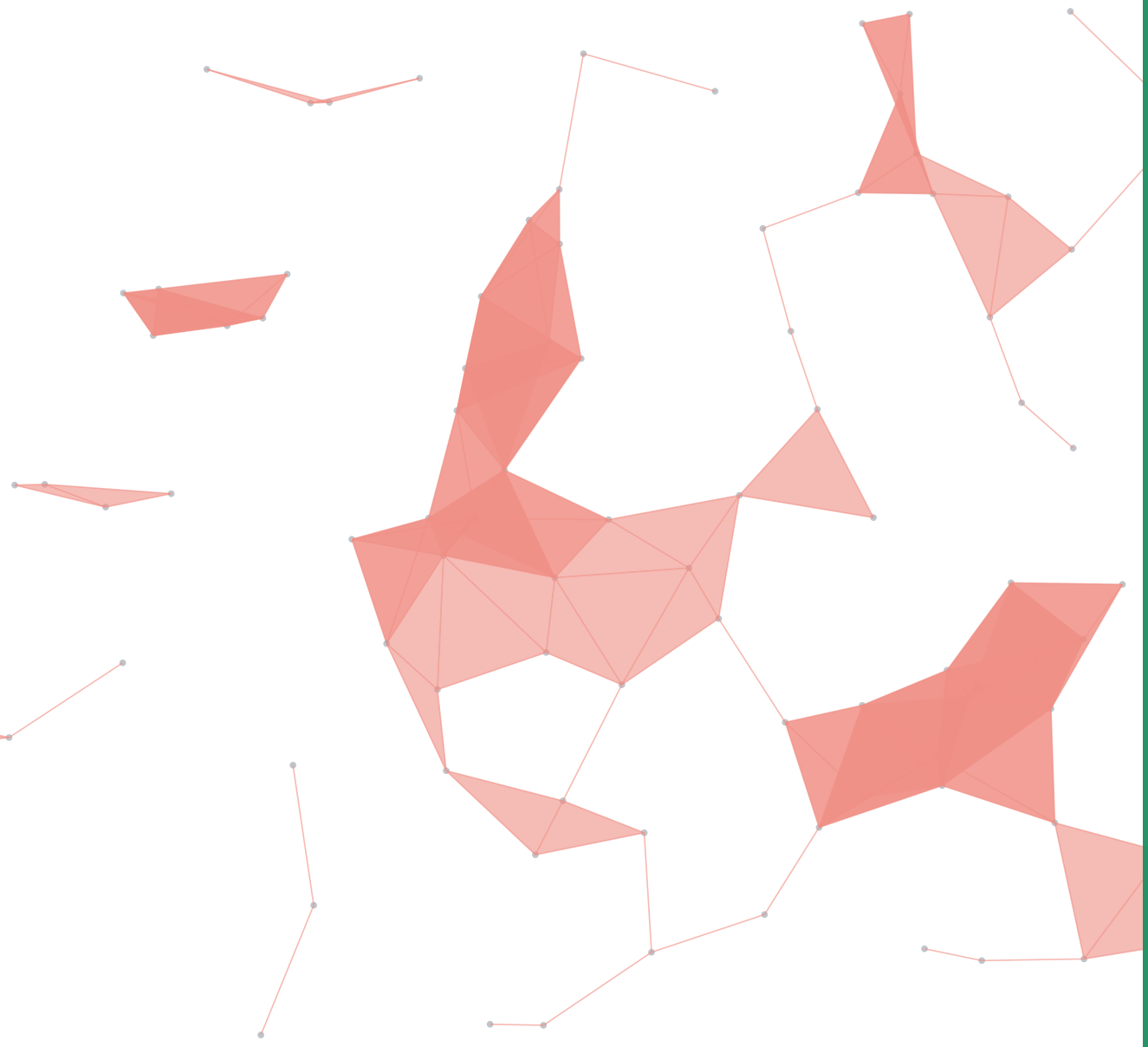

Sushovan Majhi

Topological Methods in Shape Reconstruction and Comparison

a dissertation
submitted on the Fourth day of December 2020
to the department of mathematics
in partial fulfillment of the requirements
of the school of science and engineering
of tulane university
for the degree
of
doctor of philosophy
by

Sushovan Majhi

approved:

Carola Wenk, PhD
chairwoman

Rafal Komendarczyk, PhD

Brittany Fasy, PhD

David Yang, PhD

Morris Kalka, PhD

Abstract

In the last two decades, topological data analysis (TDA) has started to become part of the data science toolkit. In this thesis, we study topological methods to address the challenges in developing provable shape reconstruction techniques. We focus on the topological and geometric reconstruction of a (hidden) geodesic subspace of $\mathbb{R}^N$ from a finite, noisy point-cloud sampled around it. We use the Čech and Vietoris-Rips complexes to devise novel and provable reconstruction algorithms. Our reconstruction technique leverages the intrinsic length metric induced by the geodesics on a geodesic space. We recognize the distortion and convexity radius as new sampling parameters for a successful reconstruction. For a geodesic subspace with finite distortion and positive convexity radius, we guarantee a correct computation of its homotopy and homology groups from a Hausdorff-close sample. Being inspired by the practical applications in road-network or map reconstruction, we also consider the geometric reconstruction of embedded metric graphs. To take our study of metric graphs one step further, we delve into a discrete Morse theoretic approach for the geometric reconstruction of graphs from a non-uniform sample with outliers. We survey the recent density-based developments, and propose an improved noise model that leads to a more efficient algorithm for better geometric guarantees. The Gromov-Hausdorff distance has been proposed as a robust framework for shape comparison. We investigate the pivotal challenges pertaining to the efficient computation of the distance measure between two Euclidean sets. We advance our understanding of the distance by answering an open question posed recently. In effect, our findings give rise to an $O(n \log n)$-time approximation algorithm with an approximation factor of $\left(1 + \frac{1}{4}\right)$.

Topological Methods in Shape Reconstruction and Comparison
by **Sushovan Majhi**

Printed in the United States of America.
December 2020.

To my ever-inspiring parents, beloved wife Nita, thesis adviser Carola Wenk, and the mathematics department at Tulane University.

Time is not measured by the passing of years but by what one does, what one feels, and what one achieves.

—Jawaharlal Nehru

Publications from the Thesis

- Sushovan Majhi, Jeffrey Vitter, and Carola Wenk. Approximating Gromov-Hausdorff Distance in Euclidean Space. *arXiv:1912.13008 [math.MG]*, 2019
- Brittany Terese Fasy, Sushovan Majhi, and Carola Wenk. Threshold-based graph reconstruction using discrete Morse theory. In *Fall Workshop on Computational Geometry*, New York, NY, November 2018
- Brittany Terese Fasy, Rafal Komendarczyk, Sushovan Majhi, and Carola Wenk. On the Reconstruction of Geodesic Subspaces of $\mathbb{R}^n$. *arXiv:1810.10144 [math.AT]*, 2018, submitted to *Journal of Computational Geometry*
- Brittany Terese Fasy, Rafal Komendaczyk, Sushovan Majhi, and Carola Wenk. Topological reconstruction of metric graphs in $\mathbb{R}^n$. In *Fall Workshop on Computational Geometry*, New York, NY, October 2017

Acknowledgement

Like any long and uncertain voyage, the venture into earning a doctorate degree—the highest academic degree—in mathematics has its own fair share of twists and turns, pain and payoff, frustration and fulfillment. Such a walk would not have been this seamless and successful without the prudent advice, support, and help I received from a great number of people around me. Some of them I worked really closely with; whereas some were remote and distant, and the rest I am not even acquainted with. I would like to take this grand opportunity to proclaim my gratitude to most of them. I would also like to extend my sincere apology to all whose contributions, mistakenly, went slipped by and remained unacknowledged here.

First of all, I would like to thank my thesis advisor Carola Wenk for her frequent advice, generous support, and the occasional nudge to keep me on track during my transition from a graduate student to an independent researcher.

I would like to thank all my co-authors for working with me so closely, exposing me to the big world of scientific research, putting me in touch with research groups, and helping me improve my academic writing. I thank Rafal Komendarczyk for teaching me topology, sharing his valuable ideas; Brittany Fasy for kick-starting my thesis by exposing me to the grandeur of Topological Data Analysis, showing the right research directions, helping me write grant proposals; Jeffrey Vitter for all his helpful inputs, countless hours of discussions, and being always so readily available for research meetings.

I sincerely thank Yusu Wang and Facundo Mémoli for hosting me at OSU and for the enlightening discussions on Gromov-Hausdorff distance during the visit in the fall of 2019. I also thank Helmut Alt for his valuable feedback during his visit to Tulane University in the Spring of 2019, and Henry Adams for the discussions on Vietoris-Rips complex during the lunch breaks at the machine learning workshop at the College of Charleston in the summer of 2019.

I also extend my thanks to the anonymous reviewers of my papers, the authors of numerous books and research articles that I read. For my research and hobby, I use

a myriad of open-source libraries, frameworks, and software developed by countless volunteers. I highly appreciate their altruistic gesture.

I thank all my committee members for taking up the time from their busy schedules, and for being so patient and available—sometimes in short notice—at the milestone events of my degree at Tulane. On this occasion, I would like to thank Ricardo Cortez for being the department chair, sharing his valuable suggestions on academic and professional matters, and teaching us Scientific Computing. He is a great and motivating teacher—his courses have reacquainted me with applied mathematics and numerical analysis. I would like to thank David Yang for offering me the reading course on Differentiable Manifolds, it helped me a lot to prepare for the Differential Geometry qualifying exam.

I also thank Robert Herbert and Michael Joyce for their help on improving my teaching; Gustavo Didier for letting me audit his wonderfully crafted course on Probability Theory. I would also like to thank Ramgopal Mettu for teaching us Algorithms and Data Structures, and also for doing a wonder job pulling off instructing an intricate topic like Complexity Theory. I extend my thanks to the faculty, administrative and technical staff of the mathematics and computer science department at Tulane University.

I would also like to acknowledge my gratitude to Satyajit Das for his earnest efforts to show a sixth-grader the wonderland of mathematics, and continuing to boost the zeal during my entire school life. My gratitude also extends to all teachers and tutors of my school and college life.

I thank my wife Nita for standing beside me, especially during the times of upheaval and frustration. I would like to thank my parents for all their effort; Shyamal, Priti, Bhaskar Das, and Tamal Da for their help and support.

I thank Karl and Isolde Hofmann for letting us stay in their majestic house at the corner of Hillary and Hampson Street. I also thank them for their inspiration, support, and care throughout our stay. I thank them for maintaining the beautiful backyard and the table beneath the Magnolia tree—where some of the elegant ideas of this thesis sprang up.

I thank Franz for helping me settle down here, for the bike, and for being the go-to person for my questions on statistics. I would like to thank Forest for the guitar lessons, canoe adventures, occasional rants on philosophy! I also thank Megan for being a co-host for our trip to Colorado in the summer of 2019. I thank Alexej for our discussions on data science and tech; Ozlem for studying together for the topology qualifier; Selvi for her encouragement and advice; Majid for such a wonderful time in New York.

I would like to thank Sankho and Abin for their support and for being good friends and considerate roommates; Akshay for helping me with job interviews, competitive

programming, and for giving me a greater perspective on the industry jobs; Hassan for being such a good friend. I thank Umar and his family for all the help, care, enlightening religious discourse, and advice on life.

A hundred times every day I remind myself that my inner and outer life are based on the labors of other men, living and dead, and that I must exert myself in order to give in the same measure as I have received and am still receiving.

—Albert Einstein

Contents

List of Tables

List of Figures

Standard Notations

$\mathbb{R}$: the set of real numbers
$\mathbb{R}^N$: the N-dimensional Euclidean space
$I = [0,1]$: the unit interval
$\emptyset$: the empty set
$A \subseteq B$ or $B \supseteq A$: set-theoretic containment
$A \subset B$ or $B \supset A$: set-theoretic proper containment
$f : A \to Y$: set-theoretic function from set A to B
1_X: the identity map of X, $1_X : X \to X$ defined by $1_X(x) = x$
$f \simeq g \text{ rel } A$: maps f and g are homotopic relative to A (Definition 2.1.1)
$X \simeq Y$: spaces X and Y are homotopy equivalent (Definition 2.1.3)
$G_1 \approx G_2$: group G_1 is isomorphic to G_2
$\pi_1(X, b)$: the fundamental group of X at the basepoint b
$\pi_k(X, b)$: the k-dimensional homotopy group of X at the basepoint b
M: manifold
$\mathcal{K}$: abstract simplicial complex
$\tau < \sigma$: the simplex τ is a face of the simplex σ
$|\mathcal{K}|$: the underlying topological space of the complex $\mathcal{K}$
$\mathcal{C}_\alpha(A)$: the Euclidean Čech complex
$\mathcal{R}_\alpha(A)$: the Euclidean Vietoris-Rips complex
$\mathcal{N}(\mathcal{K})$: the nerve of the complex $\mathcal{K}$
τ: normal injectivity radius of a Euclidean sub-manifold
$\mathbb{B}(x, r)$: r-radius Euclidean ball centered at $x \in \mathbb{R}^N$
$\mathtt{wfs}$: weak feature size
$l(\gamma)$: length of the path γ $d_L(\cdot,\cdot)$: the length metric
$\mathcal{C}^L_\alpha(A)$: the Čech complex w.r.t. d_L
$\mathcal{R}^L_\alpha(A)$: the Vietoris-Rips complex w.r.t. d_L
$\mathbf{Sh}(\mathcal{K})$: the shadow of the complex $\mathcal{K}$ (Definition 5.3.2)
$d_H(X, Y)$: Hausdorff distance in the Euclidean space (Definition 3.1.1)
$d^Z_H(X, Y)$: Hausdorff distance in (Z, d_Z)
$d_{GH}(X, Y)$: Gromov-Hausdorff distance (Definition 7.2.2)
$\mathcal{C}$: a correspondence (Definition 7.2.3)
$\mathtt{dist}(\mathcal{C})$: distortion of the correspondence $\mathcal{C}$ (Definition 7.2.4)

Chapter 1

Introduction

The beginning is the most important part of the work.
—Plato, *The Republic*

This introductory chapter sets the stage for the chapters ahead. Along with delineating our general motivation behind the problems considered, this chapter serves as the manifesto of this thesis. We take the readers on a quick tour to catch a bird's-eye view of the major inspirations and contributions of the corpus. We spare the readers of the mathematical details in this introduction, hoping to make the ride as gentle as possible.

Section 1.1 introduces the readers to the field of *topological data analysis*—the area where we think our contributions are best recognized. With a brief introduction to the realm of shape reconstruction and some of the pivotal challenges, the section also lays out our motivation behind the type of problems we consider in this work. The summary of our contributions is bestowed in Section 1.2.

1.1 Motivation

The success of computer science and engineering in developing sophisticated technologies to acquire and store large amounts of complex *data* has overwhelmed—as well as intrigued—the curious minds from almost all fields of science. With increasing CPU clock-speed, data sampling-rates have become unprecedented. Alongside, there have been constant efforts to develop database designs to suit diverse data-structures, and to enhance storage, query, and portability considerably. As a result,

large data repositories are being produced and made available for analysis. In the last two decades, such a turn of advancements in the *data-world* has brewed industrial incentives, as well as sheer attention from academic researchers.

In the early days of science, one would stare at a physical or chemical process for a long time in the hope to unveil its nature and cause. Instruments used for such observations were primitive, hence the tabulated data were erroneous. Analysis of data—spatial and time-series—has always been an inseparable part of science. In spite of its power, *data* had been disparagingly conceived of as a mere tool for science—never been considered a science itself.

In the last two decades, the emergence of data of astronomical volume and great complexity brought about a new school of thought: *data-driven* and *data-centered* research. Data has become a *science* now. Unlike the old times, the objective has now become to obtain knowledge *about* the data, rather than *from* the data. Researchers from all fields of science are lending themselves to organizing, denoising, and analyzing data. Such an invitation was naturally extended to topologists and geometers as well. Computational topology—and its subfield topological data analysis—started to become part of the data science toolkit.

Topological data analysis (TDA) is a growing field of study that helps address data analysis questions. TDA is deemed a better alternative to traditional statistical approaches when the data inherit a topological and geometric structure. Examples of such data include medical images of brain-tumors, 3D point-clouds scanned around a geometric shape, GPS locations sampled from vehicles on a road-network.

In such real-world applications, the data approximate a (hidden) geometric shape. In the last decade, topological and geometric *reconstruction* of a hidden shape from a point-cloud *sample* has received increasing attention. Notable developments have been made to encompass shapes of various types: smooth manifolds [5,6], compact sets with positive *weak feature size* [7–9], geodesic spaces [3], metric graphs [10–12], etc.

The challenges in developing provable and efficient shape reconstruction algorithms come from the noise present in the sample. As with the type of shape, reconstruction techniques change considerably with the type of noise present in the sample. A commonly assumed noise model is *Hausdorff noise*, where data are assumed to be sampled from a very-thin tubular neighborhood of the underlying shape. Shape reconstruction faces additional challenges under *non-Hausdorff noise*, where the data is non-uniform and noisy with distant outliers. Although the literature of shape reconstruction expanded relatively wide in the former realm, reconstruction under non-Hausdorff noise is not yet well-understood.

We undertake the reconstruction problem of Euclidean geodesic subspaces under Hausdorff noise. Using Rips and Čech complexes, we develop novel and provable reconstruction techniques—both topological and geometric. Our investigation is

also extended to the reconstruction of road-networks (viewed as metric graphs) under non-Hausdorff type noise that more closely reflect real data. Road-networks are special types of geodesic spaces. And, a great amount of spatial GPS data is publicly available for analysis. Although many map construction algorithms work well in practice, most of them suffer from the lack of theoretical guarantees. We take a discrete Morse theoretic approach, accounting for a more realistic noise model.

Along with reconstruction, our investigation also reaches to an equally important domain of topological data analysis: shape *comparison*. Being a natural distance measure between two metric spaces, Gromov-Hausdorff distance is receiving a fair amount of attention as a robust framework for shape comparison and matching [13]. We advance our understanding of Gromov-Hausdorff distance between Euclidean subsets by solving an open problem posed in [14], addressing some of the major challenges pertaining to its efficient computation.

1.2 Contributions of this Thesis

The contribution of this work straddles between topological data analysis and computational geometry. Euclidean shape reconstruction claims the lion's share of our work; whereas, only the last chapter is devoted to shape comparison. Here we give a quick preview of the major developments that entail our investigation. Chapter 2 makes our readers (re)acquainted with the basic and relevant notions from topology and geometry. As the title of this thesis alludes, the work is divided into two logical parts: reconstruction (Chapter 3–Chapter 6) and comparison (Chapter 7).

In Chapter 3—following a brief introduction to the domain of shape reconstruction—we present our result on smooth curve reconstruction. We also introduce here some of the important developments and techniques in the reconstruction of compact subsets of Euclidean spaces.

We develop our topological reconstruction techniques for geodesic subspaces (Definition 4.2.1) in Chapter 4. One of the major contributions of this work is to reconstruct geodesic subspaces of $\mathbb{R}^N$, both topologically and geometrically. In our pursuit, we recognize distortion (Definition 7.2.4) and convexity radius (Definition 4.2.4) as new sampling parameters. These sampling parameters are very natural properties of geodesic spaces, and they are not very difficult to estimate. Also, when comparing with `wfs`, convexity radius and distortion appears to be more stable under small perturbations of the underlying space.

In Section 4.3 and Section 4.4, our main topological reconstruction results for a geodesic subspace X of $\mathbb{R}^N$ are presented. If the distortion is finite and the convexity radius is positive, the persistent homology of both the Čech and Vietoris-Rips filtration of the sample are shown to successfully capture the homology and homotopy groups of X as proved in Theorem 4.3.4 and Theorem 4.4.5 respectively.

Theorem 4.3.4 (Reconstruction via Rips Filtration)**.** *Let X be a geodesic subset of $\mathbb{R}^N$ with a positive convexity radius ρ and finite distortion δ. Let S be a finite subset of $\mathbb{R}^N$, and let ε be a positive number such that*

$$d_H(X,S) < \frac{\varepsilon}{4} < \frac{\rho}{2\delta(3\delta+2)}.$$

Then, for any non-negative integer k, the homology group $H_k(X)$ is isomorphic to the image of the homomorphism induced by the simplicial inclusion

$$j : \boldsymbol{\mathcal{R}}_\varepsilon(S) \hookrightarrow \boldsymbol{\mathcal{R}}_{\frac{1}{2}(3\delta+1)\varepsilon}(S).$$

Theorem 4.4.5 (Reconstruction via Čech Filtration)**.** *Let X be a geodesic subset of $\mathbb{R}^N$ with a positive convexity radius ρ and finite distortion δ. Let S be a finite subset of $\mathbb{R}^N$, and let ε be a positive number such that*

$$d_H(X,S) < \varepsilon < \frac{\rho}{2\delta(4\delta+1)}.$$

Then, for any non-negative integer k, the homology group $H_k(X)$ is isomorphic to the image of the homomorphism induced by the simplicial inclusion

$$j : \boldsymbol{\mathcal{C}}_\varepsilon(S) \longrightarrow \boldsymbol{\mathcal{C}}_{(4\delta+1)\varepsilon}(S).$$

Taking the investigation one step further in Chapter 5, we present our geometric reconstruction results for metric graphs (Definition 5.3.1). We consider the geometric reconstruction of geodesic subspaces. We construct a complex on the sample as our geometric reconstruction of the space of interest. Theorem 5.2.3 establishes the isomorphism of their fundamental groups. As an interesting application in Section 5.3, we consider the geometric reconstruction of embedded graphs of $\mathbb{R}^2$. In Theorem 5.3.4, we compute a homotopy equivalent geometric complex in the same ambient space that is also Hausdorff-close to X. Since the sample S can be taken to be finite, our result gives rise to an Algorithm 1 for the geometric reconstruction of planar embedded graphs.

Theorem 5.3.4 (Geometric Reconstruction of Embedded Graphs)**.** *Let G be a connected embedded graph in $\mathbb{R}^2$. Let b be the length of the shortest simple cycle of G, and let δ be its distortion. Let $S \subseteq \mathbb{R}^2$ and $\varepsilon > 0$ be such that $d_H(G,S) < \frac{\varepsilon}{3} < \frac{b}{4\delta(15\delta+2)}$. Then, the shadow of $\boldsymbol{\mathcal{R}}^{\varepsilon}_{5\varepsilon\delta}(S)$, denoted $\widetilde{G}$, has the same homotopy type as G. Moreover, we have*

$$d_H(G,\widetilde{G}) < \left(5\delta + \frac{1}{3}\right)\varepsilon.$$

We extend our study of metric graphs in Chapter 6 to consider a discrete Morse theoretic approach to their geometric reconstruction. Following the trail of the recent development in [15], we investigate the application of discrete Morse theory

([16]) to develop provable and efficient algorithms for geometric reconstruction of embedded graphs. We propose an improved threshold-based noise model to account for more realistic use cases and to achieve better geometric reconstruction guarantees.

Finally, we devote Chapter 7 to address the computational aspects of Gromov-Hausdorff distance (Definition 7.2.2) for Euclidean subsets. Our major contribution is to provide a satisfactory answer to the quest of understanding the relation between $d_{H,iso}$ (Definition 7.3.1) and d_{GH} when X, Y are compact subsets of $\mathbb{R}^1$ equipped with the standard Euclidean metric. At the same time, we keep our broader goal of addressing the challenges in computing Gromov-Hausdorff distance in higher Euclidean dimensions. We introduce and explore some of the nice structural properties of nearest neighbor correspondence (Definition 7.3.5) in connection to d_{GH}; see Lemma 7.3.6, Theorem 7.3.7. In Theorem 7.4.3, we show that $d_{H,iso}(X,Y) \leq \frac{5}{4} d_{GH}(X,Y)$ for any compact $X, Y \subset \mathbb{R}^1$. For subsets of the real line, it was believed for a long time that $d_{GH} = d_{H,iso}$. Providing an answer to the open question posed by the authors of [14], we show in Theorem 7.4.11 that this is, in fact, not true by showing that the bound $\frac{5}{4}$ in Theorem 7.4.3 is tight. Since $d_{H,iso}(X,Y)$ can be computed in $O(n \log n)$-time ([17]), our result effectively gives rise to an $O(n \log n)$-time algorithm to approximate $d_{GH}(X,Y)$ for finite $X, Y \subset \mathbb{R}^1$ with an approximation factor of $(1 + \frac{1}{4})$.

Today is only one day in all the days that will ever be. But what will happen in all the other days that ever come can depend on what you do today. It's been that way all this year. It's been that way so many times.

—Ernest M. Hemingway

Chapter 2

Preliminaries on Topology

Point set topology is a disease from which the human race will soon recover.
—Henri Poincare

Concepts and tools from topology—especially algebraic topology—inspire our methodologies and results. In order to better appreciate the contribution of this work, our readers are expected to have a basic understanding of algebraic and combinatorial topology. Concepts—like simplicial complexes, nerve lemma, homology, homotopy groups—make appearances throughout the work. The purpose behind squirreling away these important notions in the very beginning is two-fold: to make the thesis self-contained, and to allow readers skip or skim through the chapter at their own discretion.

In this chapter, we provide some useful notations and classical results from algebraic and combinatorial topology. We give a brief overview here; for more detailed and complete treatment, we refer the interested readers to [18–20].

Section 2.1 presents the important concepts from algebraic topology: homotopy of maps, fundamental group, and higher homotopy groups. In Section 2.3, we describe the notions from the simplicial category.

Remarks 2.0.1. Unless otherwise stated, a *space* means a topological space, and a *map* between two topological spaces is assumed to be continuous.

2.1 Homotopy

The intuitive concept of continuously deforming a shape into another shape is embodied in the notion of *homotopy*.

Definition 2.1.1 (Homotopy)**.** Let $f, g : X \to Y$ be maps. A map $H : X \times I \to Y$ is called a ***homotopy between*** f ***and*** g if for all $x \in X$,

$$H(x, 0) = f(x), \text{ and } H(x, 1) = g(x).$$

the maps f and g are called ***homotopic***, denoted as $f \simeq g$.

We state that the relation of homotopic maps is an equivalence relation. An interested reader is encouraged to take a detour to [20, p.24] for the proof.

We now define a more general notion: homotopy relative to a subset $A \subset X$. For maps $f, g : X \to Y$ that agree on a subset $A \subset X$, if there exists a homotopy $H : X \times I \to Y$ such that $H(a, t) = f(a)$ for $a \in A$, then f, g are called homotopic relative to A. We write $f \simeq g \text{ rel } A$. For $A = \emptyset$, we are back to our usual homotopy, and we simply call f and g homotopic.

Finding a homotopy between maps can sometimes be a non-trivial task. In case of convex subsets of a vector space, however, the *straight-line homotopy* is a popular choice (see Example 2.2.1).

Example 2.1.2 (Straight-line Homotopy)**.** Let X be any topological space and $Y \subset \mathbb{R}^N$ be convex. Then, any two maps $f, g : X \to Y$ are homotopic. Using the fact that Y is convex, we can use the straight-line homotopy $H : X \times I \to Y$ defined by

$$H(x, t) = tf(x) + (1 - t)g(x).$$

□

The concept of homotopy gives rise to the definition of continuous deformation of spaces via homotopy equivalence.

Definition 2.1.3 (Homotopy Equivalence)**.** A map $f : X \to Y$ is called a *homotopy equivalence* if there exists another map $g : Y \to X$ such that

$$g \circ f \simeq 1_X \text{ and } f \circ g \simeq 1_Y.$$

We note that g is also a homotopy equivalence. In this case, the spaces X and Y are called *homotopy equivalent* or said to have the *same homotopy type*. Like homotopy of maps, homotopy equivalence between spaces is also an equivalence relation. The relation is weaker than homeomorphism; however, strong enough to force two homotopy equivalent spaces to share the same homotopy and homology groups. See Example 2.1.5 for an example.

We conclude this section with a very special case: when the inclusion $A \overset{i}{\hookrightarrow} X$ is a homotopy equivalence. The space X is thought to be continuously deformable to the subset A.

Definition 2.1.4 (Deformation Retract)**.** Let A be a subset of a space X, and let i denote the inclusion map. If there exists a map $r : X \to A$ such that $i \simeq r$ *rel* A, then X is said to deformation retract or retraction onto A.

Example 2.1.5 (Homeomorphism and Deformation Retration)**.** Consider the (compact) Möbius band M and the unit circle S^1. They are definitely *not* homeomorphic—punctured M is not contractible, whereas punctured S^1 is. However, M is homotopy equivalent to S^1 because there is a deformation retraction of M to its center circle. □

2.2 Homotopy Groups

In this section, we touch upon the basics of fundamental group and higher homotopy groups.

2.2.1 The Fundamental Group

With the concept of homotopy at our disposal, we can now define the fundamental group $\pi_1(X, x_0)$ of a space X at a base-point $x_0 \in X$. The underlying set of the group is defined to be the homotopy classes of loops $\gamma : I \to X$ on X with $\gamma(0) = \gamma(1) = x_0$, where the homotopies H are required to follow $H(0, t) = H(1, t) = x_0$ for all $t \in I$. The homotopy class of a loop γ is denoted by $[\gamma]$. We illustrate the concept of loop homotopy in Example 2.2.1.

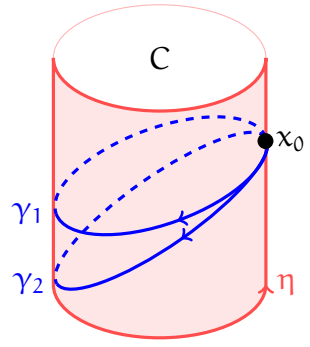

Figure 2.1: Three loops γ_1, γ_2, and η are are based at x_0 on the hollow cylinder C.

Example 2.2.1 (Loops on Cylinder)**.** We take the (hollow) cylinder C as show in Figure 2.1. Three loops are considered at the base-point x_0. The two (blue) loops γ_1, γ_2 are homotopic, i.e., $[\gamma_1] = [\gamma_2]$. Unlike them, the (red) loop η does not *wrap around* C. So, $[\eta] \neq [\gamma_1]$.

The cylinder is homotopy equivalent to a circle, consequently $\pi_1(\mathbb{S}^1, x_0) = \mathbb{Z}$; follow [21] for a proof. The class $[\eta]$ provides the identity element, and $[\gamma_1]$ is a generator of the cyclic fundamental group of S. □

In order to turn the set $\pi_1(X, x_0)$ into a group, we first define the binary operation: composition of loops. Given two loops $\gamma_1, \gamma_2 : I \to X$ with $\gamma_1(0) = \gamma_1(1) = \gamma_2(0) = \gamma_2(1) = x_0$, define their composition

$$(\gamma_1 \cdot \gamma_2)(s) = \begin{cases} \gamma_1(2s), & s \in \left[0, \frac{1}{2}\right] \\ \gamma_2(2s-1), & s \in \left[\frac{1}{2}, 1\right] \end{cases}.$$

The operation respects the homotopy equivalence relative to the base x_0. Therefore, the operation extends to homotopy classes of loops, i.e., the operation $[\gamma_1] \cdot [\gamma_2] = [\gamma_1 \cdot \gamma_2]$ on $\pi_1(X, x_0)$ is well-defined. Now, it is a matter of following the definition to check that $(\pi_1(X, x_0), \cdot)$ is, in fact, a group ([20, p.46]). This group is called the fundamental group of X at the base-point x_0. The fundamental group becomes independent of the base-point if X is path-connected. See any of the references mentioned before for the computation of fundamental groups of widely used topological spaces.

2.2.2 Higher Homotopy Groups and Whitehead's Theorem

To generalize the definition of the fundamental group, we define higher homotopy groups $\pi_k(X, x_0)$ for any $k \geq 0$. Let $I^k = [0, 1]^k$ denote the k-dimensional unit cube. We also let ∂I^k denote the boundary of I^N. For $k \geq 2$ and base-point $x_0 \in X$, we first define $\pi_k(X, x_0)$ to be the set of homotopy classes of maps $f : I^k \to X$ with $f(\partial I^k) = \{x_0\}$, where the homotopies $H(x, t)$ follow $H(x, t) = x_0$ for all $t \in I$ and $x \in \partial I^k$.

For $k = 0$, in the degenerate case, I^0 can be taken to be just a point, so $\partial I^0 = \emptyset$. Therefore, $\pi_0(X, x_0)$ is the set of the path-connected components of X.

For $k \geq 1$ and $f, g : I^k \to X$ with $f(\partial I^k) = g(\partial I^k) = \{x_0\}$, we define the composition

$$(f \cdot g)(s_1, s_2, \ldots, s_k) = \begin{cases} f(2s_1, s_2, \ldots, s_k), & s_1 \in \left[0, \frac{1}{2}\right] \\ g(2s_1 - 1, s_2, \ldots, s_k), & s_1 \in \left[\frac{1}{2}, 1\right] \end{cases}.$$

One can also check that under composition, $\pi_k(X, x_0)$ forms a group: the k-dimensional homotopy group of X at the base-point x_0.

If $\phi : X \to Y$ such that $f(x_0) = y_0$, then it induces a homomorphism $\phi_* : \pi_k(X, x_0) \to \pi_k(Y, y_0)$ defined by $\phi([\gamma]) = [\phi(\gamma)]$. It can be proven that ϕ_* is well-defined and is a homomorphism.

We conclude our discussion on homotopy groups by stating the prestigious Whitehead's theorem.

Theorem 2.2.2 (Whitehead [18]). *Let X, Y be connected CW-complexes. If a map $f : X \to Y$ induces isomorphisms $f_* : \pi_k(X, x_0) \to \pi_k(Y)$ for all $k \geq 0$, then f is a homotopy equivalence.*

Furthermore, if X is a subcomplex of Y and f is the inclusion map, then X is a deformation retraction of Y.

2.3 Simplicial Complexes

The combinatorial analog of a topological space, often used in algebraic and combinatorial topology, is an abstract simplicial complex.

2.3.1 Abstract Simplicial Complex

An ***abstract simplicial complex*** $\mathcal{K}$ consists of a set $\mathcal{V}(\mathcal{K})$ and a collection $\mathcal{F}(\mathcal{K})$ of finite non-empty subsets of $\mathcal{V}(\mathcal{K})$ such that

(i) each singleton subset of $\mathcal{V}(\mathcal{K})$ belongs to $\mathcal{F}(\mathcal{K})$, and

(ii) if σ is an element of $\mathcal{F}(\mathcal{K})$, then so are all its non-empty subsets.

The elements of $\mathcal{V}(\mathcal{K})$ are called the *vertices* of $\mathcal{K}$ and elements of $\mathcal{F}(\mathcal{K})$ are called the *simplices* of K. If a simplex $\sigma \in \mathcal{F}(\mathcal{K})$ has $(q+1)$ elements, it is called a q-*simplex* (or the *dimension* of σ is q or $\dim(\sigma) = q$). A q-simplex σ is also sometimes denoted as $\sigma^{(q)}$.

If $\tau^{(p-1)} \subseteq \sigma^{(p)}$, then τ is called a *face* of σ, written as $\tau < \sigma$. If $\tau < \sigma$, then σ is called a *co-face* of τ. When there is no possibility of confusion, the abstract simplicial complex is sometimes abbreviated to "complex".

Example 2.3.1 (Abstract Simplicial Complex). To give an example of an abstract simplicial complex $\mathcal{K}$, take the vertex set

$$\mathcal{V}(\mathcal{K}) = \{v_0, v_1, v_2, v_3\},$$

and the simplices

$$\mathcal{F}(\mathcal{K}) = \Big\{\{v_0\}, \{v_1\}, \{v_2\}, \{v_3\}, \{v_0, v_1\}, \{v_1, v_2\}, \{v_0, v_2\}, \{v_0, v_1, v_2\}, \{v_2, v_3\}\Big\}.$$

The complex has four 0-simplices, four 1-simplices, and one 2-simplex; see Figure 2.2.

2.3.2 Simplicial Maps and Contiguity

Let $\mathcal{K}_1 \to \mathcal{K}_2$ be abstract simplicial complexes. A map $\phi : \mathcal{V}(\mathcal{K}_1)$ to $\mathcal{V}(\mathcal{K}_2)$, also called a *vertex map*, is said to induce a ***simplicial map*** $\phi : \mathcal{K}_1 \to \mathcal{K}_2$ if $\phi(\sigma) \in \mathcal{F}(\mathcal{K}_2)$

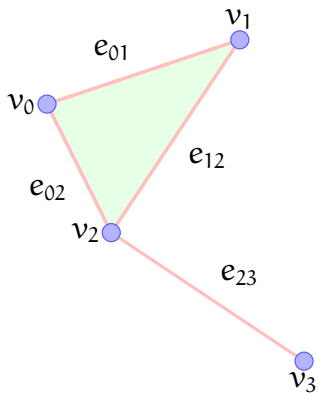

Figure 2.2: The blue points constitute the vertex set of the abstract simplicial complex. The red edges denote the 1-simplices, and the green triangle denote the 2-simplex. The union, in the subspace topology of the plane, is the associated geometric complex.

whenever $\sigma \in \mathcal{F}(\mathcal{K}_1)$. A simplicial map between abstract simplicial complexes is the combinatorial analogue of a continuous map between topological spaces. Likewise, contiguous simplicial maps play the role of homotopic maps in the combinatorial world. Two simplicial maps $\phi_1, \phi_2 : \mathcal{K}_1 \to \mathcal{K}_2$ are called ***contiguous*** if for every simplex $\sigma_1 \in \mathcal{K}_1$ there exists $\sigma_2 \in \mathcal{K}_2$ such that $\phi_1(\sigma_1) \cup \phi_2(\sigma_1) \subseteq \sigma_2$.

Although abstract simplicial complexes have enough combinatorial structure to define simplicial homology and homotopy, they are not topological spaces. For an abstract simplicial complex $\mathcal{K}$, one can define its ***underlying topological space*** denoted $|\mathcal{K}|$, to be the union of the formal convex-hulls of its simplices. As a set, $|\mathcal{K}|$ is the space of all functions $\alpha : \mathcal{V}(\mathcal{K}) \to [0,1]$, also called *barycentric coordinates*, satisfying the following two properties:

(i) $\textbf{supp}\ (\alpha) := \{v \in \mathcal{V}(\mathcal{K}) \mid \alpha(v) \neq 0\} \in \mathcal{F}(\mathcal{K})$

(ii) $\sum_{v \in \mathcal{V}(\mathcal{K})} \alpha(v) = 1.$

The details on the topologies on $|\mathcal{K}|$ and their relations can be found in [19, 20]. In this work, we use the standard metric topology on $|\mathcal{K}|$. Naturally, a simplicial map $\phi : \mathcal{K}_1 \to \mathcal{K}_2$ induces a continuous map $|\phi| : |\mathcal{K}_1| \to |\mathcal{K}_2|$ defined by

$$|\phi|(\alpha)(v) = \sum_{v \in \mathcal{V}(\mathcal{K}_1)} \alpha(v).$$

As one expects, the contiguous simplicial maps induce homotopic continuous maps between their respective underlying topological spaces; see [20] for a proof.

2.3.3 Čech and Vietoris Rips Complexes

Consider a subspace A of a metric space (M, d) and a positive scale ε.

The nerve (defined in Section 2.4) of the collection of open ε-balls centered on the points of A is known as the ***Čech Complex*** of A at a scale ε. For $X \subseteq \mathbb{R}^N$ under the standard Euclidean metric, we denote it simply by $\mathcal{C}_\varepsilon(X)$. In the case when $A \subseteq X$ under the length metric (X, d_L) (defined in Chapter 4), we denote the Čech complex by $\mathcal{C}^L_\varepsilon(A)$.

The ***Vietoris-Rips Complex*** is an abstract simplicial complex having a k-simplex for every set of $(k+1)$ points in A of diameter less than ε. It is clear from the definition that explicit knowledge about the entire metric space (M, d) is not needed to compute the complex. Unlike the Čech complex, the Vietoris-Rips complex is completely determined by the restriction of the metric to the subset A. For $X \subseteq \mathbb{R}^N$ under the standard Euclidean metric, we denote it simply by $\mathcal{R}_\varepsilon(X)$. In the case when $A \subseteq X$ under the length metric (X, d_L), we denote the Čech complex by $\mathcal{R}^L_\varepsilon(A)$.

2.4 Nerve Lemma

Most of the proofs in this work depend on the Nerve Lemma or a modification thereof. An open cover $\mathcal{U} = \{U_i\}_{i\in\Lambda}$ of a topological space X is called a *good cover* if all finite intersections of its elements are contractible. The *nerve* of $\mathcal{U}$, denoted $\mathcal{N}(\mathcal{U})$, is defined to be the simplicial complex having Λ as its vertex set, and for each non-empty k-way intersection $U_{i_1} \cap U_{i_2} \cap \ldots \cap U_{i_k}$, the subset $\{i_1, i_2, \ldots, i_k\}$ is a simplex of $\mathcal{N}(\mathcal{U})$. Under the right assumptions, the nerve preserves the homotopy type of X, as stated by the following fundamental result.

Lemma 2.4.1 (Nerve Lemma [22])**.** *Let $\mathcal{U} = \{U_i\}_{i\in\Lambda}$ be a good open cover of a para-compact topological space X. Then, the underlying topological space $\left|\mathcal{N}(\mathcal{U})\right|$ is homotopy equivalent to X.*

Remarks 2.4.2. A homotopy equivalence $h : X \longrightarrow \left|\mathcal{N}(\mathcal{U})\right|$ in the Nerve Lemma is usually constructed with the help of a *partition of unity* $\{\varphi_i\}_{i\in\Lambda}$ subordinate to the locally finite open cover $\mathcal{U}$ (c.f. [18]). Specifically, for $x \in X$, $h(x)$ is defined as follows:

$$h(x) = \sum_{i\in\Lambda} \varphi_i(x) v_i, \qquad x \in X, \tag{2.1}$$

where v_i denotes the vertex of $\mathcal{N}(\mathcal{U})$ corresponding to the cover element U_i. And, each $\varphi_i : X \longrightarrow [0, 1]$ is a continuous function satisfying the following two requirements: (i) $\text{supp}(\varphi_i) \subseteq U_i$, for all $i \in \Lambda$, and (ii) $\sum_{i\in\Lambda} \varphi_i(x) = 1$, for all $x \in X$.

Chapter 3

Introduction to Shape Reconstruction

It is the mark of an educated mind to rest satisfied with the degree of precision which the nature of the subject admits and not to seek exactness where only an approximation is possible.
—Aristotle

This chapter presents the basic concepts and challenges of Euclidean shape reconstruction. Along with some of the important developments in applying topological tools to shape reconstruction, we also discuss their limitations. In light of the shortcomings, the discussion motivates our methodologies, and helps the reader discern the importance of our contribution, which is presented in Chapter 4, Chapter 5, and Chapter 6.

3.1 Motivation

With the advent of modern sampling technologies, such as GPS, sensors, medical imaging, etc., Euclidean point-clouds are becoming widely available for analysis. In the last decade, the problem of reconstructing an (unknown) Euclidean shape, from a (noisy) sample around it, has received far and wide attention both in theoretical and applied literature; see [5, 7–9, 23, 24]. The nature of such a reconstruction attempt can commonly by classified as being *topological* or *geometric*. A topological reconstruction is usually attributed to inferring the significant topological features—such as homology and homotopy groups—of the hidden shape of interest. A much stronger paradigm is a geometric reconstruction, where one is

interested in computing, from the sample, a homotopy equivalent shape that is geometrically "close" to the ground truth.

The nature of the problem and the techniques of the solution change depending on the type of the shape X and the sample S considered, as well as how their "closeness" is measured. The most natural distance measure between two abstract metric spaces is the Gromov-Hausdorff distance (Definition 7.2.2), it measures how much two metric spaces are "metrically close". The reconstruction of a geodesic metric space X from another metric space S, that is Gromov-Hausdorff close to X, is considered both in [25, 26]. For a Euclidean shape X and a Euclidean sample S, however, the sample density is usually quantified by their Hausdorff distance (Definition 3.1.1).

Definition 3.1.1 (Directed Hausdorff Distance)**.** For any two compact subsets X, Y of a metric space (Z, d_Z), the ***directed Hausdorff distance*** from X to Y, denoted $\overrightarrow{d}_H^Z(X, Y)$, is defined by

$$\sup_{x \in X} \inf_{y \in Y} d_Z(x, y).$$

Unfortunately, the directed Hausdorff distance is not symmetric. To retain symmetry, the ***Hausdorff distance*** is defined in the following way:

Definition 3.1.2 (Hausdorff Distance)**.** For any two compact subsets X, Y of a metric space (Z, d_Z), their ***Hausdorff distance***, denoted $d_H^Z(X, Y)$, is defined by

$$\max\left\{\overrightarrow{d}_H^Z(X, Y), \overrightarrow{d}_H^Z(Y, X)\right\}.$$

To keep our notations simple, we drop the superscript when it is understood that Z is taken to be a Euclidean space and X, Y are Euclidean subsets equipped with the standard Euclidean metric $|\cdot|$.

The definition immediately imply that $d_H(A, B) < \varepsilon \iff A^\varepsilon \subset B$ and $B^\varepsilon \subset A$, where

$$A^\varepsilon := \bigcup_{a \in A} \mathbb{B}(a, \varepsilon).$$

For the Hausdorff-type reconstruction of Euclidean shapes, see [5, 7–9]. These results do not apply when considering shapes beyond the class of Euclidean submanifolds and shapes that do not have a positive weak feature size (defined later in Subsection 3.4.1). This chapter briefly surveys some of the important and related developments in shape reconstruction from point-clouds using topological methods. Table 3.1 presents a list of some of the most related results alongside our contribution.

3.2 Manifold Reconstruction

The most well-behaved spaces are smooth Euclidean (compact) sub-manifolds. Examples include smooth, closed curves of $\mathbb{R}^N$, the smoothly embedded n-dimensional

Table 3.1: Reconstruction results. Parameters (params.) are: normal injectivity radius (τ_0), weak feature size (wfs), reach (μ), shorted edge length (b), global reach (ξ), smallest turning angle (α), distortion (δ), and convexity radius (ρ).

Authors	**Shape** $X \subseteq \mathbb{R}^N$	**Params**	**Conditions on Sample** S	**Reconstruction Result**
Niyogi et al. [5]	manifolds	τ	$\varepsilon < \sqrt{\frac{3}{5}}\tau$ and $S \subset X$ is $\frac{\varepsilon}{2}$-dense	S^ε deformation retracts to X
Chazal, Lieutier [9]	compact sets	wfs	$d_H(X,S) < \varepsilon < \frac{\text{wfs}(X)}{4}$	$\text{Im}(i_*) \simeq H_*(X^\alpha)$, where $i : S^\varepsilon \to S^{3\varepsilon}$ and α is sufficiently small
Chazal, Oudot [7]	compact sets	wfs	$d_H(X,S) < \varepsilon < \frac{1}{9}\text{wfs}(X)$, S is finite	$\text{Im}(i_*) \simeq H_*(X^\alpha)$, where $i : \mathcal{R}_\varepsilon(S) \to \mathcal{R}_{4\varepsilon}(S)$, α is sufficiently small
Attali et al. [27]	compact sets	μ	$d_H(X,S) \leq \varepsilon < \lambda^{\text{cech}}(\mu)R$	$\mathcal{C}_\alpha(S)$ is homotopy equivalent to X^η for $\eta \in (0,R)$
Anjaneya et al. [11]	metric graphs	b, r	S is an (ε, R)-approximation, $\frac{15\varepsilon}{2} < b < \min\left\{\frac{R}{4}, \frac{3}{5}(b-2\varepsilon)\right\}$	homeomorphic graph
Wasserman et al. [28]	metric graphs	μ of each edge, ξ, α, b, τ	S is $\frac{\delta}{2}$-dense in X^α, $0 < r+\delta < \xi - 2\sigma$, and $0 < \delta < f(b,\alpha,\tau,\xi,\sigma)$	isomorphic pseudo-graph
Theorem 4.3.4	geodesic subspaces	δ, ρ	$d_H(X,S) < \frac{\varepsilon}{4} < \frac{\rho}{2\delta(3\delta+2)}$	$\text{Im}(i_*) \simeq H_*(X)$, where $i : \mathcal{R}_\varepsilon(S) \to \mathcal{R}_{\frac{1}{2}(3\delta+1)\varepsilon}(S)$
Theorem 5.3.4	planar metric graphs	δ, b	$d_H(X,S) < \frac{\varepsilon}{3} < \frac{b}{4\delta(15\delta+2)}$	Hausdorff-close, homotopy equivalent graph

sphere $\mathbb{S}^n$, etc. Geometric and topological inference about an *unknown* manifold from point samples is commonly known as *manifold learning*.

Smooth Euclidean sub-manifolds—being free of topological anomalies, like punctures, corners, singularities—seem deceptively easy to reconstruct. The authors of [5] were the first to successfully apply geometric and topological tools to manifold reconstruction from a dense point-cloud. The novelty lies in providing provable guarantees of correct reconstruction and introducing a new sampling parameter: *normal injectivity radius*; see Definition 3.2.1.

Definition 3.2.1 (Normal Injectivity Radius [5])**.** Let M be a compact smooth n-manifold embedded in $\mathbb{R}^N$. The normal injectivity radius τ is defined as the largest number r having the property: the open normal bundle of M of radius r is embedded in $\mathbb{R}^N$.

The normal injectivity radius is a property of the embedding, rather than the manifold. It follows from the definition that τ of a sphere of radius R is R.

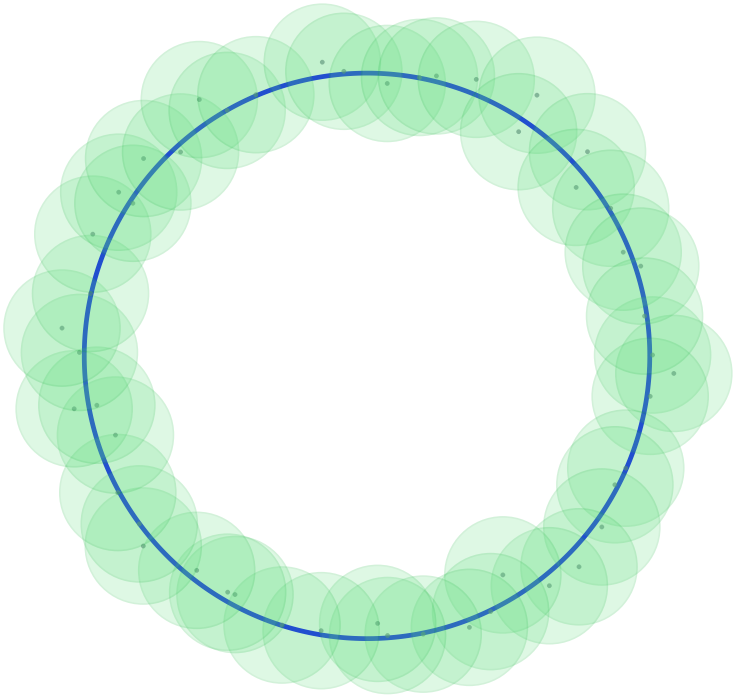

Figure 3.1: Consider the unknown manifold M to be a circle $\mathbb{S}^1$ of unit radius embedded in $\mathbb{R}^2$. The injectivity radius is 1. The sample points are shown in black. For a radius smaller than $\tau = 1$, the union of (green) Euclidean balls around them is shown to be homotopy equivalent to the shape. The picture has been generated using www.smajhi.com/shape-reconstruction.

In [5], the authors consider the union of Euclidean balls of sufficiently small radius around a dense sample S; see Figure 3.1. The density of a sample is quantified by the following notion of ε-density.

Definition 3.2.2 (ε-dense Sample)**.** For positive $\varepsilon > 0$ and $X \subseteq \mathbb{R}^N$, a subset S of $\mathbb{R}^N$ is called ε-dense if X is covered by the ε-thickening S^ε of S, i.e.,

Here $\mathbb{B}(s, \varepsilon)$ denotes the ε radius Euclidean ball centered at the point s.

We now state the main manifold reconstruction result of [5].

Theorem 3.2.3 (Manifold Reconstruction [5])**.** *Let M be a smooth submanifold of $\mathbb{R}^N$ with the normal injectivity radius τ. Let $S \subset M$ be an $\frac{\varepsilon}{2}$-dense sample and $0 < \varepsilon < \sqrt{\frac{3}{5}}\tau$. Then, the union $\mathcal{U} = \bigcup_{x_i \in S} \mathbb{B}(x, \varepsilon)$ deformation retracts to M. Therefore, homology of $\mathcal{U}$ equals homology of M.*

We first present a sketch of the proof of Theorem 3.2.3, and make a few remarks on the conditions of the theorem. For a point $p \in M$, let us denote the tangent

space and the normal space at p by T_p and N_p respectively. Let us also define the fiber $\pi^{-1}(p)$ to be $N_p \bigcap \mathcal{U}$. It has been argued that $\pi^{-1}(p)$ becomes path-connected if $\varepsilon < \sqrt{\frac{3}{5}}\tau$ and the sample is $\frac{\varepsilon}{2}$-dense. Finally, the required deformation retraction is devised along those fibers.

The obligatory $\sqrt{\frac{3}{5}}$ factor comes as a side-effect of the technique used. However, the result seems to hold without the factor and for just an ε-dense sample. In Figure 3.2, the unknown manifold is taken to be a smooth planar curve. The fiber at the point p is not path-connected, so the technique of the proof is not applicable in this case. However, the result still holds.

In Section 3.3, we use a different approach for a stronger reconstruction of the 1-dimensional case: smooth (closed) curve of $\mathbb{R}^N$, but under conditions weaker than those of Theorem 3.2.3.

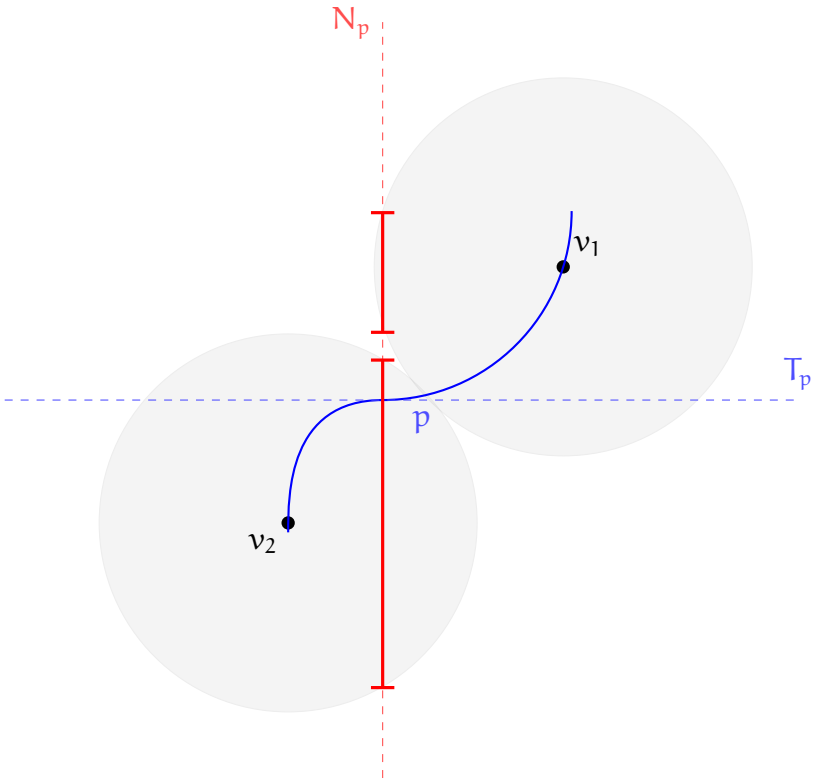

Figure 3.2: The part of the manifold is shown in blue. The Euclidean balls of radius $\varepsilon < \tau$ around v_1, v_2 are shown in grey. The fiber (red perpendicular) at p is disconnected. A case where the proof of [5] does not work, however the result holds true. Note that the sample is not $\frac{\varepsilon}{2}$ dense.

3.3 Smooth Curve Reconstruction

We consider M to be a closed, smooth curve embedded in $\mathbb{R}^N$. The homology of M is not very interesting here, as M is homotopy equivalent to a circle. Although the

homotopy type of a closed one-manifold is not very interesting, our homeomorphic approximation sheds light on the geometric embedding of the (hidden) manifold. Also, our proof works even in the bad case shown earlier in Figure 3.2.

Theorem 3.3.1 (Geometric Reconstruction of Smooth Curves)**.** *Let M be a closed, smooth curve in $\mathbb{R}^N$ and let τ be its normal injectivity radius. Let $0 < \varepsilon \leq \tau$, and let $S \subset M$ be an ε-dense sample. Then, the medial axis of S^ε is homeomorphic to M.*

As a consequence, S^ε and M are homotopy equivalent, since the author of [29] have shown that any bounded open subset of Euclidean space is homotopy equivalent to its medial axis.

Proof. We denote the curve by $\gamma : I \to M$ with $\gamma(0) = \gamma(1) = x_0$. Let us also denote the tubular neighborhood of M by M^ε. We now enumerate the points of S by $\{x_1, x_2, \ldots, x_k\}$, where $x_i = \gamma(t_i)$ and $t_i \leq t_{i+1}$; see Figure 3.3.

Now, $\{t_i\}$ introduces a partition M_i of γ, where $M_i = \gamma([t_i, t_{i+1}])$ and $i \in \{1, ..., k\}$.

Observe that, each $\mathbb{B}(x_i, \varepsilon)$—the ball around x_i—touches the tubular neighborhood M^ε exactly at two points, say u_i and l_i. Let's denote $N_i = \overline{u_i l_i}$, the normal passing through the sample point x_i. These special normal lines partition the tubular neighborhood into k regions $\{M_i^\varepsilon\}_i$.

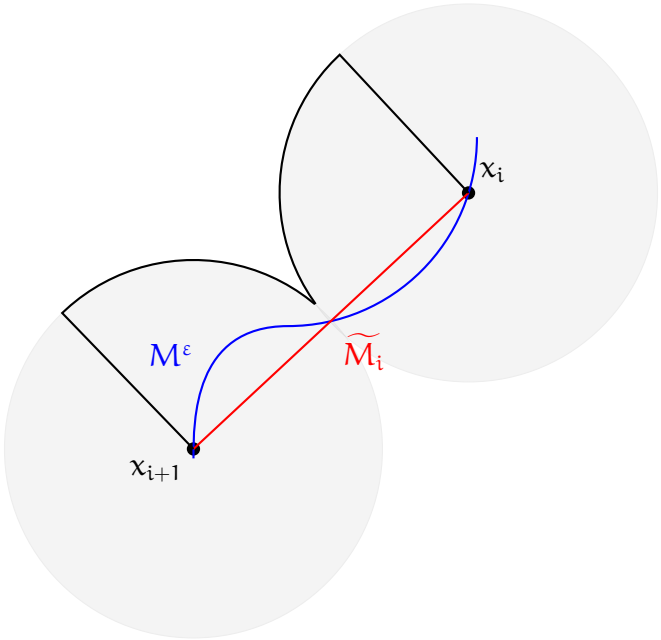

Figure 3.3: The part M^ε of the smooth curve between the sample points x_i and x_{i+1} is shown in blue. The red segment denotes $\widetilde{M}_i$.

Let's introduce $\widetilde{M}$ to be the piecewise linear curve joining x_i's in the respective order and $\widetilde{M}_i = \overline{x_i x_{i+1}}$. We show that $\widetilde{M}$ is homeomorphic to M.

Observe that $\widetilde{M}$ is also the medial axis of S^ε. Within M_i^ε we introduce a homeomorphism between $\widetilde{M}_i$ and M_i locally, and extend it globally so that it retains continuity since they agree on each N_i.

We define a homeomorphism $\phi_i : \widetilde{M}_i \to M_i$ for each M_i^ε in the following way. If we draw a perpendicular L at any point z on $\tilde{M}_i$, we show that L cuts $\widetilde{M}_i$, the manifold at exactly one point y and define $\phi_i(x) := y$. As a consequence, this proves that M_i is a continuous graph on $\widetilde{M}_i$, hence a homeomorphism.

On the contrary, let's assume that there is a perpendicular L at a point x on M_i that intersects $\widetilde{M}_i$ at least two points z_1 and z_2. We arrive at a contradiction by showing that there is a point z on M_i such that the normal T_z at z is parallel to $\widetilde{M}_i$.

Without the loss of generality, we assume that L cuts the manifold at both z_1 and z_2. We note that z_1 and z_2 are points on the manifold and tangents T_{z_1} and T_{z_2} are not parallel to L. By continuity of the tangents of M we conclude that there exists a point z on M_i such that T_z is parallel to L. Consequently, the normal N_z at z is parallel to $\widetilde{M}_i$.

Now, we arrive at a contradiction in either of the following cases:

(1) If length of $M_i \leq \varepsilon$, then ε-radius normal, $N_z \cap M^\varepsilon$, at z intersects either N_i or N_{i+1}. This contradicts the fact that τ is the injectivity radius.

(2) If length of $M_i > \varepsilon$, then ε-radius normal, $N_z \cap M^\varepsilon$, at z lies completely in the interior of M_i^ε. And, that's a contradiction because the boundary of each ε-radius normal lies on the boundary of the tubular neighborhood M^ε of the manifold.

Therefore, ϕ_i is a well-defined, invertible continuous map on a compact domain, hence a homeomorphism. Since, ϕ_i's agree on the boundary of each $\widetilde{M}_i$, we glue them to get a global homeomorphism $\phi : \widetilde{M} \to M$. This completes the proof. □

We conclude our discussion on the reconstruction of smooth manifolds by pointing out a few limitations of the normal injectivity radius approach, which led us to take a more robust approach to reconstruction in the following chapters.

Manifolds with Dents. The normal injectivity radius τ decides both the radius of the balls around the sample and the sample density. From a practical standpoint, a very small τ makes the implementation of the results difficult. However, it is very susceptible to small *dents* on the manifold: τ can drop significantly if a small noise is assumed to exist as a dent on the manifold.

Noisy Sample. Also, the results are only valid when the sample points are coming directly from the manifold. In practice, the density of the sample is seldom a

concern, noise is what makes the inference a challenge. We have covered reconstruction results that assume the finite sample is *perfect*: sample points lie directly on the manifold. A more robust reconstruction result should be able to handle noisy samples.

Non-manifolds. The shapes that we often encounter in real-world problems are not manifolds. The manifold reconstruction techniques do not apply in such cases; see Figure 3.4 for an example. Moreover, the definition of the normal injectivity radius heavily depends on the fact that the manifold is smoothly embedded. There is no natural way to extend the definition of τ to non-smooth manifolds or non-manifolds.

Because of its applications in data analysis and growing challenges, reconstruction of a general compact, Euclidean subset from a noisy sample has been receiving increasing attention in the last decade. The next section quickly surveys the developments made and challenges faced in the realm of compact set reconstruction.

3.4 Compact Set Reconstruction

Although much success has been made for Euclidean submanifolds, the topological and geometric reconstruction of spaces beyond this regime is not well-understood. As shown in Figure 3.4 for a (non-manifold) shape with branching, the union of Euclidean balls of sufficiently small radius around a dense sample is not always guaranteed to deformation retract to the shape.

We first discuss the successful topological reconstruction attempt of [8,9] using the notion of *weak feature size*.

3.4.1 Weak Feature Size

A sampling theory for general compact sets was developed in [7, 9]. The authors introduced the notion of *weak feature size* (`wfs`) for a compact subset of $\mathbb{R}^N$ as its distance from the set of critical points of the distance function. The authors consider the `wfs` of the compact shape in their sampling condition. In order to compute the homology groups of the unknown shape, a persistence-based treatment ([7]) on filtrations of the point cloud is used.

Although the results encompass spaces beyond smooth submanifolds of $\mathbb{R}^N$, they do not apply to a large class of compact sets that have a zero `wfs` or spaces whose `wfs` is not defined. Embedded trees, i.e., acyclic graphs are examples of spaces whose `wfs` is undefined, for their complements do not have any bounded component. For an example of a space with zero `wfs`, consider the space X in Figure 3.5(a). The top part of the space X is the graph of a rectifiable curve $\gamma : [0, 1] \to \mathbb{R}^2$ such that, when restricted to the segment $\left[\frac{1}{n+1}, \frac{1}{n}\right]$, it is a half-circle with the segment as its diameter.

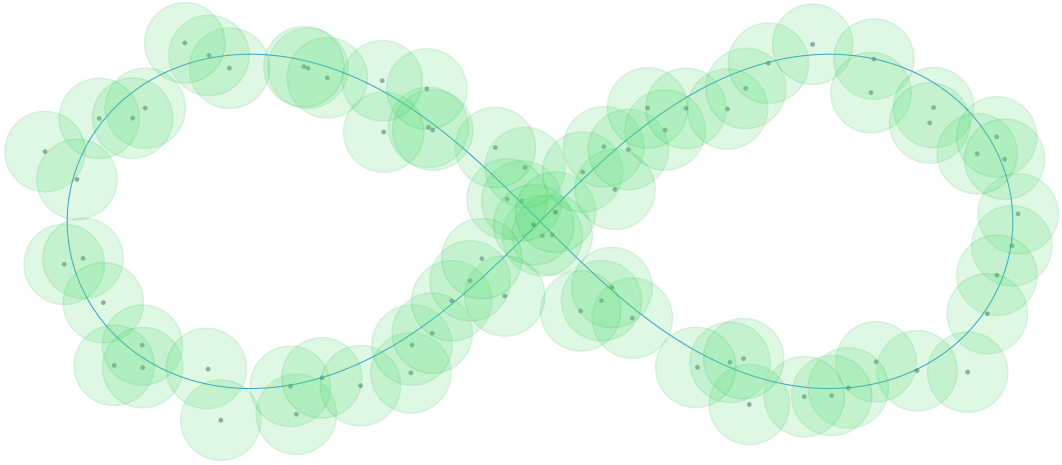

Figure 3.4: The (hidden) compact set X (shown in blue) is not a manifold—X is a bouquet of two circles. The sample S (the black points) is dense, however the union of balls S^{ε} is not homotopy equivalent to X. We see an extra 1-cycle formed right beneath the branching point.

For this space, the set of critical points of the distance function is an infinite set with an accumulation point at $(0,0)$. Consequently, $\texttt{wfs}(X) = 0$. However, X has a finite distortion and a positive convexity radius. So, our approaches presented in Chapter 4 encompass such a case.

The results of [7, 9] require the underlying space to have a positive `wfs`. Unfortunately, for a large class of shapes that frequently interest topological data analysts, `wfs` is not defined or `wfs` vanishes; examples include embedded graphs and simplicial complexes. In order to elude such difficulty, the authors of [8] introduce the notion of μ-reach to replace `wfs`. However, choosing a suitable μ so that the μ-reach is positive is not always clear.

We also note that a small Hausdorff perturbation may inflict a big fluctuation on the `wfs`. In Figure 3.5(b), the small bump on the circle introduces a new critical point, hence reducing the `wfs` of the circle significantly.

In comparison, the reconstruction results in [7–9] compute the homology groups of a small offset X^{α} of X, rather than of X itself. In Figure 3.6, we see a compact set X, where any small thickening is not homotopy equivalent to X. In our setting, however, we reconstruct the space X itself upto homotopy type.

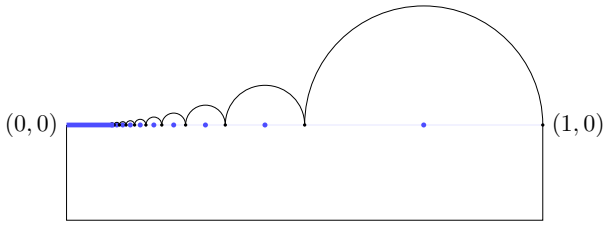

((a)) The space X is a compact Euclidean subspace with $\texttt{wfs}(X) = 0$. The critical points of the distance function are shown in blue; they accumulate at $(0, 0)$. However, X has a finite distortion and a positive convexity radius.

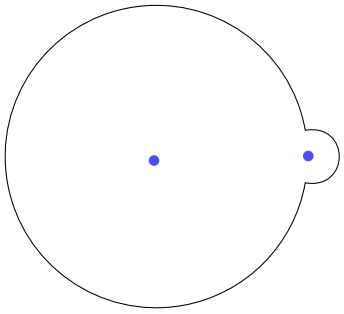

((b)) The blue dots show the critical points of the distance function. The small bump on the boundary introduces an additional critical point, hence the `wfs` drops drastically under such a small noise. However, the convexity radius and distortion remain almost the same.

Figure 3.5: Zero `wfs` and `wfs` under small noise

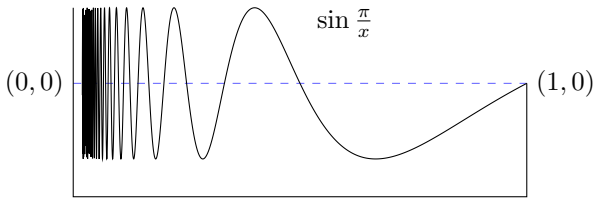

Figure 3.6: The compact set X has a positive `wfs`, but X and X^{α} do not have the same homotopy type for any $\alpha > 0$. The space X is contractible whereas X^{α} has the homotopy type of a circle.

3.4.2 Čech and Vietoris-Rips Complex-based Reconstruction

In shape reconstruction, the use of various simplicial complexes built on the point-clouds is becoming increasingly popular; see for example [27, 30, 31]. The most common of them are Vietoris-Rips and Čech complexes. In this work, we use filtrations of both of them, and we recognize the ***distortion*** and ***convexity radius*** of X to be the most natural sampling parameters when geodesic subspaces of $\mathbb{R}^N$ are considered; see Section 4.2 for their formal definitions. The distortion quantifies the maximum ratio of the length metric to the standard Euclidean metric.

Consider a (compact) subset X of $\mathbb{R}^N$ and a finite Euclidean sample S around it. In the most desirable scenario, we aim to compute a geometric complex $\widetilde{X}$ that is homotopy equivalent to X. If such a strong reconstruction goal is elusive, we resort to computing only the homotopy and homology groups of X from S. In such a pursuit, we ask the most fundamental question: for what scale ε and under what density condition on S are the Čech or Vietoris-Rips complexes of S homotopy equivalent to X? In [5], the authors provide a very satisfying answer when X is a smooth submanifold. For sufficiently small scale $\varepsilon > 0$ and sufficiently dense sample S, the authors show that the union of Euclidean balls around the sample points has a deformation retraction onto X. As a consequence of the Nerve Lemma (Lemma 2.4.1), the Čech complex $\mathcal{C}_{\varepsilon}(S)$ of S is homotopy equivalent to X. When X is a planar circle, the result is demonstrated in Figure 3.7. The Vietoris-Rips complex

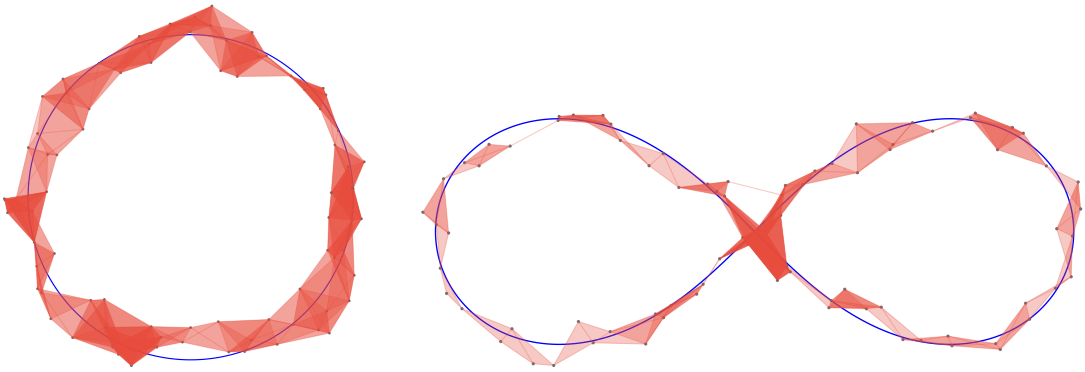

Figure 3.7: On the left, a sample (shown in gray) around a planar circle (thick blue) is considered. For a small scale, the Vietoris-Rips complex, whose shadow is shown in red, correctly reflects the homotopy type of the circle. On the right, a reasonably dense sample around a planar lemniscate is considered. However, the Vietoris-Rips complex in this case fails to capture the correct one-dimensional Betti number. We see an extra 1-cycle (containing the green edge) introduced just above the four-way intersection. The pictures were generated using the shape reconstruction library available on www.smajhi.com/shape-reconstruction.

also behaves similarly in the manifold case; see [31]. These results can also be extended, under some restrictions, to spaces with positive reach; see [27].

3.5 Discussions

Although much success has been made for Euclidean shapes with positive reach, the homotopy type reconstruction of spaces beyond this regime is not well-understood. As shown in Figure 3.7 for a (non-manifold) space with branching, the existence of such a small scale ε is not always guaranteed for neither the Vietoris-Rips complex nor the Čech complex. A very small ε may introduce anomalous features, whereas a large ε may potentially destroy a significant feature. In Chapter 4, we consider a persistence-based approach with filtrations of these combinatorial complexes of the sample S, and use it to compute the homology and homotopy groups of X. The idea is to start with a scale ε so that the Vietoris-Rips complex (or Čech complex) contains all the homological features of X, along with some unwanted features or "noise", as shown in Figure 3.7. A bigger scale ε' is then carefully conjured up so that the noise features of the former complex become trivial in the (larger) complex at this scale. Such an idea of looking at two different scales ε and ε' in order to rule a homological feature significant pervades the developments in Chapter 4 and Chapter 5.

Chapter 4

Topological Reconstruction of Geodesic Subspaces

Geometry has two great treasures; one is the Theorem of Pythagoras; the other, the division of a line into extreme and mean ratio. The first we may compare to a measure of gold; the second we may name a precious jewel.
— Johannes Kepler

We gave a brief introduction to the growing field of topological shape reconstruction in Chapter 3. The discussion has also shed some light on the challenges a non-manifold shape particularly brings forth. This chapter introduces *geodesic subspaces* (see Definition 4.2.1), and presents our methods to reconstruct them. As we will see—the class of such spaces encompasses smooth submanifolds, along with a large class of compact sets that are important from the topological data analysis standpoint.

This chapter presents our contribution to the reconstruction of geodesic spaces from a Hausdorff-close, finite sample. Following the formal definition in Section 4.2, we discuss two important concepts: distortion (Subsection 4.2.1) and convexity radius (Subsection 4.2.2). In Section 4.3 and Section 4.4, we discuss topological reconstruction using Vietoris-Rips and Čech complexes, respectively.

4.1 Introduction

In many applications, a point-cloud approximates a geodesic subspace (see Definition 4.2.1) of Euclidean space. Examples include GPS trajectory data sampled around a road-network, which can be thought of as a graph in $\mathbb{R}^2$, earthquake data

sampled around an embedded graph inside the earth, or 3D scans of a simplicial complex. The spaces of interest in such applications do not always enjoy a manifold structure or have a desired positive `wfs`. However, the intrinsic geodesics of such shapes enjoy a rich geometric structure. The length metric d_L (defined in Section 4.2) turns them into geodesic subspaces of $\mathbb{R}^N$. In this work, we consider both topological and geometric reconstruction of a geodesic subspace (X, d_L) of $\mathbb{R}^N$ from a Hausdorff-dense, finite, noisy Euclidean sample $(S, \|\cdot\|)$.

Our reconstruction approach is similar to [7], which is based on the `wfs` of the underlying space. However, the use of partition of unity, for example, in the proof of Theorem 4.4.5, makes our methods very different. The novelty of this paper is discerned by the introduction of distortion and convexity radius as sampling parameters—as opposed to the typically used concepts, like reach or `wfs`. As a consequence, the results apply to a different (generally larger) class of spaces that includes smooth submanifolds of $\mathbb{R}^N$, finite embedded graphs, higher dimensional simplicial complexes, etc. Our geometric reconstruction technique in Chapter 5 also brings a robust and new approach to topological graph reconstruction.

4.2 Geodesic Subspaces

Let $\gamma : I = [0, 1] \to \mathbb{R}^N$ be a (continuous) path. The length of γ is defined as:

$$\sup \sum_{i=1}^{k} \|\gamma(t_{i-1}) - \gamma(t_i)\|,$$

where the supremum is taken over all partitions $\mathcal{P} = \{0 = t_0, \ldots, t_{i-1}, t_i, \ldots, t_k = 1\}$ of I. Furthermore, γ is called *rectifiable* if $L(\gamma) < \infty$.

For a path-connected subset $X \subseteq \mathbb{R}^N$, we call the restriction of the standard Euclidean metric $\|\cdot\|$ to X the *induced metric* on X. We define the *length metric*, sometimes called the *geodesic metric*, $d_L : X \times X \to \mathbb{R}$ by

$$d_L(x, y) = \inf_{\gamma:[0,1]\to X} L(\gamma),$$

where the infimum is taken over all (continuous) paths $\gamma : I \to X$ from x to y.

Definition 4.2.1 (Geodesic Subspace)**.** We call $X \subseteq \mathbb{R}^N$ a ***geodesic subspace*** if between any pair of points $x, y \in X$, there always exists a rectifiable path on X whose length is $d_L(x, y)$. In other words, the infimum in the definition of d_L is realized.

For a compact subset X of $\mathbb{R}^N$ with a finite distortion, that we define now, is in fact a geodesic subspace.

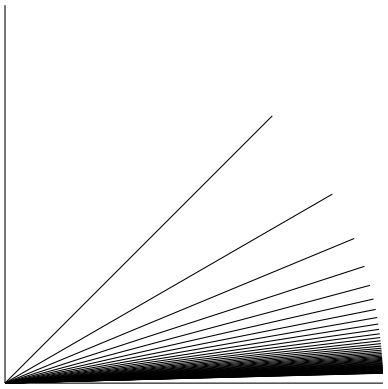

Figure 4.1: The union X of the falling segments in the figure is known as the *infinite broom*. The topology of $(X, \|\cdot\|)$ is strictly finer than the length metric topology of (X, d_L). In the latter topology, it is locally path-connected; whereas; the former is not.

4.2.1 Distortion

The concept of distortion was first introduced by M. Gromov in the context of knots on Riemannian manifolds in [32–34]. Since then, various questions regarding bounds on distortion, both lower and upper, of embedded spaces interest researchers in the field of geometry and topology. We follow the book ([34]) by Gromov to define distortion here. For an $X \subseteq \mathbb{R}^N$, let us consider the identity map $f : (X, \|\cdot\|) \to (X, d_L)$. The distortion of X is defined by the best Lipschitz constant of f. More formally, we have the following definition.

Definition 4.2.2 (Distortion)**.** The ***distortion*** of $X \subseteq \mathbb{R}^N$ is defined by

$$\delta = \sup_{x,y \in X, x \neq y} \frac{d_L(x,y)}{\|x-y\|}.$$

In general, the distortion is bounded below by 1 and above by $+\infty$, and both the bounds can be achieved. The lower bound is attained when X is a straight line segment. On the other extreme, if X is a planar cusp: the union of points $(x, y) \in \mathbb{R}^2$ such that $x^2 = y^3$, we have $\delta = +\infty$. For more on distortion, see [34, 35].

Remarks 4.2.3 (Equivalence of Topologies). We reconstruct the length metric space (X, d_L) in Section 4.3 and Section 4.4. Under the finite distortion condition, however, we note that the topology of (X, d_L) is equivalent to the induced metric topology $(X, \|\cdot\|)$. The equivalence of the two topologies is a direct consequence of the following inequalities:

$$\|x-y\| \leq d_L(x,y) \leq \delta\|x-y\|, \text{ where } x, y \in X. \tag{4.1}$$

We also note that the equivalence of the topologies does not generally hold if the distortion of X is not finite. For an example, let $X \subset \mathbb{R}^2$ to be the union of planar line segments $\left\{\left[(0,0), \left(\cos\frac{\pi}{2i}, \sin\frac{\pi}{2i}\right)\right]\right\}_{i\in\mathbb{N}}$, as shown in Figure 4.1. Such a space is also known as *infinite broom*. We see that the distortion of the space is infinite by

considering the sequence $a_i = \left(\cos \frac{\pi}{2i}, \sin \frac{\pi}{2i}\right)$ of points on the right end of the spokes of the broom:

$$\lim_{i\to\infty} \frac{d_L\big((0,1), a_i\big)}{\|(0,1) - a_i\|} = \infty.$$

The Euclidean metric topology, in this case, is strictly finer than the length metric topology, as (X, d_L) is locally path-connected, but $(X, \|\cdot\|)$ is not.

4.2.2 Convexity Radius

In our reconstruction technique, the convexity radius of the underlying geodesic subspace plays an important role. We start with its formal definition from [36]. Although the concept is defined for general length spaces, here we restrict ourselves to only geodesic subspaces. Here, $\mathbb{B}_L(x, r)$ denotes the ball of radius r around $x \in X$ in the d_L metric.

Definition 4.2.4 (Convexity Radius)**.** We define the *convexity radius*, denoted ρ, of a geodesic subspace $X \subseteq \mathbb{R}^N$ to be the supremum of all $r > 0$ with the following two properties: for any $x \in X$ and $y, y' \in \mathbb{B}_L(x, r)$,

(i) there exists a unique length-minimizing geodesic path joining y and y', and this path lies entirely inside $\mathbb{B}_L(x, r)$.

(ii) this unique geodesic is continuous with respect to its endpoints.

For example, the convexity radius of a sphere of radius R is $\frac{R}{4}$. Also, the convexity radius of an embedded graph is $\frac{b}{4}$, where b is the length of its smallest simple cycle. It is well-known that the convexity radius of a compact Riemannian manifold is positive. The definition of convexity radius immediately implies the following fact, which we use later for our reconstruction results.

Lemma 4.2.5. *Let $X \subseteq \mathbb{R}^N$ be a geodesic subspace with a positive convexity radius ρ, and let $0 < \varepsilon < \rho$. Let $A \subseteq X$ be ε-dense w.r.t the d_L metric. Then, the Čech complex $\mathcal{C}^L_\varepsilon(A)$ is homotopy equivalent to X.*

Proof. Since $\varepsilon < \rho$, an ε-radius (metric) ball is contractible using condition (ii) of Definition 4.2.4, also so is any finite intersection of ε-balls. The reason is we can define a homotopy along the unique length-minimizing path joining any point of the ball to its center. Now, the density assumption implies that the collection of ε-balls around A is a cover of (X, d_L). Hence, it is a good cover. By the Nerve Lemma (Lemma 2.4.1), we conclude that $\mathcal{C}^L_\varepsilon(A)$ is homotopy equivalent to X. □

We consider the problem of topological reconstruction of a geodesic subspace X of $\mathbb{R}^N$ from a noisy sample S.

Remarks 4.2.6. From now on, unless otherwise stated, we assume that the underlying shape X has a positive convexity radius and a finite distortion, also the sample S is a finite subset of $\mathbb{R}^N$.

We show that both Čech and Vietoris-Rips filtrations of S can be used to compute the homology and homotopy groups of X. Before we treat each type of complex separately in Section 4.3 and Section 4.4, we show how the Vietoris-Rips and Čech complexes behave under Hausdorff perturbation.

Lemma 4.2.7 (Hausdorff Distance and Complexes)**.** *Let $A, B \subseteq \mathbb{R}^N$, and ε be a positive number such that $d_H(A,B) < \varepsilon$. Then for any $\alpha > 0$, there exist simplicial maps*

$$\xi_1 : \mathcal{C}_\alpha(A) \longrightarrow \mathcal{C}_{\alpha+\varepsilon}(B)$$

and

$$\xi_2 : \mathcal{R}_\alpha(A) \longrightarrow \mathcal{R}_{\alpha+2\varepsilon}(B)$$

such that for every vertex $a \in A$, we have $\|a - \xi_i(a)\| < \varepsilon$ for $i = 1, 2$. Moreover, such simplicial maps are unique, up to contiguity.

Proof. By the definition of Hausdorff distance and since $d_H(A,B) < \varepsilon$, there exists a (possibly non-unique, non-continuous) map $\xi : A \to B$ such that $\|a - \xi(a)\| < \varepsilon$. We show that this vertex map extends to a simplicial map between both Čech and Vietoris-Rips complexes.

Let $\sigma = \{a_0, a_1, \ldots, a_k\}$ be a k-simplex of $\mathcal{C}_\alpha(A)$. By definition, there exists a $z \in \mathbb{R}^N$ such that $\|a_i - z\| < \alpha$ for all $i \in \{0, 1, \ldots, k\}$. From the triangle inequality we then have, $\|\xi(a_i) - z\| \leq \|\xi(a_i) - a_i\| + \|a_i - z\| < \varepsilon + \alpha$. So, $\{\xi(a_0), \cdots, \xi(a_k)\}$ is a simplex of $\mathcal{C}_{\alpha+\varepsilon}(B)$. Hence, ξ extends to a simplicial map ξ_1 between the Čech complexes. To argue for the uniqueness of the simplicial map, let us assume that η is another simplicial map with the property that for every vertex $a \in A$, we have $\|a - \eta(a)\| < \varepsilon$. Again from the triangle inequality, we have $\|\eta(a_i) - z\| < \varepsilon + \alpha$. So, $\xi_1(\sigma) \cup \eta(\sigma)$ is a simplex of $\mathcal{C}_{\alpha+\varepsilon}(B)$. Hence, ξ_1 and η are contiguous.

For the Vietoris-Rips complex part, we follow a similar argument. Let $\sigma = \{a_0, a_1, \ldots, a_k\}$ be a k-simplex of $\mathcal{R}_\alpha(A)$. By definition, the diameter of σ is not greater than α. From the triangle inequality, we have $\|\xi(a_i) - \xi(a_j)\| \leq \|\xi(a_i) - a_i\| + \|a_i - a_j\| + \|\xi(a_j) - a_j\| < 2\varepsilon + \alpha$. So, $\{\xi(a_0), \cdots, \xi(a_k)\}$ is a simplex of $\mathcal{R}_{\alpha+2\varepsilon}(A)$. Hence, ξ extends to a simplicial map ξ_2 between Vietoris-Rips complexes. □

4.3 Homology Groups via Vietoris-Rips Filtration

We use the following fundamental result from [25] to compute the homology groups of X from a filtration of Vietoris-Rips complexes on a finite sample.

Theorem 4.3.1 (Homotopy Equivalence [25])**.** *Let X be a geodesic subspace with a positive convexity radius ρ. For $0 < \varepsilon < \rho$, then there exists a homotopy equivalence $T : \left|\mathcal{R}_\varepsilon^L(X)\right| \longrightarrow X$.*

Note that $\mathcal{R}_\varepsilon^L(X)$ is usually an infinite Vietoris-Rips complex on the entire space X. As a quick corollary of this result, we show the following:

Corollary 4.3.2. *Let X be a geodesic subspace with a positive convexity radius ρ. For $0 < \varepsilon' \leq \varepsilon < \rho$, the inclusion $i : \boldsymbol{\mathcal{R}}^L_{\varepsilon'}(X) \hookrightarrow \boldsymbol{\mathcal{R}}^L_{\varepsilon}(X)$ induces isomorphisms on homology and homotopy groups.*

Proof. It follows from the construction of the map T in [25] that the following diagram commutes:

$$\begin{array}{ccc} \left|\boldsymbol{\mathcal{R}}^L_{\varepsilon'}(X)\right| & \xhookrightarrow{\ i\ } & \left|\boldsymbol{\mathcal{R}}^L_{\varepsilon}(X)\right| \\ & {\scriptstyle T'} \searrow \quad \swarrow {\scriptstyle T} & \\ & X & \end{array}$$

The maps T and T' are homotopy equivalences from Theorem 4.3.1, and T' is the restriction of T. Hence, i induces isomorphisms on the homology and homotopy groups. □

The (hidden) space X is equipped with both the Euclidean metric $\|\cdot\|$ and the geodesic metric d_L; whereas, the sample S only has the Euclidean metric, as geodesics do not exist in a discrete set. In order to achieve our result, we use certain simplicial maps to compare $\boldsymbol{\mathcal{R}}^L_*(X)$, $\boldsymbol{\mathcal{R}}_*(X)$, and $\boldsymbol{\mathcal{R}}_*(S)$.

Lemma 4.3.3 (Euclidean and Intrinsic Rips Complexes)**.** *Let X a geodesic subspace of $\mathbb{R}^N$ with a finite distortion δ. Then for $A \subseteq X$ and any positive number α, we have the following simplicial inclusions*

$$\boldsymbol{\mathcal{R}}^L_\alpha(A) \hookrightarrow \boldsymbol{\mathcal{R}}_\alpha(A) \hookrightarrow \boldsymbol{\mathcal{R}}^L_{\delta\alpha}(A).$$

Proof. The fact that $\|x - y\| \leq d_L(x, y)$ implies the first inclusion $\boldsymbol{\mathcal{R}}^L_\alpha(A) \hookrightarrow \boldsymbol{\mathcal{R}}_\alpha(A)$. Similarly, $d_L(x, y) \leq \delta\|x - y\|$ implies the second inclusion. □

Theorem 4.3.4 (Reconstruction via Rips Filtration)**.** *Let X be a geodesic subset of $\mathbb{R}^N$ with a positive convexity radius ρ and finite distortion δ. Let S be a finite subset of $\mathbb{R}^N$, and let ε be a positive number such that*

$$d_H(X, S) < \frac{\varepsilon}{4} < \frac{\rho}{2\delta(3\delta + 2)}.$$

Then, for any non-negative integer k, the homology group $H_k(X)$ is isomorphic to the image of the homomorphism induced by the simplicial inclusion

$$j : \boldsymbol{\mathcal{R}}_\varepsilon(S) \hookrightarrow \boldsymbol{\mathcal{R}}_{\frac{1}{2}(3\delta+1)\varepsilon}(S).$$

Proof. We derive the following chain of simplicial maps:

$$\boldsymbol{\mathcal{R}}^L_{\frac{\varepsilon}{2}}(X) \xrightarrow{\phi_1} \boldsymbol{\mathcal{R}}_\varepsilon(S) \xrightarrow{\phi_2} \boldsymbol{\mathcal{R}}^L_{\frac{3\varepsilon}{2}\delta}(X) \xrightarrow{\phi_3} \boldsymbol{\mathcal{R}}_{(3\delta+1)\frac{\varepsilon}{2}}(S) \xrightarrow{\phi_4} \boldsymbol{\mathcal{R}}^L_{\frac{1}{2}(3\delta+2)\delta\varepsilon}(X).$$

The first map ϕ_1 is the composition of the simplicial inclusion $\mathcal{R}^L_{\frac{\varepsilon}{2}}(X) \hookrightarrow \mathcal{R}_{\frac{\varepsilon}{2}}(X)$ from Lemma 4.3.3 and the simplicial map $\mathcal{R}_{\frac{\varepsilon}{2}}(X) \longrightarrow \mathcal{R}_{\varepsilon}(S)$ from Lemma 4.2.7, thanks to the assumption $d_H(S,X) < \frac{\varepsilon}{4}$.

Similarly, starting with $\mathcal{R}_{\varepsilon}(S)$ and composing maps from Lemma 4.2.7 and Lemma 4.3.3, respectively, we get the second simplicial map ϕ_2. The other two maps ϕ_3 and ϕ_4 are obtained repeating the exact same argument for a given scale.

From Lemma 4.2.7, we first note that the composition $\phi_3 \circ \phi_2$ is contiguous to the inclusion:

$$j : \mathcal{R}_{\varepsilon}(S) \hookrightarrow \mathcal{R}_{(3\delta+1)\frac{\varepsilon}{2}}(S).$$

Therefore, they induce homotopic maps on the respective underlying topological spaces. Consequently, we have $(\phi_3 \circ \phi_2)_* = j_*$. We first argue that ϕ_{2*} is surjective and ϕ_{3*} is injective.

By the choice of the simplicial maps in Lemma 4.3.3 and Lemma 4.2.7, we observe that $\phi_2 \circ \phi_1$ is contiguous to the inclusion

$$\mathcal{R}^L_{\frac{\varepsilon}{2}}(X) \hookrightarrow \mathcal{R}^L_{\frac{3\varepsilon}{2}\delta}(X).$$

By Corollary 4.3.2, the inclusion induces isomorphism on homology, hence so does $\phi_2 \circ \phi_1$. In particular, $(\phi_2 \circ \phi_1)_*$ is surjective. Hence, we have ϕ_{2*} is surjective, and ϕ_{1*} is injective.

Also, $\phi_4 \circ \phi_3$ is contiguous to the inclusion

$$\mathcal{R}^L_{\frac{3\varepsilon}{2}\delta}(X) \hookrightarrow \mathcal{R}^L_{\frac{1}{2}(3\delta+2)\delta\varepsilon}(X),$$

which induces an isomorphisms on homologies. Therefore, ϕ_{3*} induces an injective homomorphism.

Since we have $j_* = \phi_{3*} \circ \phi_{2*}$ and ϕ_{2*} is surjective, the image of j_* is the image of ϕ_{3*}. On the other hand, we know that $\mathrm{Im}(\phi_{3*})$ is isomorphic to $H_*\left(\mathcal{R}^L_{\frac{3\varepsilon}{2}\delta}(X)\right)/\mathrm{Ker}(\phi_{3*})$. As we have already shown that ϕ_{3*} is injective, its kernel is trivial. Therefore, the image of j_* is isomorphic to $\mathcal{R}^L_{\frac{3\varepsilon}{2}\delta}(X)$. Since $\frac{3\varepsilon}{2}\delta < \rho$, Theorem 4.3.1 implies that $\mathcal{R}^L_{\frac{3\varepsilon}{2}\delta}(X)$ is, in fact, homotopy equivalent to X. This completes the proof. □

The above reconstruction result works also for an infinite sample S. In applications, however, we are computationally constrained to use only finite samples.

4.4 Homology Groups via Čech Filtration

The reconstruction of homology groups via the Vietoris-Rips filtration (Theorem 4.3.4) was due to the homotopy equivalence theorem by Hausmann [25].

In this subsection, we use Čech filtrations to obtain similar reconstruction results. The Nerve Lemma (Lemma 2.4.1) is used here as the Čech alternative to the Hausmann's theorem. Like the Vietoris-Rips case, we still use different simplicial maps to compare $\mathcal{C}^L_*(X)$, $\mathcal{C}_*(X)$, and $\mathcal{C}_*(S)$. Unfortunately due to the technical assumption on the local-finiteness of the open cover in the Nerve Lemma, the (infinite) Čech complex $\mathcal{C}^L_*(X)$ is no longer guaranteed to be homotopy equivalent to X. In order to elude such a technical difficulty in the Čech case, a different technique of proof is adapted. The approach involves a (controlled) variant of the partition of unity; see Lemma 4.4.3.

Lemma 4.4.1 (Euclidean and Intrinsic Čech Complexes)**.** *Let* X *a geodesic subspace of* $\mathbb{R}^N$ *with a finite distortion* δ*. Then for* $A \subseteq X$ *and any positive number* α*, we have the following simplicial inclusions*

$$\mathcal{C}^L_\varepsilon(A) \hookrightarrow \mathcal{C}_\alpha(A) \hookrightarrow \mathcal{C}^L_{2\delta\alpha}(A).$$

Proof. The fact that $\|x-y\| \leq d_L(x,y)$ implies the first inclusion.

On the other hand, for any $x, y \in X$ we have $d_L(x,y) \leq \delta\|x-y\|$. Let $\sigma = \{x_0, ..., x_k\}$ be a simplex of $\mathcal{C}_\alpha(A)$. Then $\|x_i - x_j\| < 2\alpha$, consequently $d_L(x_i, x_j) < 2\delta\alpha$ for all $1 \leq i, j \leq k$. This implies

$$\{x_0, x_1, \ldots, x_k\} \subset \bigcap_{i=0}^{k} \mathbb{B}_L(x_i, 2\delta\alpha),$$

where $\mathbb{B}_L(x_i, r)$ denotes the r-ball centered at x_i in the metric (X, d_L). Therefore $\sigma \in \mathcal{C}^L_{2\delta\alpha}(A)$, and this verifies the second inclusion. □

We begin with a lemma that is analogous to Corollary 4.3.2 in the Čech regime; the result will find its use in the proof of Theorem 4.4.5.

Lemma 4.4.2 (Inclusion of Covers)**.** *Let* $\mathcal{U} = \{U_i\}_{i\in\Lambda}$ *and* $\mathcal{U}' = \{U'_i\}_{i\in\Lambda}$ *be good open covers of a para-compact topological space* X *such that* $U_i \subseteq U'_i$ *for each* i*. Then, the inclusion*

$$i : \mathcal{N}(\mathcal{U}) \hookrightarrow \mathcal{N}(\mathcal{U}')$$

induces isomorphisms on the homology and homotopy groups of the respective geometric complexes.

Proof. Consider the following diagram:

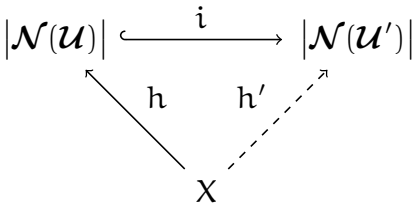

where the map $h = \sum \varphi_i u_i$ is obtained from an arbitrary partition of unity $\{\varphi_i\}$ subordinate to $\boldsymbol{\mathcal{U}}$. By the Nerve Lemma (Lemma 2.4.1), h is a homotopy equivalence ([18]). Since $U_i \subseteq U_i'$, the partition of unity $\{\varphi_i\}$ is also subordinate to $\boldsymbol{\mathcal{U}}'$. We can then choose the homotopy equivalence h' to be h. Therefore, the diagram commutes. Since the maps h and h' are homotopy equivalences, we conclude that i induces an isomorphism on homology and homotopy groups. □

We now prove the following extension of the partition of unity.

Lemma 4.4.3 (Controlled Partition of Unity)**.** *Let $\{U_i\}$ and $\{V_i\}$ be open covers of a paracompact, Hausdorff space X such that $\overline{V_i} \subseteq U_i$ for each i. Then, there exists a partition of unity $\{\varphi_i\}$ subordinate to $\{U_i\}$ such that $V_i \subseteq$ **supp** $\varphi_i \subseteq U_i$ for all i.*

Proof. Since X is a paracompact Hausdorff space, we know that X is normal (see, e.g., [37]). Since X is normal and $\overline{V_i} \subseteq U_i$ for each i, there exists open subset W_i such that $\overline{V_i} \subseteq W_i$ and $\overline{W_i} \subseteq U_i$. Note that $\{W_i\}$ is also a locally finite cover of X. Now, $(X - W_i)$ and $\overline{V_i}$ are closed, disjoint subsets of X. Using Urysohn's Lemma (see [37]), for each i, we choose a continuous function $\psi_i : X \to [0, 1]$ such that

$$\psi_i(\overline{V_i}) = \{1\} \text{ and } \psi_i(X - W_i) = \{0\}.$$

So, we have **supp** $\varphi_i \subseteq \overline{W_i} \subseteq U_i$. Also, $V_i \subseteq$ **supp** φ_i for each i.

Because the collection $\{W_i\}$ is a locally finite cover of X, the sum $\Psi = \sum_i \psi_i$ is finite at every point, and also Ψ is nowhere zero. We can then normalize to get our desired partition of unity.

$$\varphi_i(x) := \frac{\psi_i(x)}{\Psi(x)}.$$

□

We now use the controlled partition of unity to prove the following important lemma.

Lemma 4.4.4 (Commuting Diagram)**.** *Let X, Y be paracompact, Hausdorff spaces with a continuous map $f : X \to Y$. Let $\boldsymbol{\mathcal{U}} = \{U_i\}$ and $\boldsymbol{\mathcal{V}} = \{V_i\}$ be good, locally finite, open covers of X and Y respectively, such that*

(a) $\bigcap_i V_i \neq \emptyset$ implies $\bigcap_i U_i \neq \emptyset$, i.e., we have the simplicial inclusion $j : \boldsymbol{\mathcal{N}}(\boldsymbol{\mathcal{V}}) \to \boldsymbol{\mathcal{N}}(\boldsymbol{\mathcal{U}})$ that sends the vertex corresponding to V_i to the vertex corresponding to U_i,

(b) $\overline{f^{-1}(V_i)} \subseteq U_i$ for all i.

Then, the following diagram commutes, up to homotopy:

$$\begin{array}{ccc} |\boldsymbol{\mathcal{N}}(\boldsymbol{\mathcal{V}})| & \xhookrightarrow{\quad j \quad} & |\boldsymbol{\mathcal{N}}(\boldsymbol{\mathcal{U}})| \\ \Big\uparrow{\scriptstyle h_Y} & & \Big\uparrow{\scriptstyle h_X} \\ Y & \xleftarrow{\quad f \quad} & X \end{array}$$

where h_X, h_Y *are homotopy equivalences from (2.1).*

Proof. We make use of the controlled partition of unity lemma to prove our result. Let us choose a partition of unity $\{\phi_i\}$ subordinate to $\{V_i\}$. One can choose h_Y so that for each $y \in Y$

$$h_Y(y) = \sum_i \phi_i(y)v_i,$$

where v_i is the vertex of $\mathcal{N}(\mathcal{V})$ corresponding to V_i.

Since $\{f^{-1}(V_i)\}$ is an open cover of X with $\overline{f^{-1}(V_i)} \subseteq U_i$ for each i, by Lemma 4.4.3 we can choose a partition of unity $\{\psi_i\}$ subordinate to $\{U_i\}$ such that for each i

$$f^{-1}(V_i) \subseteq \textbf{supp}\ \psi_i.$$

Also, choose h_x such that for each $x \in X$

$$h_X(x) = \sum_i \psi_i(x)u_i,$$

where u_i is the vertex of $\mathcal{N}(\mathcal{U})$ corresponding to U_i.

To see that the diagram commutes, up to homotopy, it suffices to show that $(j \circ h_Y \circ f)$ is homotopic to h_X. We start with a point $x_0 \in X$

$$(j \circ h_Y \circ f)(x_0) = j\big(\sum_i \phi_i(f(x_0))v_i\big) = \sum_i \phi_i(f(x_0))j(v_i) = \sum_i \phi_i(f(x_0))u_i.$$

On the other hand, $h_X(x_0) = \sum_i \psi_i(x_0)u_i$. Now if $\phi_i(f(x_0))$ is non-zero for some i, then $f(x_0) \in V_i$, and consequently $x_0 \in f^{-1}(V_i) \subseteq U_i$. From our choice of the support of ψ_i, $\psi_i(x_0)$ has to be non-zero. This shows that both $(j \circ h_Y \circ f)(x_0)$ and $h_X(x_0)$ lie in an (open) simplex of $\mathcal{N}(\mathcal{V})$. Due to convexity of simplices, the following (straight-line) homotopy is well-defined:

$$F(x,t) = \sum_i [t\psi_i(x) + (1-t)\phi_i(x)]\, u_i.$$

to see that $(j \circ h_Y \circ f)$ is homotopic to h_X. □

Now we are in a position to prove our reconstruction result for Čech complexes.

Theorem 4.4.5 (Reconstruction via Čech Filtration)**.** *Let* X *be a geodesic subset of* $\mathbb{R}^N$ *with a positive convexity radius* ρ *and finite distortion* δ*. Let* S *be a finite subset of* $\mathbb{R}^N$*, and let* ε *be a positive number such that*

$$d_H(X,S) < \varepsilon < \frac{\rho}{2\delta(4\delta+1)}.$$

Then, for any non-negative integer k*, the homology group* $H_k(X)$ *is isomorphic to the*

image of the homomorphism induced by the simplicial inclusion

$$j : \mathcal{C}_\varepsilon(S) \longrightarrow \mathcal{C}_{(4\delta+1)\varepsilon}(S).$$

Proof. We first note from $d_H(X, S) < \varepsilon$ and Lemma 4.2.7 that there is a map $\xi : S \to X$ such that for each $s \in X$,

$$\|s - \xi(s)\| < \varepsilon. \tag{4.2}$$

Let $X' = \xi(S)$. Then (4.2) implies $d_H(S, X') < \varepsilon$, hence $d_H(X, X') < 2\varepsilon$ by the triangle inequality.

We now derive the following chain of simplicial maps:

$$\mathcal{C}_\varepsilon(S) \xrightarrow{\phi_1} \mathcal{C}^L_{4\varepsilon\delta}(X') \xrightarrow{\phi_2} \mathcal{C}_{(4\delta+1)\varepsilon}(S) \xrightarrow{\phi_3} \mathcal{C}^L_{2\delta(4\delta+1)\varepsilon}(X').$$

The first map ϕ_1 is the composition of the simplicial map $\mathcal{C}_\varepsilon(S) \hookrightarrow \mathcal{C}_{2\varepsilon}(X')$ from Lemma 4.2.7 (due to $d_H(S, X') < \varepsilon$) and the simplicial inclusion $\mathcal{C}_{2\varepsilon}(X') \hookrightarrow \mathcal{C}^L_{4\delta\varepsilon}(X')$ from Lemma 4.4.1.

Similarly, starting with $\mathcal{C}^L_{4\delta\varepsilon}(X')$ and composing maps from Lemma 4.4.1 and Lemma 4.2.7, respectively, we get the second simplicial map ϕ_2. The other map ϕ_3 is also obtained repeating the exact same argument for a different scale.

We first observe that the choice of simplicial maps in Lemma 4.4.1 and Lemma 4.2.7 makes $(\phi_2 \circ \phi_1)$ contiguous to the given natural inclusion j of $\mathcal{C}_\varepsilon(S)$ into $\mathcal{C}_{2\delta(4\delta+1)\varepsilon}(S)$. We now consider the following diagram:

$$\begin{array}{ccccccc}
\left|\mathcal{C}_\varepsilon(S)\right| & \xrightarrow{\phi_1} & \left|\mathcal{C}^L_{4\delta\varepsilon}(X')\right| & \xrightarrow{\phi_2} & \left|\mathcal{C}_{(4\delta+1)\varepsilon}(S)\right| & \xrightarrow{\phi_3} & \left|\mathcal{C}^L_{2\delta(4\delta+1)\varepsilon}(X')\right| \\
\uparrow{\scriptstyle h_1} & & \uparrow{\scriptstyle h_2} & & & & \uparrow{\scriptstyle h_3} \\
S^\varepsilon & \xleftarrow{\quad i \quad} & X & & \xleftarrow{\qquad\qquad Id \qquad\qquad} & & X
\end{array} \tag{4.3}$$

to show the diagram commutes, up to homotopy. We first explain the horizontal maps in the bottom row of (4.3). Since $d_H(X, S) < \varepsilon$, we get the first inclusion $X \subseteq S^\varepsilon$. The three vertical maps are homotopy equivalences that come from the Nerve Lemma (Lemma 2.4.1) for various good open covers as constructed in Lemma 4.4.4. The first vertical map h_1 is obtained for the open cover $\mathcal{U}_1 = \{\mathbb{B}(x, \varepsilon)\}_{x \in S}$ of S^ε by Euclidean balls. The other two vertical maps, h_2 and h_3, are corresponding to the (intrinsic) covers $\mathcal{U}_2$ and $\mathcal{U}_3$ of (X, d_L) by the intrinsic balls of radii $2\delta\varepsilon$ and $4\delta(2\delta+1)\varepsilon$ respectively. The assumption $4\delta(2\delta+1)\varepsilon < \rho$ implies that they are indeed good (intrinsic) covers of X. Therefore, by Lemma 4.2.5 we get the homotopy equivalences h_2 and h_3.

Apply Lemma 4.4.4 to each of the rectangles in the diagram (4.3) to show that the diagram is homotopy commutative, and therefore it commutes on the homology level. The commutativity would then imply that ϕ_1 induces a surjective homomorphism and ϕ_2 induces an injective homomorphism on the homology groups, implying $\mathrm{Im}(\phi_{2*} \circ \phi_{1*}) = \mathrm{Im}(\phi_{2*}) = H_k(X)$ on the k-th homology group. Also, we note that $\phi_2 \circ \phi_1$ is homotopic to the given simplicial inclusion j.

To see that the first rectangle commutes, we consider the covers $\boldsymbol{\mathcal{U}}_1$ and $\boldsymbol{\mathcal{U}}_2$ of S^ε and (X, d_L). Note that for any $x \in S$, the choice of $\xi(x)$ implies that $i^{-1}(\mathbb{B}(x,\varepsilon)) = \mathbb{B}(x,\varepsilon) \cap X \subseteq \mathbb{B}_L(\xi(x), 2\delta\varepsilon)$. Consequently, $\overline{\mathbb{B}(x,\varepsilon)} \cap X \subseteq \mathbb{B}_L(\xi(x), 4\delta\varepsilon)$. A similar argument also applies to the other rectangle. Therefore by Lemma 4.4.4, the diagram (4.3) commutes. □

4.5 Discussions

We remark that Theorem 4.3.4 and Theorem 4.4.5 can be formulated in terms of any natural functor

$$\mathcal{F} : \mathbf{Top} \longrightarrow \mathbf{Grp}.$$

In particular, the results extend immediately to homology groups $H_*(\,\cdot\,; G)$ with coefficients in any abelian group G, or homotopy groups $\pi_*(\,\cdot\,)$.

The difference between a simpleton and an intelligent man, according to the man who is convinced that he is of the latter category, is that the former wholeheartedly accepts all things that he sees and hears while the latter never admits anything except after a most searching scrutiny. He imagines his intelligence to be a sieve of closely woven mesh through which nothing but the finest can pass.

—R. K. Narayan

Chapter 5

Reconstruction of Metric Graphs

We have the duty of formulating, of summarizing, and of communicating our conclusions, in intelligible form, in recognition of the right of other free minds to utilize them in making their own decisions.
—Sir R. A. Fisher

In Chapter 4, we used filtrations of both the Čech and the Vietoris-Rips complexes to compute the homology and homotopy groups of our hidden geodesic subspace X from a noisy sample S around it. The results fail, however, to produce a topological space that faithfully carries the topological features of X. To remedy this, we consider the problem of geometric reconstruction of geodesic subspaces of $\mathbb{R}^N$. In Section 5.2, we introduce a new metric d_ε on S. We then show in Theorem 5.2.3 that the Vietoris-Rips complex of (S, d_ε) and X have isomorphic fundamental groups. In Section 5.3, we further use this complex for the geometric reconstruction of embedded graphs. Finally, in Section 5.4, we conclude our investigation of metric graphs with a probabilistic analysis under random sampling. We estimate the smallest sample size needed to guarantee a given probability of reconstruction.

5.1 Introduction

In the last decade, both abstract and embedded metric graphs are considered for reconstruction; see [10–12]. In [11], the authors consider an abstract metric graph and a sample that is close to it under the Gromov-Hausdorff metric (Definition 7.2.2), and reconstruct the structure of the metric graph along with the metric on it. In a more recent work [12], the authors show a statistical treatment of metric

graph reconstruction. They consider an embedded metric graph and a Euclidean sample around it. The Gromov-Hausdorff proximity used in [11] is replaced by the density assumption. The algorithm presented in [11] only reconstructs the connectivity of the vertices of the underlying metric graph and outputs an isomorphic pseudo-graph.

And lastly, we mention in [10, Lemma 6.1], where the first Betti number of an abstract metric graph is computed by considering the persistent cycles in the Vietoris-Rips complexes of a sample that is very close to it, with respect to the Gromov-Hausdorff distance. In Gromov-Hausdorff type reconstruction schemes, a small Gromov-Hausdorff distance between the graph and the sample guarantees a successful reconstruction. These methods are not a good choice when embedded graphs in $\mathbb{R}^N$ are considered. Also, none of the above-mentioned works give a geometrically close embedding for the reconstruction. Whereas our technique, presented in Section 5.3, can successfully reconstruct embedded graphs from a Hausdorff-close sample.

5.2 Recovery of Fundamental Group

For any fixed $\varepsilon > 0$, we first consider the Euclidean Vietoris-Rips complex $\boldsymbol{\mathcal{R}}_\varepsilon(S)$ on the sample S. In general, $\boldsymbol{\mathcal{R}}_\varepsilon(S)$ is not guaranteed to be homotopy equivalent to X; as shown in Figure 5.1. This is not surprising, because the Euclidean metric on S, used to compute the complex, can be very different from the length metric d_L on X. Our goal is to approximate d_L by the shortest path metric, denoted d_ε, on the one-skeleton of $\boldsymbol{\mathcal{R}}_\varepsilon(S)$. Let us denote the one-skeleton of $\boldsymbol{\mathcal{R}}_\varepsilon(S)$ by G_ε. Since $\boldsymbol{\mathcal{R}}_\varepsilon(S)$ is an abstract simplicial complex, G_ε inherits the structure of an abstract graph. However, we turn its underlying topological space $\left|G_\varepsilon\right|$ into a metric graph by defining the metric d_ε in the following way: the metric, when restricted to an edge (s,t), is isometric to a real interval of length $\|s-t\|$.

We show in Lemma 5.2.1 that d_ε approximates the metric d_L, which the Euclidean sample is oblivious to. For any positive scale α, we denote the Vietoris-Rips complex of S in the d_ε metric by $\boldsymbol{\mathcal{R}}^\varepsilon_\alpha(S)$. The following lemma helps us to compare the metric d_ε with the standard Euclidean metric $\|\cdot\|$ and the length metric d_L in Lemma 5.2.2.

Lemma 5.2.1 (Minimal Covering of Paths)**.** *Let X be a geodesic subspace of $\mathbb{R}^N$. Let $S \subseteq \mathbb{R}^N$ and $\varepsilon > 0$ such that $d_H(X,S) < \frac{\varepsilon}{3}$. For any path γ joining any two points $x, y \in X$, we can find a sequence $\{a_i\}_{i=0}^k \subseteq S$ with $\|a_{i+1} - a_i\| < \varepsilon$ such that*

$$\sum_{i=0}^{k-1} \|a_{i+1} - a_i\| < 3l(\gamma).$$

Moreover, a_0 and a_k can be chosen to be any points with $\|x - a_0\| < \frac{\varepsilon}{3}$ and $\|y - a_K\| < \frac{\varepsilon}{3}$.

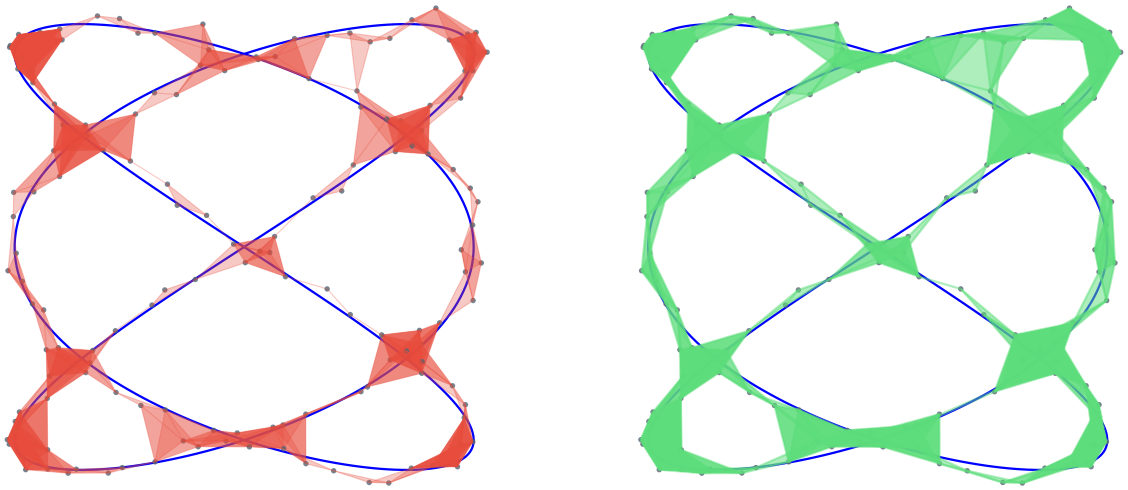

Figure 5.1: We implement Algorithm 1 on a Lissajous G with $\beta_1(G) = 8$. On the left, the Euclidean Vietoris-Rips complex $\mathcal{R}_\varepsilon(S)$ (in red) at a scale $\varepsilon = 65$ on a dense sample S of size 150 fails to capture the homotopy type, as its $\beta_1 = 9$. On the right, the shadow $\widetilde{G}$ (green) of $\mathcal{R}^{\varepsilon}_{5\delta\varepsilon}(S)$ is shown to correctly reconstruct G. The pictures were generated using the shape reconstruction webapp available on www.smajhi.com/shape-reconstruction.

Proof. Since $d_H(X,S) < \frac{\varepsilon}{3}$, there exists $a_0 \in S$ such that $\|x - a_0\| < \frac{\varepsilon}{3}$. We now iteratively define the sequence $\{a_i\} \subseteq S$, along with a sequence $\{t_i\}_0^k \subset [0,1]$ that defines a partition of $[0,1]$. We set $t_0 = 0$. Assuming both a_i and t_i are defined, we define $t_{i+1} \in [0,1]$ in the following way: if $\gamma([t_i,1]) \cap \partial\mathbb{B}_{\frac{2\varepsilon}{3}}(a_i) \neq \emptyset$, we set

$$t_{i+1} = \min\{t \in [t_i,1] \mid \gamma(t) \in \partial\mathbb{B}_{\frac{2\varepsilon}{3}}(a_i)\}.$$

Otherwise, if $\gamma([t_i,1]) \cap \partial\mathbb{B}_{\frac{2\varepsilon}{3}}(a_i) = \emptyset$, set $t_{i+1} = 1$. Since $d_H(S,X) < \frac{\varepsilon}{3}$, we set $a_{i+1} \in S$ to be a point in S such that $\|\gamma(t_{i+1}) - a_{i+1}\| < \frac{\varepsilon}{3}$. The procedure forces t_{i+1} to be strictly greater than t_i, hence $\{t_i\}$ defines a partition of $[0,1]$. Therefore,

$$l(\gamma) = \sum_{i=0}^{k} l(\gamma|_{[t_i,t_{i+1}]}) \geq \sum_{i=0}^{k} \|\gamma(t_i) - \gamma(t_{i+1})\| \geq \sum_{i=0}^{k} \frac{\varepsilon}{3} \geq \frac{1}{3}\sum_{i=0}^{k} \|a_{i+1} - a_i\|.$$

We also note that

$$0 < \|a_{i+1} - a_i\| \leq \|a_{i+1} - \gamma(t_{i+1})\| + \|\gamma(t_{i+1}) - a_i\| < \frac{\varepsilon}{3} + \frac{2\varepsilon}{3} = \varepsilon.$$

□

Analogous to Lemma 4.2.7, we get the following useful simplicial maps.

Lemma 5.2.2 (Vietoris-Rips Inclusion by d_ε). *Let X be a geodesic subspace $X \subseteq \mathbb{R}^N$. Let $S \subseteq \mathbb{R}^N$ and $\varepsilon > 0$ be such that $d_H(X,S) < \frac{\varepsilon}{3}$. For any $\alpha > 0$,*

(i) there exists a natural simplicial inclusion

$$\mathcal{R}^{\varepsilon}_{\alpha}(S) \hookrightarrow \mathcal{R}_{\alpha}(S).$$

(ii) there exists a simplicial map

$$\xi : \mathcal{R}^{L}_{\alpha}(X) \longrightarrow \mathcal{R}^{\varepsilon}_{3\alpha}(S)$$

induced by the vertex map ξ, that sends a vertex $x \in X$ to $s \in S$ such that $\|x-s\| < \frac{\varepsilon}{3}$.

Proof of (i). follows immediately from the definition of the metric d_ε. □

Proof of (ii). By Lemma 4.2.7, there is a vertex map $\xi : X \to S$ such that for each $x \in X$ we have $\|x - \xi(x)\| < \frac{\varepsilon}{3}$.

We show that the map extends to a simplicial map. Let $\sigma = \{x_0, x_1, \cdots, x_k\}$ be a k-simplex of $\mathcal{R}^{L}_{\alpha}(X)$. Then, $d_L(x_i, x_j) \leq \alpha$ for all i, j. Now by Lemma 5.2.1, there exists a path joining $\xi(x_i)$ and $\xi(x_j)$ in G_ε, moreover $d_\varepsilon(\xi(x_i), \xi(x_j)) < 3\alpha$. So, $\xi(\sigma)$ is a simplex of $\mathcal{R}^{\varepsilon}_{3\alpha}(S)$. Hence, the vertex map extends to a simplicial map. □

We now show that the fundamental group of the Vietoris-Rips complex on S under the metric d_ε is isomorphic to that of X. We tolerate the sloppiness from ignoring the basepoint.

Theorem 5.2.3 (Fundamental Group)**.** *Let X be a connected geodesic subspace of $\mathbb{R}^N$ with a positive convexity radius ρ and a finite distortion δ. Let $S \subseteq \mathbb{R}^N$ and $\varepsilon > 0$ be such that $d_H(X, S) < \frac{\varepsilon}{3} < \frac{\rho}{\delta(15\delta+2)}$. Then, the fundamental group of $\mathcal{R}^{\varepsilon}_{5\varepsilon\delta}(S)$ is isomorphic to the fundamental group of X.*

Proof. We derive the following chain of simplicial maps:

$$\mathcal{R}_\varepsilon(S) \xrightarrow{\phi_1} \mathcal{R}^{L}_{\frac{5\varepsilon\delta}{3}}(X) \xrightarrow{\phi_2} \mathcal{R}^{\varepsilon}_{5\delta\varepsilon}(S) \xhookrightarrow{\phi_3} \mathcal{R}_{5\delta\varepsilon}(S) \xrightarrow{\phi_4} \mathcal{R}^{L}_{\delta(15\delta+2)\varepsilon/3}(X).$$

The map ϕ_1 is the composition of the simplicial map $\mathcal{R}_\varepsilon(S) \longrightarrow \mathcal{R}_{\frac{5\varepsilon}{3}}(X)$ from Lemma 4.2.7 and the simplicial inclusion $\mathcal{R}_{\frac{5\varepsilon}{3}}(X) \hookrightarrow \mathcal{R}^{L}_{\frac{5\varepsilon\delta}{3}}(S)$ using Lemma 4.3.3 for $\alpha = \frac{5\varepsilon}{3}$, thanks to the assumption $d_H(S, X) < \frac{\varepsilon}{3}$. By a similar composition but at different scale of $5\delta\varepsilon$, we get ϕ_4. We also obtain ϕ_2 from Lemma 5.2.2 and ϕ_3 from Lemma 5.2.2.

We argue that ϕ_2 induces the desired isomorphism on the fundamental groups. Since $\varepsilon < \frac{\rho}{\delta(15\delta+2)}$, we have already seen in Theorem 4.3.4 that the simplicial map $\phi_4 \circ \phi_3 \circ \phi_2$ induces an isomorphism on all homotopy groups. Therefore, ϕ_2 induces an injective homomorphism on the homotopy groups, particularly the fundamental group of X.

We now show that the induced homomorphism is also surjective on the fundamental groups by showing that $\phi_2 \circ \phi_1$ induces a surjection. As observed in Theorem 4.3.4, it suffices to show the surjection for the the natural inclusion $i : \mathcal{R}_\varepsilon(S) \hookrightarrow \mathcal{R}^{\varepsilon}_{5\delta\varepsilon}(S)$, because i is contiguous to $\phi_2 \circ \phi_1$.

We start with a loop η in $\mathcal{R}^{\varepsilon}_{5\delta\varepsilon}(S)$. We can assume that η is made up of edges (one-simplices) of $\mathcal{R}^{\varepsilon}_{5\delta\varepsilon}$. Let us consider an edge $\sigma = \{a, b\}$ in η, then we have $d_\varepsilon(a, b) \leq 5\delta\varepsilon$. By the definition of d_ε, there must be a sequence of points $a = x_0, x_1, \cdots, x_k = b$ such that for each i, the segment $[x_i, x_{i+1}]$ is an edge of $\mathcal{R}_\varepsilon(S)$. Moreover, we observe for later that the diameter of the whole set $\{x_0, \cdots, x_k\}$ in the d_ε metric is not greater than $5\varepsilon\delta$.

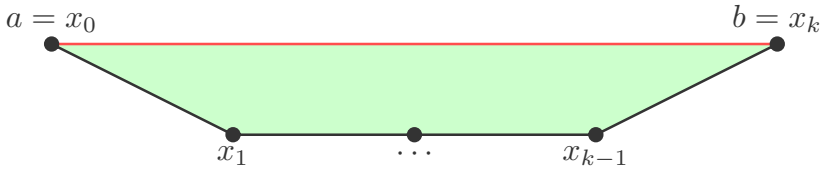

Figure 5.2: The red one-simplex $[a, b]$ of $\mathcal{R}^{\varepsilon}_{5\delta\varepsilon}(S)$ is shown to be pushed off to a path $a = x_0, x_1, \cdots, x_k = b$ in $\mathcal{R}_\varepsilon(S)$. All the nodes form a simplex (shown in green) in $\mathcal{R}^{\varepsilon}_{5\delta\varepsilon}(S)$.

Now, we define a loop η' in $\mathcal{R}_\varepsilon(S)$ by replacing each edge $[a, b]$ in η with the path joining the points in the sequence $a = x_0, x_1, \cdots, x_k = b$ consecutively, as shown in Figure 5.2. We note that η' is indeed a loop in $\mathcal{R}_\varepsilon(S)$. We now show that $(\phi_2 \circ \phi_1)(\eta')$ is homotopic to the loop η in $\mathcal{R}^{\varepsilon}_{5\delta\varepsilon}(S)$. As observed before, $\{a = x_0, \cdots, x_k = b\}$ is a simplex of $\mathcal{R}^{\varepsilon}_{5\delta\varepsilon}(S)$. We can then use a (piece-wise) straight line homotopy that maps each edge $[a, b]$ of η to the subpath $[a = x_0, x_1] \cup \cdots \cup [x_{k-1}, x_k = b]$ of η'. Hence, $[\eta']$ is, in fact, a pre-image of $[\eta]$. This shows, in turn, that ϕ_2 induces a surjective homomorphism on π_1. This completes the proof. □

5.3 Reconstruction Algorithm

We finally turn our attention to the geometric reconstruction of embedded graphs. We start with the formal definition of an embedded graph.

Definition 5.3.1 (Embedded Metric Graph)**.** An ***embedded metric graph*** G is a subset of $\mathbb{R}^N$ that is homeomorphic to a 1-dimensional simplicial complex, where the length metric d_L is the shortest path distance on G.

We simply call them embedded graphs. We also note that if G has finitely many vertices and b is the length of its shortest simple cycle, then the convexity radius ρ is $\frac{b}{4}$. In this paper, we always assume that G is a planar graph, i.e., $N = 2$ and it has finitely many vertices. We consider the *shadow* of the Vietoris-Rips complex $\mathcal{R}^{\varepsilon}_{\bullet}(S)$ considered in Section 5.2.

Definition 5.3.2 (Shadow of a Complex)**.** Let A be a subset of $\mathbb{R}^N$, and let $\mathcal{K}$ be an abstract simplicial complex whose vertex set is A. For each simplex $\sigma = \{x_1, x_2, \ldots, x_k\} \in \mathcal{K}$, we define its ***shadow***, denoted $\mathbf{Sh}(\sigma)$, as the convex-hull of the Euclidean point set $\{x_1, x_2, \ldots, x_k\}$. The shadow of $\mathcal{K}$ in $\mathbb{R}^N$, denoted by $\mathbf{Sh}(\mathcal{K})$, is the union of the shadows of all its simplices, i.e., $\mathbf{Sh}(\mathcal{K}) := \bigcup_{\sigma \in \mathcal{K}} \mathbf{Sh}(\sigma)$.

We, therefore, have the following natural projection map $p : \left|\mathcal{K}\right| \to \mathbf{Sh}(\mathcal{K})$. In general, $\mathbf{Sh}(\mathcal{K})$ may not have the same homotopy type as $|\mathcal{K}|$. However, as proved in [38], the fundamental group of the Vietoris-Rips complex of a planar point set is isomorphic to the fundamental group of its shadow. In [39], the authors further the understanding of shadows of Euclidean Rips complexes. In the case of planar graphs and $\mathcal{K} = \mathcal{R}^{\varepsilon}_{\bullet}(S)$, we prove a similar result now.

Lemma 5.3.3 (Shadow)**.** *Let G be a connected embedded graph with a positive convexity radius ρ and a finite distortion δ. Let $S \subseteq \mathbb{R}^2$ and $\varepsilon > 0$ be such that $d_H(G,S) < \frac{\varepsilon}{3} < \frac{\rho}{\delta(15\delta+2)}$. Then, the shadow projection $p : \left|\mathcal{R}^{\varepsilon}_{5\varepsilon\delta}(S)\right| \longrightarrow \mathbf{Sh}(\mathcal{R}^{\varepsilon}_{5\varepsilon\delta}(S))$ induces isomorphism on the fundamental groups.*

Proof. From Theorem 5.2.3, we have the following chain of simplicial maps:

$$\mathcal{R}_{\varepsilon}(S) \xrightarrow{\phi_1} \mathcal{R}^{L}_{5\varepsilon\delta/3}(G) \xrightarrow{\phi_2} \mathcal{R}^{\varepsilon}_{5\delta\varepsilon}(S) \xhookrightarrow{\phi_3} \mathcal{R}_{5\delta\varepsilon}(S) \xrightarrow{\phi_4} \mathcal{R}^{L}_{\delta(15\delta+2)\varepsilon/3}(G).$$

We have shown that ϕ_2 induces an isomorphism on π_1. As we have also noted that $(\phi_4 \circ \phi_3 \circ \phi_2)$ induces an isomorphism on all homotopy groups. So, we conclude first that ϕ_3 induces an injective homomorphism on π_1 .

Now, we consider the following commutative diagram:

$$\begin{array}{ccc} \mathcal{R}_{\varepsilon}(S) & \xhookrightarrow{i} & \mathcal{R}^{\varepsilon}_{5\delta\varepsilon}(S) \xhookrightarrow{\phi_3} \mathcal{R}_{5\delta\varepsilon}(S) \\ & & \downarrow p \qquad\qquad \downarrow \widetilde{p} \\ & & \mathbf{Sh}(\mathcal{R}^{\varepsilon}_{5\delta\varepsilon}(S)) \xhookrightarrow{j_2} \mathbf{Sh}(\mathcal{R}_{5\delta\varepsilon}(S)) \end{array} \tag{5.1}$$

where i is contiguous to the composition $(\phi_2 \circ \phi_1)$, and $p, \widetilde{p}$ are the natural (shadow) projections.

We show that the induced map p_* is an isomorphism on the fundamental groups. From the commutativity of the diagram (5.1), we note that p_* is an injection on π_1, since ϕ_{3*} is injective and $\widetilde{p}_*$ is also injective on π_1 by [38]. For surjectivity, we follow the same lifting argument presented in [38]. □

As a consequence of Lemma 5.3.3, we finally present our main geometric reconstruction result.

Theorem 5.3.4 (Geometric Reconstruction of Embedded Graphs)**.** *Let G be a connected embedded graph in $\mathbb{R}^2$. Let b be the length of the shortest simple cycle of G, and let δ be its distortion. Let $S \subseteq \mathbb{R}^2$ and $\varepsilon > 0$ be such that $d_H(G,S) < \frac{\varepsilon}{3} < \frac{b}{4\delta(15\delta+2)}$. Then, the shadow of $\mathcal{R}^{\varepsilon}_{5\varepsilon\delta}(S)$, denoted $\widetilde{G}$, has the same homotopy type as G. Moreover, we have*

$$d_H(G,\widetilde{G}) < \left(5\delta + \frac{1}{3}\right)\varepsilon.$$

Proof. As noted before, the convexity radius of G is $\frac{b}{4}$. Therefore by Lemma 5.3.3, the shadow $\widetilde{G}$ and G have isomorphic fundamental groups. Since the higher homotopy groups are trivial, we conclude that they are homotopy equivalent.

For the Hausdorff distance, we note that $\sigma \subseteq \mathbf{Sh}(\sigma)$ for any $\sigma \subseteq S$. So, $d_H(\sigma, \mathbf{Sh}(\sigma)) \leq diam(\sigma)$. As a consequence, $d_H(\widetilde{G}, S) \leq 5\delta\varepsilon$. By the triangle inequality, we then conclude the result. □

Based on Theorem 5.3.4, we devise the following algorithm for the geometric reconstruction of (planar) embedded graphs. For a demonstration, see Figure 5.1. The algorithm takes $O(k^3)$-time if the sample S has at most k points.

Algorithm 1 Graph Reconstruction Algorithm

Require: Finite sample $S \subseteq \mathbb{R}^2$, $\varepsilon > 0, \delta$, and b
Ensure: $d_H(G, S) < \frac{\varepsilon}{3} < \frac{b}{4\delta(15\delta+2)}$

```
Initialize G̃ ← ∅
Compute the one-skeleton of R_ε(S)
Compute (S, d_ε)
for all {a, b, c} ∈ S do
    if d_ε(a, b) < 5δε and d_ε(b, c) < 5δε and d_ε(c, a) < 5δε then
        G̃ ← G̃ ∪ CONVEX-HULL({a, b, c})
    end if
end for
return G̃
```

5.4 Random Sampling and Length Estimate

We now consider a finite sample $S = \{x_1, \ldots, x_n\}$ that is sampled at random from G. Our reconstruction results in Theorem 4.4.5, Theorem 4.3.4 have the primary assumption that the Euclidean thickening of S covers the graph G. A randomly drawn sample may fail to meet such a condition. However, given the chance of covering—we estimate a lower bound on the sample size. We first need the following lemma from [5]:

Lemma 5.4.1. *Let $\{A_i\}$ for $i = 1, \ldots, l$ be a finite collection of measurable sets and let μ be a probability measure on $\bigcup_{i=1}^{l} A_i$ such that for all $1 \leq i \leq l$, we have $\mu(A_i) > \alpha$. Let $S = \{x_i, \ldots, x_n\}$ be a set of n i.i.d. draws according to μ. Then if $n \geq \frac{1}{\alpha}\left(\log l + \log \frac{1}{\lambda}\right)$ we are guaranteed that with probability $> 1 - \lambda$, the following is true*

$$S \cap A_i \neq \emptyset \text{ for all } 1 \leq i \leq l.$$

For a positive number ε, suppose we cover G by Euclidean ε-balls. Let $\{y_1, \ldots, y_l\}$ be the set of points on G such that balls $\mathbb{B}(y_i, \varepsilon)$ form minimal cover of G. Here l is the *ε-covering number* $C(\varepsilon)$ of G. Also, the ε-packing number $P(\varepsilon)$ is the maximum number of non-overlapping sets of the form $(\mathbb{B}(x, r) \cap G)$ that can be packed inside G. The following inequality have been shown in [5].

$$P(2\varepsilon) \leq C(2\varepsilon) \leq P(\varepsilon)$$

Before we prove the final theorem of this section, we show a technical result in the following lemma.

Lemma 5.4.2 (Length Estimate)**.** *If* $p \in G$ *and* $0 < \varepsilon < \frac{b}{2\delta}$. *Then* $l(N) \geq \varepsilon$, *where* $N = G \cap \mathbb{B}(p, \varepsilon)$ *and* b *is the length of the shortest edge of* G.

Proof. Let p lies on an edge e of G and the endpoints of e are v_1 and v_2. We claim that e intersects the boundary of $\mathbb{B}(p, \varepsilon)$. If we assume the contrary, then the entire edge e must lie inside N. This implies that $d_L(v_1, v_2) \leq \delta\|v_1 - v_2\| \leq \delta(2\varepsilon) < b$, i.e., the length of the edge e is smaller than b, which is a contradiction. Therefore, there is a point $q \in e$ such that $\|p - q\| = \varepsilon$ and the segment γ of e joining p to q lies inside N. Since $l(\gamma) \geq \|p - q\| = \varepsilon$, we have $l(N) \geq \varepsilon$. □

Now, we present the final result of this section.

Theorem 5.4.3 (Random Sampling for Graph)**.** *Let* $0 < \varepsilon < \frac{b}{2\delta}$ *and* $S = \{x_1, \ldots, x_n\} \subseteq G$ *be a set of* n *i.i.d. draws according to the uniform probability measure on* G. *If*

$$n \geq \frac{2\, l(G)}{\varepsilon}\left(\log \frac{4\, l(G)}{\varepsilon} + \log \frac{1}{\lambda}\right),$$

with a probability $> (1 - \lambda)$ *we have that* $G \subseteq S^{\varepsilon}$. *Here* $l(G)$ *denotes the total length of the graph* G.

Proof. Consider $A = \{y_1, \ldots, y_l\} \subseteq G$ such that the Euclidean $\frac{\varepsilon}{2}$-balls around A form a minimal cover of G. We choose $A_i = \mathbb{B}(y_i, \frac{\varepsilon}{2}) \cap G$ in order to apply Lemma 5.4.1 in our setting. As shown in Lemma 5.4.2, $l(A_i) \geq \frac{\varepsilon}{2}$. So, we can choose $\alpha = \frac{\varepsilon}{2l(G)}$.

To estimate the $\frac{\varepsilon}{2}$-covering number l, we use the inequality $P(2\varepsilon) \leq C(2\varepsilon) \leq P(\varepsilon)$, to conclude $l \leq P(\frac{\varepsilon}{4})$. On the other hand, as the packing number is realized by non-overlapping sets of vol at least $\frac{\varepsilon}{4}$, we have

$$l(G) \geq \sum_{P(\frac{\varepsilon}{4})} (\frac{\varepsilon}{4})$$

to get $l \leq P(\frac{\varepsilon}{4}) \leq \frac{4\, l(G)}{\varepsilon}$. Using this lower bound on l in Lemma 5.4.1, we conclude the result. □

5.5 Discussions

In this work, we successfully reconstruct the topology of general geodesic spaces. We also reconstruct the geometry of an embedded graph. Currently, the output of such geometric reconstruction is a thick region around the hidden graph; see Figure 5.1. One can consider a post-processing step to prune the output shadow $\widetilde{G}$ in order to output an embedded graph that is isomorphic to the hidden graph G. A natural extension of our work is to consider the geometric reconstruction of higher-dimensional simplicial complexes. Unlike the graphs, such a space may have non-trivial homotopy groups. We have seen that the output of Algorithm 1 computes the fundamental group correctly. However, it is not clear whether the higher homotopy groups of the output are also isomorphic to the respective homotopy groups of the underlying space.

We know what we are, but know not what we may be.
—William Shakespeare, *Hamlet*

Chapter 6

Discrete Morse Theory in Graph Reconstruction

Religion is a luxury, which India, in its present condition, cannot possibly afford. India will never be free until the Hindus and Moslems are as rabidly enthusiastic about their religion as we are about the Church of England. If I were an Indian millionaire, I would leave all my money for the endowment of an Atheist mission.

—Aldous Huxley, *Benares*

In our investigation into geodesic shape reconstruction so far, we have studied the topological reconstruction of geodesic subspaces in Chapter 4, with a full geometric reconstruction of metric graphs in Chapter 5. We have been successfully forging ideas from metric geometry with topological tools—like Vietoris-Rips Complexes, Nerve Lemma, etc—to develop provable shape reconstruction techniques. Maintaining the same spirit, we now consider a discrete Morse theoretic approach to the geometric reconstruction of metric graphs.

Road-networks or maps are modeled as embedded metric graphs. And, a great amount of spatial GPS data is publicly available for analysis. Graph reconstruction from noisy samples has been studied extensively in the last decade; see e.g., [10–12, 15, 40–42]. Although many map construction algorithms work well in practice, most of them suffer from the lack of theoretical guarantees. Along with reconstruction guarantees, providing good embedding is also desired.

One can typically classify noise models for reconstruction problems into two categories: Hausdorff noise and non-Hausdorff noise. The sample S may not lie exactly on the metric graph G of interest, however S is sampled from a very small offset

of G. In this case, the Hausdorff distance between the sample and ground truth is assumed to be very small. We call such a noise *Hausdorff* noise. The situation becomes different in the presence of outliers in S. If outliers in S are far away from G, they contribute to an uncontrollably large Hausdorff distance. We study how discrete Morse theory can lend itself to developing an efficient algorithm for the geometric reconstruction of Euclidean graphs under *non-Hausdorff* type noise.

In Section 6.1, following the general motivation, we briefly discuss the density-based approach to graph reconstruction. Then, we give a brief introduction to discrete Morse theory in Section 6.2, along with its connection to persistent homology. Section 6.3 presents our proposed noise model and our reconstruction algorithm.

6.1 Motivation

We assume that the hidden graph G is contained in a planar, rectangular grid Ω of pixels in the plane. In the density-based reconstruction approach, a density function $\rho : \Omega \to \mathbb{R}$ is first computed from the (finite) sample $S \subset \Omega$. One can define ρ on the planar grid in several ways. A *histogram computation* or a *kernel density estimation (KDE)* ([43]) are usually very popular and easy to implement in practice. Then, an appropriate threshold is chosen to get a thickened graph as the super-level set of the density at the threshold. Some algorithms work by choosing this threshold empirically, whereas others, e.g., [42], use systematic topological techniques to choose a set of thresholds just big enough to capture the desired topological changes in the sub-level set filtration dictated by the density function. While most of the previous approaches gained success in practice, not much has been proved theoretically to guarantee the desired topological or geometric correctness.

Our work is inspired by the recent development by Dey et al. [15]. The authors use discrete Morse theory to extract the cycles of the underlying graph G from a density function. They show that if the density function satisfies a noise model, which the authors call an (ω, β, ν)-approximation, then the output $\widehat{G}$ of their algorithm has the same homotopy type as G. However, the noise model is too simplistic to locate the branchings of G. Also, the results of [15] fail to capture the leaves or the "hairs" of G, resulting in a large Hausdorff distance between $\widehat{G}$ and G.

In order to overcome the above-mentioned limitations of the algorithm developed in [15], we propose a two-threshold based noise model for the density function that is more practical and that can localize all vertices of G. Using different thresholds for the graph vertices and the graph edges, we develop a more efficient algorithm (Algorithm 2) that can output a reconstruction that is also geometrically very close to G. We prove in Theorem 6.3.1 that the output of our algorithm successfully captures both the topology and geometry of the underlying graph G.

6.2 Discrete Morse Theory

Morse theory—in its original form—was first introduced by Marston Morse ([44]). The *smooth* Morse theory analyzes the topology of smooth manifolds through the lens of well-behaved, real-valued smooth functions on the manifold, called *Morse functions*. Each Morse function gives rise to a CW-complex that has the same homotopy type as the manifold, whose cells are in one-to-one correspondence with the critical points of the function. Morse inequalities (strong and weak) and Morse-Smale complex are just two among many other far-reaching and important consequences of the theory. We encourage an interested reader to follow [44, 45] for a more detailed treatment on the subject.

In many applied fields, like TDA, the topology of a simplicial complex also needs to be analyzed. Robin Forman's discrete Morse theory ([16]) has successfully brought (smooth) Morse theory into the combinatorial world of simplicial complexes and simplex-wise maps. Discrete Morse theory has recently been gaining popularity in data science. Areas of successful application include simplification of persistent homology computation [46], de-noising point-clouds [47], grey-scale image analysis [48, 49], and graph reconstruction [15]. We adapt discrete Morse theory to our setup and leverage Morse cancellation, stable and unstable manifolds to aid the extraction of features of a (hidden) metric graph from a finite sample.

We touch upon the basic definitions and relevant results from discrete Morse theory. We refer the readers to [16, 45, 50] for an in-depth introduction to the elegant subject. We start with the definition of a discrete Morse function.

Definition 6.2.1 (Forman's Discrete Morse Function [50])**.** Let $\mathcal{K}$ be a simplicial complex. A simplex-wise function $\rho : \mathcal{K} \to \mathbb{R}$ is called a *discrete Morse function* on $\mathcal{K}$ if, for every p-simplex $\sigma^{(p)}$ in $\mathcal{K}$, we have

$$\left|\left\{\tau^{(p-1)} < \sigma^{(p)} : f(\tau) \geq f(\sigma)\right\}\right| \leq 1, \text{ and}$$

$$\left|\left\{\tau^{(p+1)} > \sigma^{(p)} : f(\tau) \leq f(\sigma)\right\}\right| \leq 1.$$

The above definition takes a while to grasp. The basic idea is the faces of a simplex must be assigned *strictly* greater values by ρ, with at most one exception. Likewise, the co-faces of a simplex must be assigned *strictly* smaller values, with at most one exception. So, each simplex of $\mathcal{K}$ is allowed at most one exception at all. See Figure 6.1 for an example.

A curious reader might wonder: does there always exist a discrete Morse function on a given complex $\mathcal{K}$? And, the answer is yes—one can take $f\left(\sigma^{(p)}\right) := p$. The function, however, is not a very good discrete Morse function because it has *many* critical simplices.

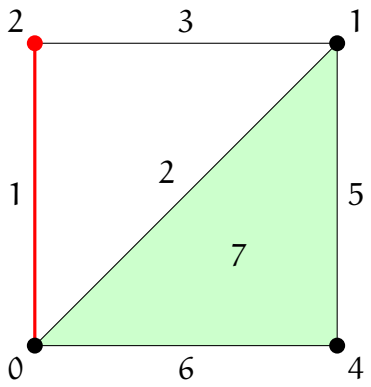

Figure 6.1: The simplicial complex $\mathcal{K}$ consists of four vertices, five edges, and a (green) triangle. The values assumed by the simplex-wise function f are shown by the simplices. The thick, red edge has an exception, the red vertex. Consequently, the red vertex has an exception, the red edge. Therefore, f is a valid discrete Morse function on $\mathcal{K}$.

Definition 6.2.2 (Critical Simplex)**.** Let $\mathcal{K}$ be a simplicial complex and $f : \mathcal{K} \to \mathbb{R}$ be a discrete Morse function. A simplex $\sigma^{(p)}$ in $\mathcal{K}$ is called a *critical simplex* if

$$\left|\left\{\tau^{(p-1)} < \sigma : f(\tau) \geq f(\sigma)\right\}\right| = 0$$

and

$$\left|\left\{\tau^{(p+1)} > \sigma : f(\tau) \leq f(\sigma)\right\}\right| = 0.$$

The critical simplices are simplices with *no* exceptions. A simplex is called *regular* if it is not critical. In Figure 6.1, the red edge and the red vertex are regular, and all other simplices are critical.

Definition 6.2.3 (Discrete Vector Field)**.** Let $\mathcal{K}$ be a simplicial complex. A *discrete vector field* V on $\mathcal{K}$ is a collection of pairs $\left(\sigma^{(p)}, \tau^{(p+1)}\right)$ of simplices of $\mathcal{K}$ such that $\sigma^{(p)} < \tau^{(p+1)}$, and each simplex of $\mathcal{K}$ appears in at most one of such pairs.

A pair $\left(\sigma^{(p)}, \tau^{(p+1)}\right) \in V$ is also called and visualized by an *arrow*, of which σ and τ are the *tail* and the *head*, respectively; see Figure 6.2. A simplex is called critical if it does not appear in any of the pairs of V.

Definition 6.2.4 (Induced Gradient Vector Field)**.** Let f be a discrete Morse function on a simplicial complex $\mathcal{K}$. The *induced gradient vector field* V_f is defined as follows:

$$V_f = \left\{(\sigma^{(p)}, \tau^{(p+1)}) : \sigma < \tau, f(\sigma) \geq f(\tau)\right\}.$$

With the definition of a discrete vector field under our belts, we now define the concept of a V-path.

Definition 6.2.5 (V-path)**.** Let V be a discrete vector field on a simplicial complex $\mathcal{K}$. A *V-path* or *gradient* path is a sequence of simplices

$$\tau_0^{(p)}, \sigma_0^{(p+1)}, \tau_1^{(p)}, \sigma_1^{(p+1)}, \ldots, \sigma_r^{(p+1)}, \tau_{r+1}^{(p)},$$

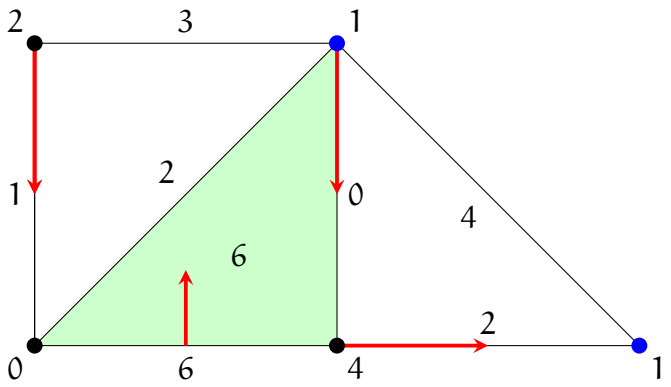

Figure 6.2: The simplicial complex $\mathcal{K}$ consists of five vertices, seven edges, and a (green) triangle. The discrete vector field V has four (red) arrows or pairs of simplices. Also, the values of a discrete Morse function $f : \mathcal{K} \to \mathbb{R}$ are shown so that V_f is the induced gradient vector field of f. Note the V-path that starts at the top blue vertex and ends at the bottom blue vertex.

where $r > 0$, $\left(\tau_i^{(p)}, \sigma_i^{(p+1)}\right) \in V$ and $\tau_{i+1}^{(p)} < \sigma_i^{(p+1)}$ for all $i \in \{0, \ldots, r\}$.

We consider the example of Figure 6.2 to illustrate the concept.

We now define (discrete) Morse cancellation, which provides a systematic way to reduce the number of critical simplices in a gradient vector field.

Definition 6.2.6 (Morse Cancellation)**.** Let V be a gradient vector field on $\mathcal{K}$, and suppose that $\tau^{(p)}$ and $\sigma^{(p+1)}$ are two critical simplices such that there exists a unique V-path

$$\tau_0^{(p)}, \sigma_0^{(p+1)}, \tau_1^{(p)}, \sigma_1^{(p+1)}, \ldots, \sigma_r^{(p+1)}, \tau^{(p)}$$

with $\tau_0 < \sigma$. Define a new gradient vector field $\widehat{V}$ by reversing the arrows; see Figure 6.3.

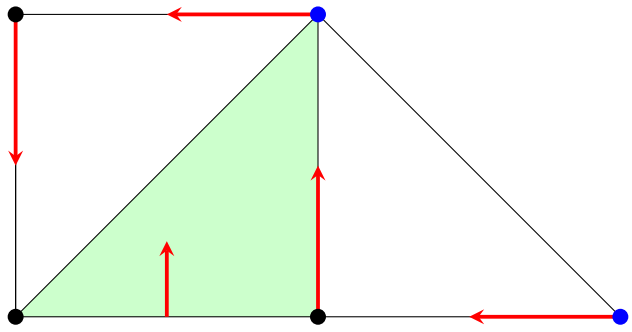

Figure 6.3: The effect of cancelling the V-path shown in Figure 6.2 is described. The new gradient field $\widehat{V}$ is shown by the red arrows. Note that $\widehat{V}$ has two fewer critical simplices!

Finally, for a critical simplex σ, we define its *stable manifold* to be the union of the V-paths that end at σ. Similarly, we define its *unstable manifold* to be the union of the V-paths that start at σ. For more details see [15, 16].

6.2.1 Persistence-Guided Morse Cancellation

In practical applications, we often consider an injective function $f : \mathcal{V}(\mathcal{K}) \to \mathbb{R}$ on the vertex set of $\mathcal{K}$. For any $\sigma \in \mathcal{K}$, we can extend the map to a simplex-wise map on $\mathcal{K}$ in the following way:

$$f(\sigma) := \max_{0 \le i \le p} \{f(v_i)\},$$

where $\sigma = \{v_0, v_1, \ldots, v_p\}$ is a p-simplex of $\mathcal{K}$.

The function f may not be a discrete Morse function. However, f is an example of a PL-function. One can define a *strict* total-ordering '$\prec$' of the simplices of $\mathcal{K}$ by using f and then the face relation '$<$' in case of a tie. A *lower-star filtration*

$$\emptyset = \mathcal{K}_0 \subseteq \mathcal{K}_1 \subseteq \ldots \subseteq \mathcal{K}_{k-1} \subseteq \mathcal{K}_k = \mathcal{K}$$

on $\mathcal{K}$ is defined by '$\prec$', where $k =$ the number of simplices in $\mathcal{K}$.

A popular strategy to remove topological features associated with the "noise" present in f is to consider a lower-star filtration ([15]), and let persistent homology ([51]) guide the Morse cancellations. We refer the readers to [15, 50, 52, 53] for more details. In our work, however, we use the style and notations of [15].

Suppose that we run persistence on a lower-star filtration, and denote by $P_f(\mathcal{K})$ the resulting persistence pairs. For a pair $(\sigma, \tau) \in P_f(\mathcal{K})$, its persistence $Pers(\sigma, \tau)$ is defined by $f(\tau) - f(\sigma)$. As a consequence of using a lower-star filtration, every simplex in $\mathcal{K}$ participates in a persistence pair.

6.3 Reconstruction Algorithm

We first discuss the noise model we propose for the density function ρ, then follows the analysis and proof of correctness of our algorithm (Algorithm 2). For ease of presentation, we define the noise model in the smooth set-up.

Let Ω be a planar rectangle, and let G be a finite embedded graph embedded inside Ω. Let ω be a small positive number such that G^ω, the ω-offset of G, is contained in Ω and has a deformation retraction onto G. For each vertex v of G, we call the ω-ball centered at v the *vertex region* of v. Now, let $\mathcal{V}^\omega$ be the union of all vertex regions of G.

We call a density function $\rho : \Omega \to \mathbb{R}$ an $(\omega, \beta_1, \beta_2, \nu)$-approximation of G if

$$\rho(x) \in \begin{cases} [\beta_1, \beta_1 + \nu], & \text{if } x \in \mathcal{V}^\omega \\ [\beta_2, \beta_2 + \nu], & \text{if } x \in G^\omega - \mathcal{V}^\omega \\ [0, \nu], & \text{otherwise} \end{cases}$$

where $\beta_1 > \beta_2 + 2\nu$, $\beta_2 > 2\nu$. In this case, we call β_1 and β_2 the thresholds for ρ. We assume our density function is an $(\omega, \beta_1, \beta_2, \nu)$-approximation. In practice, these

Algorithm 2 Graph Reconstruction Algorithm

Require: The discretized domain $\mathcal{K}$, density function $\rho : \mathcal{K} \to \mathbb{R}$, and threshold δ
Ensure: The reconstructed graph $\widehat{G}$

```
Initialize V as the trivial vector field on K
Initialize Ĝ = ∅
Run zero-dimensional persistence to get the persistence pairs P(K)
for all (ν, e) ∈ P(K) with Pers(ν, e) < δ do
    Try to perform a Morse cancellation for the pair
    Update V
end for
for all (ν, e) ∈ P(K) with Pers(ν, e) ≥ δ do
    Ĝ = Ĝ ∪ {unstable manifold of e}
end for
return Ĝ
```

four parameters are unknown. However, in our algorithm, we use a cut-off δ such that $\nu < \delta < \min(\beta_2 - \nu, \beta_1 - \beta_2 - \nu)$ and is assumed to be known to us.

In order to reconstruct G, the density is expected to assume very large values inside G^{ω} relative to the outside region. Here, a small noise or perturbation ν has been assumed. The thresholds make this noise model close to real-world applications involving the extraction of road-networks from GPS trajectory data. Because points along trajectories make the density higher near the intersections than the edges, this noise model enables us to correctly reconstruct not only the topology but also the geometry of G as shown in Theorem 6.3.1.

6.3.1 Analysis of Algorithm

In light of our proposed noise model, we devise Algorithm 2 for the geometric reconstruction. We start with a discretization $\mathcal{K}$ of the planar rectangle Ω. For example, $\mathcal{K}$ can be a planar two-dimensional cubical complex. Let the density function $\rho : \mathcal{K} \to \mathbb{R}$ be an $(\omega, \beta_1, \beta_2, \nu)$-approximation and let cutoff $\nu < \delta < \min(\beta_2 - \nu, \beta_1 - \beta_2 - \nu)$. Our goal is to construct a discrete vector field V on $\mathcal{K}$ that is associated to a discrete Morse function that is much simpler than ρ. This way, we clean the density function from the noise administered by ν. We initialize V with the initial vector field $\mathcal{K}$ in which all simplices are critical. In order to remove non-genuine critical simplices, we run zero-dimensional persistence on a lower-star filtration of $\mathcal{K}$ defined by $f = -\rho$, and denote by $P(\mathcal{K})$ the persistence pairs. Then, for each (vertex-edge) persistence pair $(v, e) \in P(\mathcal{K})$ with persistence smaller than δ, we try to perform Morse cancellation of the Morse pair (σ, τ) to update V. After the cancellations are done, the output V is a cleaner discrete gradient field on $\mathcal{K}$. The resulting V only contains genuine critical points, i.e., for each graph vertex we have a critical vertex v of $\mathcal{K}$ in its vertex region and for each edge of G we have a critical edge e in V. All these critical vertices and edges will be contained

in G^ω. Moreover, these critical vertices and edges are characterized by their persistence being larger than δ. Therefore, to extract the edges of G we consider each edge of $\mathcal{K}$ with persistence $\geq \delta$ and compute their unstable manifolds. The union of their unstable manifolds is the reconstruction $\widehat{G}$.

We note that Algorithm 2 runs only zero-dimensional persistence. The algorithm presented in [15], however, uses both zero-dimensional and one-dimensional persistence computations. Therefore, our algorithm avoids the complexity of matrix multiplication, and runs only in $O(k \log k)$-time, where k is the total number of vertices and edges in the grid $\mathcal{K}$.

The two thresholds help us to localize the critical vertices of the discrete gradient field inside the vertex regions. The output $\widehat{G}$ has the same homotopy type as G as shown in the following theorem.

Theorem 6.3.1 (Graph Reconstruction)**.** *Let G be a connected, embedded planar graph contained in rectangular grid Ω, and let the simplicial complex $\mathcal{K}$ be a discretization of Ω. If $\rho : \mathcal{K} \to \mathbb{R}$ is an $(\omega, \beta_1, \beta_2, \nu)$-approximation of G, then the output $\widehat{G}$ of Algorithm 2 has the same homotopy type as G. Moreover, $d_H(G, \widehat{G}) \leq \omega$.*

Proof. We prove the homotopy type by showing that G and $\widehat{G}$ have the same first Betti numbers, as the homotopy type of a connected graph is completely characterized by its first Betti number.

After the termination of Algorithm 2, by the assumption on the density function, for each graph vertex v' of G, we have exactly one critical vertex v of $\mathcal{K}$ inside the vertex region of v'. This vertex v is the local maximum of ρ inside the vertex region of v'. For the persistence pairings in $P(\mathcal{K})$ with persistence larger than δ, a vertex v of $\mathcal{K}$ has to be paired with either $+\infty$ or with a critical edge e of $\mathcal{K}$ from the edge region of a graph edge e' of G. And, e' will be incident to v', as illustrated in Figure 6.4. Now, for each critical edge e of $\mathcal{K}$, e must lie inside one of the edge regions of G. Moreover, for each each e' of G we have exactly one critical edge e of $\mathcal{K}$. For the pairings of $P(\mathcal{K})$ with persistence larger than δ, each edge e is either paired with a vertex v from the vertex region of an incident edge or a triangle from the complement of G^ω.

The one-to-one correspondence of the edges of G and the critical edges of $\mathcal{K}$ and the vertices of G and the critical vertices of $\mathcal{K}$ in V, shows that the stable manifold of a critical edge e of $\mathcal{K}$ that lies in the edge region of a graph edge e' of G is a path in G^ω joining the critical vertices of the vertex regions of the end-points of e'. This concludes that $\widehat{G}$ and G have the same first Betti numbers. Also, since the critical vertices and edges are localized inside the corresponding regions we conclude that $d_H(G, \widehat{G}) < \omega$. □

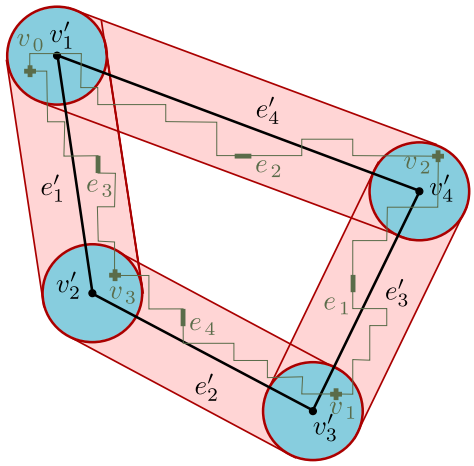

Figure 6.4: A graph G with vertex and edge regions. Critical edges and their stable manifolds are shown in green.

6.4 Discussions

With our proposed noise model, we have successfully recovered the topology and geometry of the underlying graph. Compared to [15], we improve the running-time by avoiding higher-dimensional persistence computations. In addition, our algorithm produces Hausdorff-close embedding under our noise model. For graphs, however, a better quality guarantee would be a small (edge-wise) Fréchet distance between the reconstruction and the ground truth. A better noise model that allows for such a guarantee can be a natural next step. Our reconstruction works for planar graphs, the question of higher-dimensional shape reconstruction using discrete Morse theory still remains open.

An eye for an eye only ends up making the whole world blind.
—M. K. Gandhi

Chapter 7

Computing Gromov-Hausdorff Distance in Euclidean Spaces

Most people believe the mind to be a mirror, more or less accurately reflecting the world outside them, not realizing on the contrary that the mind is itself the principal element of creation.

—Rabindranath Tagore

Thus far, our focus of exploration has been the reconstruction of shapes. We turn our attention, in this final chapter, to the comparison of shapes. As noted earlier, a reliable shape reconstruction technique is always complemented with good reconstruction guarantees. Topological invariants, such as Betti numbers, homotopy-type, persistence diagrams, etc, are some popular choices for such guarantees. In the area of metric shape reconstruction, Gromov-Hausdorff distance provides a natural framework for reconstruction guarantees: how much the reconstruction and the (hidden) shape of interest are *metrically-close*; see [10, 11, 28] for example.

As a robust framework for shape comparison and recognition ([13, 54]), we investigate the questions pertaining to the computation of the Gromov-Hausdorff distance, particularly between Euclidean subsets. Our work is primarily motivated by developing an efficient algorithm to compute Gromov-Hausdorff distance between compact sets $X, Y \subset \mathbb{R}^d$.

Section 7.1 presents our motivation and some major, related developments. We state the formal definition and some important properties of Gromov-Hausdorff distance in Section 7.2. We then bring our focus particularly onto Gromov-Hausdorff distance between Euclidean subsets. In Section 7.3, we introduce the concept of

Hausdorff distance under Euclidean isometries, discuss how it interplays with the Gromov-Hausdorff distance, and explore some of the nice structural properties of nearest neighbor correspondences (Definition 7.3.5). Finally, in Section 7.4, we dive deep into our approximation techniques for the efficient computation of the Gromov-Hausdorff distance on the real line.

7.1 Motivation

The Gromov-Hausdorff distance was first introduced by M. Gromov in ICM 1979 (see Berger [55]). The notion, although it emerged in the context of Riemannian metrics, proves to be a natural distance measure between any two metric spaces. Based on the notion of Hausdorff distance, the distance compares two metric spaces by quantifying how metrically similar they are. In the last decade, the concept surfaced its usefulness in shape matching and topological data analysis.

In shape recognition and comparison, shapes are regarded as metric spaces that are deformable under a class of transformations. Depending on the application in question, a suitable class of transformations is chosen, then the dissimilarity between the shapes are defined by a suitable notion of *distance measure* that is invariant under the desired class of transformations. For comparing Euclidean shapes under Euclidean isometry, the use of Gromov-Hausdorff distance is proposed and discussed in [13, 54, 56, 57].

7.1.1 Related Work

The concept of Gromov-Hausdorff distance has been spawning a multitude of research directions. Naturally, the scope of the topic has grown wide and vast—both in theory and applications alike. In this work, we investigation the challenges related to the efficient computation of the distance. We first briefly lay out some of the very interesting and pivotal developments addressing its computational aspects.

As we will see, a straight-forward computation of the Gromov-Hausdorff distance between two metric spaces containing at most k points takes $O(2^k)$-time. Except for a few extremely simple configurations with just a handful of points, a generic polynomial-time computational scheme is not yet known. The last decade stands witness to some major developments addressing the NP-hardness questions related to the computation of Gromov-Hausdorff distance.

For a minimization problem, like computing the Gromov-Hausdorff distance, the exact solution s_{opt} may be difficult to compute. In an attempt to solve such an optimization problem, an algorithm is sometimes devised to output an approximate solution s_{appx} instead. Such an algorithm is called an *approximation algorithm* with

an approximation factor $\rho > 1$ if $s_{opt} \leq s_{appx} \leq \rho s_{opt}$. The algorithm is also often called a ρ-approximation to the minimization problem.

We take this opportunity to quickly bring up another related and crucial concept from complexity theory: the notion of NP-hardness of a (discrete) problem. We spare the readers here of the mathematical definition of the NP-hard class of problems. Instead, we give here a brief and gentle overview. The class P is defined to be the collection of problems that are known to be solvable by an algorithm whose running time is polynomial in the input size. Some decision problems, however, may not be known to be solved in polynomial time, but checking whether a given solution does solve an instance of the problem can be done in polynomial time. This class is known as NP. It's believed by many computer scientists including myself, at least at the time of writing this thesis, that $P \subsetneq NP$. An NP-hard problem is defined to be at least as hard as any NP problem. An interested reader is referred to [58], one of the best references on such an intricate topic like complexity theory.

The authors of [59] show an NP-hardness result for approximating the Gromov-Hausdorff distance between metric trees. A *metric tree* is a metric space that has the topology of a contractible 1-dimensional simplicial complex. If X and Y are metric trees, [59] proves that it is NP-hard to approximate $d_{GH}(X, Y)$ by an approximation factor < 3. The authors use the distortion based definition (Lemma 7.2.5) of the Gromov-Hausdorff distance to establish their results.

For Euclidean subsets, the question of a polynomial-time algorithm is still vastly open. Although the distance measure puts Euclidean shape matching on a robust theoretical foundation [13, 54], the question of computing the Gromov-Hausdorff distance efficiently, or even an approximation thereof, still remains elusive. In [57], the author shows that computing the distance is related to various NP-hard problems and studies a variant of Gromov-Hausdorff distance.

As noted before, the computation of Gromov-Hausdorff distance leads to minimizing the *additive* distortion (Definition 7.2.4) over all correspondences between the sets. For completion, we mention here a parallel line of developments ([14, 58, 60]) related to minimum *multiplicative* distortion (see [60] for a definition) over the bijections between Euclidean subsets of the same cardinality. The authors of [58] prove the decision problem of finding a minimum (multiplicative) distortion bijection in three-dimensional Euclidean space is NP-hard. In [60], the authors present a polynomial-time algorithm to find the minimum distortion bijection between two subsets of the real line, provided that the sets have a distortion less than $5 + 2\sqrt{5}$. For large distortion in the real line, the distortion problem is still shown to be hard in [14].

The authors of [14] introduce the additive distortion—the one used in Gromov-Hausdorff distance—and demonstrate a polynomial-time 2-approximation algorithm for the real line case ($d = 1$). An open problem is also posed in [14]: are there

polynomial-time approximations to find the minimum bijective distortion withing a factor less than 2?

All these NP-hardness results provoke the natural curiosity about the computational hardness of Gromov-Hausdorff between Euclidean subsets. Let $d \geq 1$ and $X, Y \subseteq \mathbb{R}^d$ be compact sets, equipped with the standard Euclidean metric. Our knowledge of efficient computational schemes of $d_{GH}(X, Y)$ is still sufficiently scanty. We pose the following open questions:

(i) Is there an algorithm to compute $d_{GH}(X, Y)$ *exactly* in polynomial-time?

(ii) If not, can we find a polynomial-time approximation algorithm for $d_{GH}(X, Y)$, possibly with a reasonably small approximation factor?

(iii) If not, is it NP-hard to approximate $d_{GH}(X, Y)$, like the metric graph case?

The above questions set the pitch of our investigation into the computation of d_{GH} in Euclidean spaces.

7.2 Gromov-Hausdorff Distance and Distortion

The notion of Gromov-Hausdorff distance is closely related to the notion of Hausdorff distance (Definition 3.1.1). We follow Gromov's book([61]) to define the distance. The primary definition uses the concept of an isometry or distance-preserving map between metric spaces.

Definition 7.2.1 (Isometry)**.** A map $f : (X, d_X) \to (Y, d_Y)$ is called an *isometry* if

$$d_X(x_1, x_2) = d_Y(f(x_1), f(x_2)).$$

We immediately note that an isometry f is injective, and that $f : X \to f(X)$ is a homeomorphism.

We are now in a place to define the Gromov-Hausdorff distance formally. Unlike the Hausdorff distance, the Gromov-Hausdorff distance can be defined between two abstract metric spaces (X, d_X) and (Y, d_Y) that may not share a common ambient space. We start with the following formal definition:

Definition 7.2.2 (Gromov-Hausdorff Distance [61])**.** The ***Gromov-Hausdorff distance***, denoted $d_{GH}(X, Y)$, between two metric spaces (X, d_X) and (Y, d_Y) is defined to be

$$d_{GH}(X, Y) = \inf_{\substack{f:X\to Z \\ g:Y\to Z \\ Z}} d_H^Z(f(X), g(Y)),$$

where the infimum is taken over all isometries $f : X \to Z$, $g : Y \to Z$ and metric spaces (Z, d_Z).

The definition of Gromov-Hausdorff distance may not seem very natural at the first glance—it deserves a bit of explanation. As mentioned earlier, The definition works for abstract metric spaces X and Y, without requiring them to be embedded in a common ambient metric space. In order to anatomize Definition 7.2.2, we first observe that the maps f, g are embedding X and Y, respectively, into a common metric space (Z, d_Z). Since f, g are isometries, the subsets $f(X), g(Y)$ of Z are isometric to X and Y respectively. For the curious reader: such a Z, where both X, Y can be isometrically embedded, always exists; one can take $Z = X \sqcup Y$ for instance. As $f(X)$ and $g(Y)$ are subsets of Z, their Hausdorff distance $d_H^Z(f(X), g(Y))$ can now be considered. The Gromov-Hausdorff distance is defined to minimize (if minimum exists) this $d_H^Z(f(X), g(Y))$, subject to all isometries f, g and ambient metric space (Z, d_Z). As a consequence, Gromov-Hausdorff distance is a distance measure between abstract metric spaces X and Y that is also invariant under any isometric transformations of X or Y. A detour to [57, 61, 62] is suggested for a detailed treatment on the definitions and properties of Gromov-Hausdorff distance.

In order to present an equivalent definition of the Gromov-Hausdorff distance that is computationally viable, we first define the notion of a correspondence.

Definition 7.2.3 (Correspondence [36])**.** A ***correspondence*** $\mathcal{C}$ between any two (non-empty) sets X and Y is defined to be a subset $\mathcal{C} \subseteq X \times Y$ with the following two properties:

i) for any $x \in X$, there exists an $y \in Y$ such that $(x, y) \in \mathcal{C}$, and

ii) for any $y \in Y$, there exists a $x \in X$ such that $(x, y) \in \mathcal{C}$.

A correspondence $\mathcal{C}$ is a special *relation* that assigns all points of both X and Y a corresponding point. If the sets X and Y in the Definition 7.2.3 are equipped with metrics d_X and d_Y, respectively, we can also define the distortion of the correspondence $\mathcal{C}$.

Definition 7.2.4 ((Additive) Distortion of Correspondence)**.** Let $\mathcal{C}$ be a correspondence between two metric spaces (X, d_X) and (Y, d_Y), then its ***distortion***, denoted $\mathtt{Dist}(\mathcal{C})$, is defined to be

$$\sup_{(x_1,y_1),(x_2,y_2)\in\mathcal{C}} \left| d_X(x_1, x_2) - d_Y(y_1, y_2) \right|$$

The distortion $\mathtt{Dist}(\mathcal{C})$ is sometimes called the *additive* distortion as opposed to the *multiplicative* distortion; see [60] for a definition. For non-empty sets X, Y, we denote by $\mathcal{C}(X, Y)$ the set of all correspondences between X and Y. We note the following relation, which can be used to give an equivalent definition of the Gromov-Hausdorff distance via correspondences. For a proof of the following, the readers are encouraged to see [62].

Lemma 7.2.5. *For any two compact metric spaces (X, d_X) and (Y, d_Y), the following holds:*

$$d_{GH}(X, Y) = \frac{1}{2} \inf_{\mathcal{C}\in\mathcal{C}(X,Y)} \mathtt{Dist}(\mathcal{C}).$$

The combinatorial wrinkle in the alternative definition unveils the genuine complexity entailed in the computation of Gromov-Hausdorff distance. For two finite metric spaces X, Y containing at most n points, the computation takes $O(2^n)$-time by trying out all possible matchings between the points of X and Y.

7.3 Gromov-Hausdorff Distance in Euclidean Spaces

With the basic definitions now at our disposal, we make our readers acquainted with a related notion $d_{H,iso}(X, Y)$ here, and list a few of its relevant consequences. The notion was first introduced in [56]. In this section, we also introduce the concept of nearest neighbor correspondences, present some of its properties, then illuminate the trail that has led us to the pinnacle of our findings of Section 7.4.

7.3.1 Hausdorff Distance under Euclidean Isometry

For any dimension $d \geq 1$, a *Euclidean isometry* $T : \mathbb{R}^d \to \mathbb{R}^d$ is defined to be a map that preserves the distance, i.e.,

$$\left|T(x_1) - T(x_2)\right| = \left|x_1 - x_2\right| \text{ for all } x_1, x_2 \in \mathbb{R}^d.$$

When $d = 1$, the map T can only afford to be a translation or a reflection (flip). In $d = 2$, a Euclidean isometry is characterized by a combination of a translation, a rotation by an angle, and a mirror-reflection. For more about Euclidean isometries, see [63]. We denote by $\mathcal{E}(\mathbb{R}^d)$ the set of all isometries of $\mathbb{R}^d$.

Definition 7.3.1 (Hausdorff under Isometry)**.** For any two compact subsets X, Y of $\mathbb{R}^d$, we define

$$d_{H,iso}(X, Y) = \inf_{T \in \mathcal{E}(\mathbb{R}^d)} d_H(X, T(Y)).$$

We immediately note that $d_{H,iso}$ induces a pseudo-metric on the set of compact subsets of $\mathbb{R}^d$; $d_{H,iso}(X, Y) = 0 \implies X$ is *congruent* to Y.

Remarks 7.3.2. If X, Y are subsets of $\mathbb{R}^1$ with at most n point, the authors of [17] prove that the computation of $d_{H,iso}(X, Y)$ takes $O(n \log n)$.

The $d_{H,iso}(X, Y)$ minimizes the Hausdorff distance over only Euclidean isometries; whereas $d_{GH}(X, Y)$ considers minimizing over *all* isometries and *all* embeddings for X and Y—not just Euclidean. The observation quickly yields the following inequality:

$$d_{GH}(X, Y) \leq d_{H,iso}(X, Y).$$

It is most natural to wonder if they are, in fact, equal. To our disappointment, we can contrive the following configuration in $\mathbb{R}^2$ to show the contrary in Example 7.3.3.

Example 7.3.3 ($d_{GH} < d_{H,iso}$ in $\mathbb{R}^2$)**.** Let us consider two finite sets $X, Y \subset \mathbb{R}^2$ as shown in Figure 7.1. We take $X = \{x_1, x_2, x_3, x_4, x_5\}$, $Y = \{y_1, y_2, y_3, y_4, y_5\}$, and $x_1 = y_1$, $x_2 = y_2$. In a moment's reflection, we see that the blue edges give us the distortion-minimizing optimal correspondence:

$$\mathcal{C}_{opt} = \{(x_1, y_1), (x_2, y_2), (x_4, y_3), (x_5, y_3), (x_3, y_4), (x_3, y_5)\}.$$

with $\mathrm{dist}(\mathcal{C}_{opt}) = h+\varepsilon$. Consequently, $d_{GH}(X, Y) = \frac{h+\varepsilon}{2}$. On the other hand, $d_{H,iso}(X, Y) = h$.

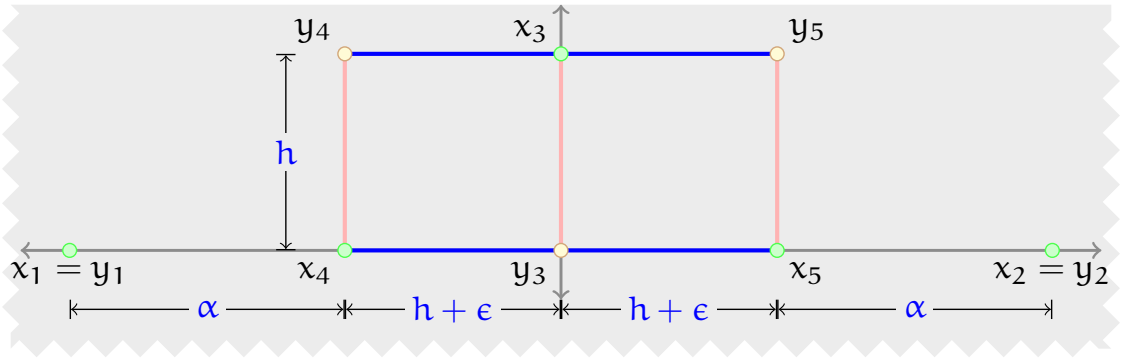

Figure 7.1: The points of X and Y are shown in green and yellow respectively. The optimal correspondence is shown by the blue edges and the nearest neighbor correspondence is shown by the red edges.

The authors show in [56] the following bounds, relating $d_{H,iso}$ and d_{GH} between two compact subsets X, Y of $\mathbb{R}^d$.

$$d_{GH}(X, Y) \leq d_{H,iso}(X, Y) \leq c'_d(M)^{\frac{1}{2}} \sqrt{d_{GH}(X, Y)}, \tag{7.1}$$

where $M = \max\{\mathrm{diameter}(X), \mathrm{diameter}(Y)\}$ and c'_d is a constant that depends only on the dimension d. In the inequality (7.1), note the upper bound depends on the diameter of the input sets X and Y. For $d \geq 2$, such a dependence is unavoidable. See Figure 7.1.

In dimension $d = 2$ and beyond, we just saw that there are examples where both the bounds shown in (7.1) are tight. This leaves us with $d = 1$, the compact subsets of the real line. For a long time, it was believed, by the deceptively simple structure of the real line, that $d_{GH} = d_{H,iso}$. If it was true, we could compute d_{GH} in near-linear time; see Remark 7.3.2. However, the following sophisticated construction shows that the conjecture is false.

Example 7.3.4 ($d_{GH} < d_{H,iso}$ in $\mathbb{R}^1$)**.** In this example, we show that for any given Gromov-Hausdorff distance $\delta > 0$, there exist $X, Y \subset \mathbb{R}^1$ such that $d_{H,iso}(X,Y) = \delta + \frac{\delta}{8}$. As a consequence, $d_{GH}(X,Y) < d_{H,iso}(X,Y)$.

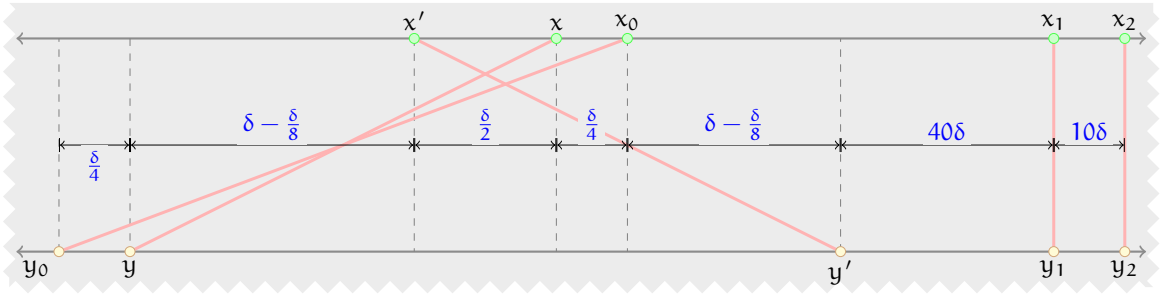

Figure 7.2: The points of X and Y are shown in green and yellow respectively. The optimal correspondence is shown by the red edges. The optimal correspondence is not crossing free.

The subsets X, Y are taken as shown in Figure 7.2. We note that $d_H(X,Y) = \delta + \frac{\delta}{8}$. Now, we claim that $d_{H,iso}(X,Y) = \delta + \frac{\delta}{8}$. For a proof of our claim, we present in Table 7.1 the summary of $d_H(X, Y + \Delta)$, which considers translations of Y by an amount $\Delta \in \mathbb{R}^1$. We also note that a translation of $-Y$ does not help to reduce the Hausdorff distance.

Δ	$\overrightarrow{d}_H(X, Y+\Delta)$	$\overrightarrow{d}_H(Y+\Delta, X)$	$d_H(X, Y+\Delta)$
$(-\infty, 0)$	–	(y_0, x')	$> \delta + \frac{\delta}{8}$
0	(x, y')	(y_0, x')	$\delta + \frac{\delta}{8}$
$(0, \frac{\delta}{8})$	–	$(y_k, x), (y_k, x_k)$	$\in (\delta + \frac{\delta}{8}, \delta + \frac{\delta}{4})$
$\frac{\delta}{8}$	$(x, y), (x, y')$	–	$\delta + \frac{\delta}{4}$
$(\frac{\delta}{8}, \frac{\delta}{4})$	(x, y)	–	$\delta + \frac{\delta}{8}$
$\frac{\delta}{4}$	(x, y)	(y', x_0)	$\delta + \frac{\delta}{8}$
$(\frac{\delta}{4}, \infty)$	–	(y', x_0)	$> \delta + \frac{\delta}{8}$

Table 7.1: A summary of $d_H(X, Y + \Delta)$ is recorded for $\Delta \in \mathbb{R}$. In the second and third columns, the directed Hausdorff distances are achieved for the shown pairs of points. The other columns are self-explanatory.

By our observation in the above example, we are intrigued by the quest of finding the tight upper bound for (7.1) in $\mathbb{R}^1$. A better and constant upper bound is presented in Section 7.4, along with the proof that the bound is tight.

7.3.2 Nearest Neighbor Correspondence

To conclude our discussion of this section, we lastly present our line of investigation into Hausdorff correspondences. As noted previously, in Example 7.3.3 and Example 7.3.4, $d_{GH}(X,Y) \neq d_{H,iso}(X,Y)$ in general. However, we take the analysis one step further, and ask in Theorem 7.3.7 if there exists an isometry T such that the Hausdorff correspondence between X and $T(Y)$ is an optimal correspondence that minimizes the distortion.

Among many possible correspondences, the following correspondence is particularly interesting when considered two Euclidean subsets.

Definition 7.3.5 (Nearest Neighbor Correspondence)**.** For any two compact subsets $X, Y \subseteq \mathbb{R}^N$, we define the ***nearest neighbor correspondence*** $\mathcal{C}_{NN}$ to be the relation defined the nearest neighbors of points of X and Y. More precisely,

$$\mathcal{C}_{NN} = \{(x,y) \in X \times Y \mid (x \text{ is a nearest neighbor of } y \text{ in } X) \\ \text{or } (y \text{ is a nearest neighbor of } x \text{ in } Y)\}.$$

Since X and Y are compact, the nearest neighbors exist. Hence, the induced relation is a correspondence. The following important structural property follows from the definition.

Lemma 7.3.6 (Crossing)**.** *For any two compact $X, Y \subset \mathbb{R}^1$, the nearest neighbor correspondence $\mathcal{C}_{NN}$ is free of crossings.*

Proof. Let us consider two edges $e = (x,y)$ and $e' = (x',y')$ in $\mathcal{C}_{NN}$ with $x < x'$. Without loss of generality, we assume that y is a nearest neighbor of x. In order to show that e cannot cross e', we assume the contrary: $y' < y$. Now, we consider the following cases based on the position of y with respect to x. In each case we show that neither y' is a nearest neighbor of y' nor x' is a nearest neighbor of x'.

Case 1 ($y \leq x$)**:** In this case, a nearest neighbor of x' cannot be smaller than y. Hence, y' cannot be its nearest neighbor. Also for $y' < y$, its nearest neighbor has to be also smaller than x, hence x' cannot be its nearest neighbor either.

Case 2 ($x < y$)**:** A nearest neighbor of x' cannot be smaller than y. Hence, y' cannot be its nearest neighbor. Since $y' < y$, we have $y' \leq x$ in this case. Therefore, a nearest neighbor y' has to be smaller than x. So, x' cannot be its nearest neighbor.

□

We wrap up this section with our final result of this section in the following theorem.

Theorem 7.3.7 (Crossing)**.** *For $d \geq 1$, there exist compact subsets $X, Y \subset \mathbb{R}^d$ such that $\mathcal{C}_{NN}$ between X and $T(Y)$ is not an optimal correspondence for any Euclidean isometry $T \in \mathcal{E}(\mathbb{R}^d)$.*

Proof. For $d \geq 2$, we refer the readers to Example 7.3.3. The optimal correspondence $\mathcal{C}_{\text{opt}}$ between X, Y is shown by the blue edges. And, the $\mathcal{C}_{\text{NN}}$ is shown by the red edges. We also note here that there does not exist any non-trivial Euclidean isometry T such that $\mathcal{C}_{\text{opt}}$ becomes the nearest neighbor correspondence.

In the case $d = 1$, we use X, Y from Example 7.3.4. The optimal correspondence $\mathcal{C}_{\text{opt}}$ is shown by the red edges. However, $\mathcal{C}_{\text{opt}}$ must have crossings—even when one considers the reflection of Y. By Lemma 7.3.6, $\mathcal{C}_{\text{opt}}$ cannot be produced by any nearest neighbor correspondence. □

7.4 Gromov-Hausdorff Distance in $\mathbb{R}^1$

This section is devoted to our main result (Theorem 7.4.3) on approximating the Gromov-Hausdorff distance between subsets of the real line. Unless stated otherwise, in this section, we assume that X, Y are compact subsets of $\mathbb{R}^1$, and both are equipped with the standard Euclidean metric denoted by $|\cdot|$.

In $\mathbb{R}^1$, we visualize $X \times Y$ on the disjoint union of two real lines in $\mathbb{R}^2$ and a correspondence $\mathcal{C} \in \mathcal{C}(X, Y)$ by edges between the corresponding points; see Figure 7.3. Such a two dimensional visualization comes in handy for the proofs.

Definition 7.4.1 (Crossing)**.** For a correspondence $\mathcal{C} \in \mathcal{C}(X, Y)$, we say a pair of edges $(x_1, y_1), (x_2, y_2) \in \mathcal{C}$ are ***crossing*** if they cross in the usual sense, i.e., either of the following happens $x_1 < x_2$ but $y_1 > y_2$ or $x_1 > x_2$ but $y_1 < y_2$; see Figure 7.3.

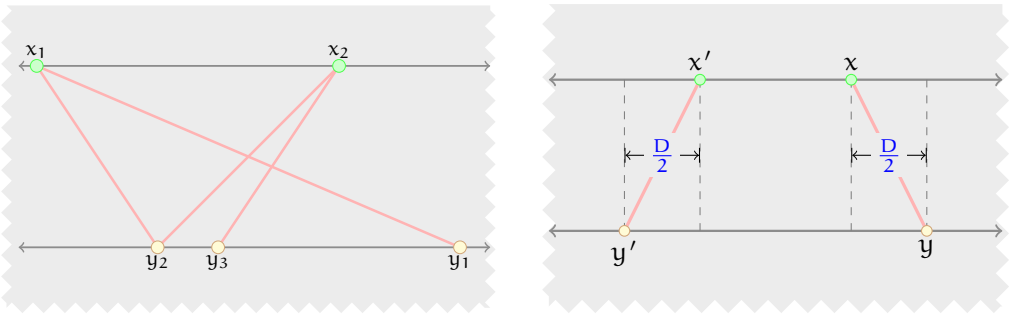

((a)) An Example Correspondence ((b)) The Standard Configuration

Figure 7.3: On the left, the (sorted) $X = \{x_1, x_2\}$ and $Y = \{y_1, y_2, y_3\}$ are identified as subsets of the top and the bottom lines respectively. The points of X are shown in green, and the points of Y are shown in yellow. We visualize the correspondence $\mathcal{C} = \{(x_1, y_1), (x_2, y_2), (x_2, y_3)\}$ by the red edges between the respective points. Also, the edges (x_1, y_1) and (x_2, y_2) are crossing. On the right, the distortion D of a correspondence is attained by the pairs (x', y') and (x, y).

7.4.1 A 2-Approximation

Theorem 7.4.2 (Approximation of the Gromov-Hausdorff Distance)**.** *For any two compact subsets X, Y of $\mathbb{R}^1$, we have the following*

$$d_{H,iso}(X,Y) \leq 2d_{GH}(X,Y).$$

Proof. Let $\mathcal{C}$ be any correspondence between two compact subsets X, Y of $\mathbb{R}^1$. There exists a pair of relatives $(x,y),(x',y') \in \mathcal{C}$ such that $\Big||x-x'|-|y-y'|\Big| = D$, where D is the distortion of $\mathcal{C}$. Without loss of generality, we assume that $x \leq x'$ and $|x-x'| \leq |y-y'|$. Then, there exists an R^1-isometry such that, when applied on Y, the pairs look like Figure 7.4. From now on, we assume this configuration for any given correspondence $\mathcal{C}$.

We must show that for any correspondence $\mathcal{C}$ with distortion D, there exists a Euclidean isometry $T \in \mathcal{E}(R^1)$ such that

$$d_H(X, T(Y)) \leq D.$$

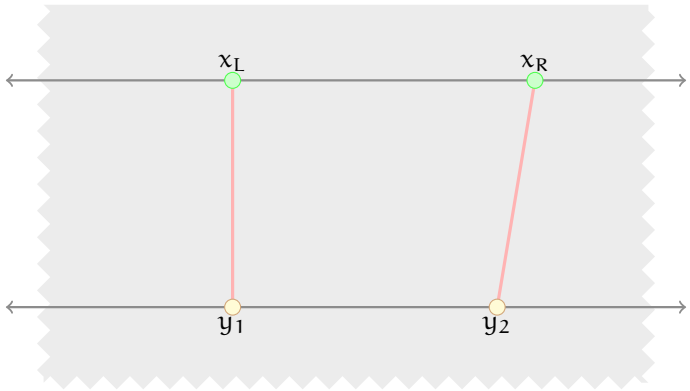

Figure 7.4: This standard alignment is assumed for $\mathcal{C}$ in this proof. We may need to apply a Euclidean isometry on Y so that (x_L, y_1) and (x_R, y_2) do not cross and $x_L = y_1$.

Let us denote $x_L = \min X$ and $x_R = \max X$. We also assume that $(x_L, y_1), (x_R, y_2) \in \mathcal{C}$ for some $y_1, y_2 \in Y$.

Without loss of generality, we can assume that the edges $(x_L, y_1), (x_R, y_2)$ do not cross, i.e., $y_1 \leq y_2$. This may require to flip Y once, but applying such an isometry is distortion-safe. We can further assume that $x_L = y_1$, which may require an additional translation. See Figure 7.4.

Case 1 (No Crossings)**:** In this case, we claim that $d_H(X,Y) \leq D$. To see the claim, consider any edge $(p,q) \in \mathcal{C}$. Since, the edge does not cross (x_L, y_1), we must have $|p-q| \leq D$. So, $d_H(X,Y) \leq D$.

Case 2 (Narrow Crossings)**:** Let us assume that there is at least an edge that crosses the edge (x_L, y_1). We now let

$$\varepsilon_1 = \max\big\{(x - x_L) \mid \text{the edge } (x,y) \in \mathcal{C} \text{ crosses } (x_L, y_1) \text{ for some } y \in Y\big\},$$

and

$$\varepsilon_2 = \max\big\{(y_1 - y) \mid \text{the edge } (x,y) \in \mathcal{C} \text{crosses} (x_L, y_1) \text{ for some } x \in X\big\}.$$

We first observe that $\varepsilon_1, \varepsilon_2 > 0$. In this case, we note that both $\varepsilon_1, \varepsilon_2 \leq D$. We claim that $d_H(X,Y) \leq D$.

To see that $\overrightarrow{d_H}(X,Y) \leq D$, consider an $x \in X$. If $x \leq x_L + \varepsilon_1$, then we have $\big|x - y_1\big| \leq D$. And, we note that $(x.y)$ cannot cross (x_L, y_1), hence we have $\big|x - y\big| \leq D$.

To show that $\overrightarrow{d_H}(Y,X) \leq D$, we take an $y \in Y$. If $y < y_1$, then we have $\big|y - x_L\big| \leq D$. If $y > y_1$, we consider $x \in X$ such that $(x,y) \in \mathcal{C}$. Then, (x,y) does not cross (x_L, y_1). Therefore, $\big|x - y\big| \leq D$. This proves the claim.

Case 3 (Wide Crossings)**:** The last case deals with the scenario of having at least one edge crossing the edge (x_L, y_1). Let ε_1, ε_2 be defined as in the previous case. Then, either $\varepsilon_1 > D$ or $\varepsilon_2 > D$. In this case, we pick T to be the translation of $\mathbb{R}^1$ to the right by D and argue that $d_H(X, T(Y)) \leq D$.

Since the edge (x_R, y_2) does not cross (x_L, y_1), we first note that $\big|x_R - y_2\big| \leq D$. Therefore, $\varepsilon_1 + \varepsilon_2 \leq 2D$.

To see that $\overrightarrow{d_H}(X, T(Y)) \leq D$, consider an $x \in X$. If $x \leq x_L + \varepsilon_1$, then we still have $\big|x - (y_1 + D)\big| \leq D$. If $x > x_L + \varepsilon_1$, then consider $(x,y) \in \mathcal{C}$. The edge (x,y) does not cross (x_L, y_1), hence we have $\big|x - y\big| \leq D$. Since $\varepsilon_1 + \varepsilon_2 > D$, we have $y \leq x$. Hence, $\big|(y + D) - x\big| \leq D$.

Now to show that $\overrightarrow{d_H}(T(Y), X) \leq D$, we take an $y \in Y$. If $y < y_1$, then we have $\big|y - x_L\big| \leq D$. If $y > y_1$, we consider $x \in X$ such that $(x,y) \in \mathcal{C}$. Then, (x,y) does not cross (x_L, y_1). Therefore, $\big|x - y\big| \leq D$. This proves the claim.

□

For a correspondence $\mathcal{C} \in \mathcal{C}(X,Y)$ between two compact sets with $\mathtt{Dist}(\mathcal{C}) = D$, there exists a pair of edges $(x', y'), (x,y) \in \mathcal{C}$ such that $\Big|\big|x - x'\big| - \big|y - y'\big|\Big| = D$. We can further assume, without loss of generality, that $x \geq x'$ and $(x - x') \leq \big|y - y'\big|$. Then, there exists an isometry $T \in \mathcal{E}(\mathbb{R}^1)$ such that the edges $(x', T(y'))$ and $(x, T(y))$ do not cross and $\big(x' - T(y')\big) = \big(T(y) - x\big) = \frac{D}{2}$; see Figure 7.3. From now on, we always assume this standard configuration for any given compact $X, Y \subset \mathbb{R}^1$ and a correspondence $\mathcal{C}$ between them.

7.4.2 The Tight Approximation

Now, we present in Theorem 7.4.3 our main result of this section. We also know that $d_{GH}(X,Y) \leq d_{H,iso}(X,Y)$ for any compact $X, Y \subset \mathbb{R}^d$; see [56]. Together with this, Theorem 7.4.3 thus gives us the approximation algorithm for d_{GH} with an approximation factor of $\left(1+\frac{1}{4}\right)$. Later in Theorem 7.4.11, we also show that the upper bound of Theorem 7.4.3 is tight.

Theorem 7.4.3 (Approximation of Gromov-Hausdorff Distance)**.** *For any two compact $X, Y \subset \mathbb{R}^1$ we have*

$$d_{H,iso}(X,Y) \leq \frac{5}{4} d_{GH}(X,Y).$$

Proof. In order to prove the result, it suffices to show that for any correspondence $\mathcal{C} \in \mathcal{C}(X,Y)$ with $\mathrm{Dist}(\mathcal{C}) = D$, there exists a Euclidean isometry $T \in \mathcal{E}(\mathbb{R}^1)$ such that

$$d_H(X, T(Y)) \leq \frac{5D}{8}.$$

Depending on the crossing behavior, we classify a given correspondence into three main types: no double crossing, wide crossing, and no wide crossing, and we divide the proof for each type into Theorem 7.4.5, Theorem 7.4.9, and Theorem 7.4.10 respectively. □

We start with the definition of a double crossing edge.

Definition 7.4.4. An edge in a correspondence $\mathcal{C} \in \mathcal{C}(X,Y)$ is said to be ***double crossing*** if it crosses both the (designated) edges (x', y') and (x, y); see Figure 7.6.

In the following theorem, we consider the case when there is no double crossing edge in $\mathcal{C}$.

Theorem 7.4.5 (No Double Crossing)**.** *For a correspondence $\mathcal{C} \in \mathcal{C}(X,Y)$ without any double crossing, there exists a value $\Delta \in \mathbb{R}$ such that*

$$d_H(X, Y+\Delta) \leq \frac{5}{8} D,$$

where $D = \mathrm{Dist}(\mathcal{C})$.

Proof. In the trivial case, when $d_H(X,Y) \leq \frac{5}{8}D$, we take $\Delta = 0$. So, we assume the non-trivial case that $d_H(X,Y) > \frac{5}{8}D$. Therefore, there exists either i) $a_0 \in X$ with $\min\limits_{b \in Y} |a_0 - b| > \frac{D}{2}$ or ii) $b_0 \in Y$ with $\min\limits_{a \in X} |a - b_0| > \frac{D}{2}$, or both.

We first note that such an a_0 cannot belong to $[x', x]$, where $\mathrm{Dist}(C) = \Big| |y - y'| - |x - x'| \Big|$. If it did, then for any edge $(a_0, t) \in \mathcal{C}$, we would have $t \in [y', y]$ and

$|a_0 - t| \leq \frac{D}{2}$ because then either $\Big||a_0 - x'| - |t - y'|\Big| \geq \frac{D}{2}$ or $\Big||a_0 - x| - |t - y|\Big| \geq \frac{D}{2}$. In fact, a_0 has to belong to A or A' as defined below (see Figure 7.5):

$$A = \{p \in X \cap (x + D, \infty) \mid \text{ there exists } q \in Y \cap [y', y] \text{ with } (p, q) \in \mathcal{C}\},$$
$$A' = \{p \in X \cap (-\infty, x' - D) \mid \text{ there exists } q \in Y \cap [y', y] \text{ with } (p, q) \in \mathcal{C}\}.$$

Similarly if b_0 exists, it has to belong to either B or B':

$$B = \{q \in Y \cap (y', y - D) \mid \text{ there exists } p \in X \cap [x, \infty) \text{ with } (p, q) \in \mathcal{C}\},$$
$$B' = \{q \in Y \cap (y' + D, y) \mid \text{ there exists } p \in X \cap [x, \infty) \text{ with } (p, q) \in \mathcal{C}\}.$$

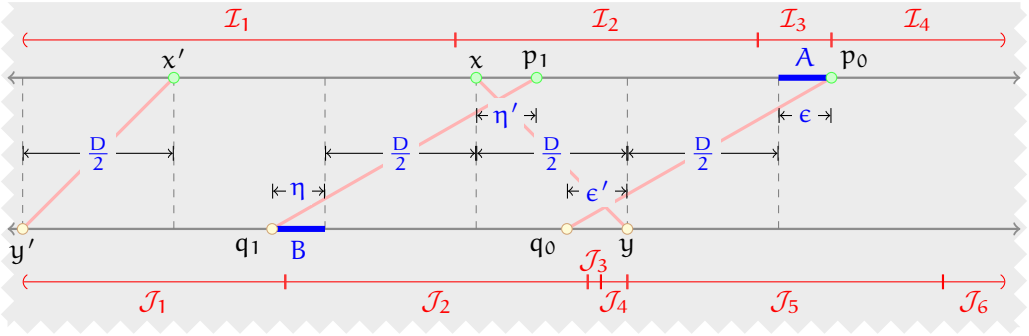

Figure 7.5: The no double crossing case is shown. The sets A and B are subsets of the top and bottom thick, blue intervals, respectively.

We now argue it suffices to study only the following three cases. If either $A \neq \emptyset$ or $A' \neq \emptyset$, we can assume, without loss of generality, that $A \neq \emptyset$ and use Case (1) and Case (2). Now if we have $A = A' = \emptyset$ and either $B \neq \emptyset$ or $B' \neq \emptyset$, we can assume, without loss of generality, that $B \neq \emptyset$ and use Case (3). For each of these cases, we will choose a positive $\Delta \leq \frac{3D}{8}$ and show that $d_H(X, Y + \Delta) \leq \frac{D}{2} + \frac{\Delta}{3}$. As a result, $d_H(X, Y + \Delta) \leq \frac{D}{2} + \frac{D}{8}$.

Case 1 ($A \neq \emptyset, B = \emptyset$)**:** We denote $p_0 = \max A$ and $\varepsilon = p_0 - x - D$. We also let $q_0 \in Y \cap [y', y]$ such that $(p_0, q_0) \in \mathcal{C}$; let $\varepsilon' = (y - q_0)$. In this case, we choose $\Delta = \frac{3}{4}\varepsilon$.

We first observe that $(p_0 - x') \geq (q_0 - y')$. From the distortion of the pair (x', y') and (p_0, q_0), and noting that $(p_0 - x') \geq (q_0 - y')$, we get

$$D \geq \big|(p_0 - x') - (q_0 - y')\big| = (p_0 - x') - (q_0 - y') = \varepsilon + \varepsilon'.$$

In particular, $\varepsilon' \leq D$. Now from the distortion of the pair (x, y) and (p_0, q_0), we also get

$$D \geq \big|D + \varepsilon - \varepsilon'\big| = D + \varepsilon - \varepsilon'.$$

This implies that $\varepsilon' \geq \varepsilon$. Combining this with $\varepsilon + \varepsilon' \leq D$, we obtain $\varepsilon \leq \frac{D}{2}$.

In order to show $\overrightarrow{d}_H(X, Y+\Delta) \leq \frac{D}{2} + \frac{\Delta}{3}$, we consider the following partition of the real line into intervals:

$$\mathbb{I}_1 = \left(-\infty, q_0 + \Delta - \frac{D}{2}\right], \ \mathbb{I}_2 = \left[q_0 + \Delta - \frac{D}{2}, q_0 + \Delta + \frac{D}{2}\right],$$
$$\mathbb{I}_3 = \left[q_0 + \Delta + \frac{D}{2}, p_0\right], \text{ and } \mathbb{I}_4 = [p_0, \infty).$$

For an arbitrary point $a \in X$ from any of the above intervals, we show that there exists a point $b \in Y$ such that $\big|a - (b+\Delta)\big| \leq \left(\frac{D}{2} + \frac{\Delta}{3}\right)$.

Let $a \in \mathbb{I}_1 \cap X$ and $b \in Y$ such that $(a,b) \in \mathcal{C}$. From $\Delta < \varepsilon \leq \varepsilon'$, it follows that $a < x$. We first note that (a,b) cannot cross (x,y). If $a \in [x', x]$, then (a,b) does not cross (x,y) because of its distortion bound with the edge (x', y'). Now if $a < x'$, then (a,b) does not cross (x,y), otherwise (a,b) would be a double crossing edge.

Now, we argue that (a,b) cannot cross (p_0, q_0) either. We assume the contrary that (a,b) crosses (p_0, q_0). Since (a,b) does not cross (x,y), we have $(b - q_0) \leq \varepsilon'$. So, we get the following contradiction:

$$\begin{aligned} D \geq \Big|\big|p_0 - a\big| - \big|q_0 - b\big|\Big| &= \left|\left[q_0 + \varepsilon' + \frac{D}{2} + \varepsilon - a\right] - (b - q_0)\right| \\ &\geq \left(\frac{D}{2} - \Delta\right) + \varepsilon' + \frac{D}{2} + \varepsilon - \varepsilon' = D + \varepsilon - \Delta > D. \end{aligned}$$

As a consequence if $b \leq a$, then it follows from the distortion of the pair (a,b) and (x,y) that $(a-b) \leq \frac{D}{2}$. If $b > a$, from the distortion of the pair (a,b) and (p_0, q_0) we get $b - a \leq \frac{D}{2} - (\varepsilon + \varepsilon')$. In either case, we conclude that $\big|a - (b+\Delta)\big| \leq \frac{D}{2}$, since $\Delta < \varepsilon$.

For $a \in \mathbb{I}_2 \cap X$ we have $\big|a - (q_0 + \Delta)\big| \leq \frac{D}{2}$.

For $a \in \mathbb{I}_3 \cap X$, the distance $\big|a - (y+\Delta)\big|$ is maximized when a is the right endpoint of the interval $\mathbb{I}_3$. Therefore,

$$\big|a - (y+\Delta)\big| \leq \Big|p_0 - (y+\Delta)\Big| = \max\left\{\left|\frac{D}{2} - \varepsilon'\right|, \frac{D}{2} + \varepsilon - \Delta\right\} = \frac{D}{2} + \frac{\Delta}{3}.$$

If $(a,b) \in \mathcal{C}$ with $a \in \mathbb{I}_4 \cap X$, we have $a > p_0 = \max A$. Therefore, (a,b) does not cross (x,y). Also, it cannot cross (x', y') because of our assumption of no double crossing. By an argument similar to $\mathbb{I}_1$, we conclude $\big|a - (b+\Delta)\big| \leq \frac{D}{2}$.

In order to show $\overrightarrow{d_H}(Y+\Delta, X) \leq \frac{D}{2} + \frac{\Delta}{3}$, we consider the following partition of the

real line into intervals:

$$\mathcal{J}_1 = \left(-\infty, x - \frac{D}{2} - \Delta\right], \mathcal{J}_2 = \left[x - \frac{D}{2} - \Delta, y - \frac{\varepsilon}{2}\right], \mathcal{J}_3 = \left[y - \frac{\varepsilon}{2}, y\right],$$
$$\mathcal{J}_4 = [y, p_0 + \frac{D}{2} - \Delta], \text{ and } \mathcal{J}_5 = (p_0 + \frac{D}{2} - \Delta, \infty).$$

For an arbitrary point $b \in Y$ from any of the above intervals, we now show that there exists a point a in X such that $\left|a - b\right| \leq \left(\frac{D}{2} + \frac{\Delta}{3}\right)$.

Since $B = \emptyset$, for any $b \in \mathcal{J}_1 \cap Y$ with edge $(a, b) \in \mathcal{C}$, the edge cannot cross (x, y) or (p_0, q_0). Therefore, $\left|a - (b + \Delta)\right| \leq \frac{D}{2}$ as before.

For $b \in \mathcal{J}_2 \cap Y$, the distance $\left|x - (b + \Delta)\right|$ is maximum at the endpoints of $\mathcal{J}_2$. Therefore,

$$\left|x - (b + \Delta)\right| \leq \max\left\{\frac{D}{2}, \left|x - y + \frac{\varepsilon}{2} - \Delta\right|\right\} = \max\left\{\frac{D}{2}, \left|-\frac{D}{2} + \frac{2\Delta}{3} - \Delta\right|\right\}$$
$$= \frac{D}{2} + \frac{\Delta}{3}.$$

Now, let $b \in \mathcal{J}_3 \cap Y$ and $(a, b) \in \mathcal{C}$. Because of the distortion bound D with the edges (x, y) and (p_0, q_0), a moment's reflection reveals that $a \in \left(p_0 - D - \frac{\varepsilon}{2}, x + D + \frac{\varepsilon}{2}\right) = \left(x + \frac{\varepsilon}{2}, p_0 - \frac{\varepsilon}{2}\right)$. So, the distance $\left|a - (b + \Delta)\right|$ is maximum when b in one of the endpoints of $\mathcal{J}_3$ and a the other endpoint of the interval $\left(x + \frac{\varepsilon}{2}, p_0 - \frac{\varepsilon}{2}\right)$. Therefore,

$$\left|a - (b + \Delta)\right| \leq \max\left\{\left|\left(x + \frac{\varepsilon}{2}\right) - \left(y - \frac{\varepsilon}{2} + \Delta\right)\right|, \left|\left(p_0 - \frac{\varepsilon}{2}\right) - (y + \Delta)\right|\right\}$$
$$= \max\left\{\frac{D}{2} - \frac{\Delta}{3}, \frac{D}{2} + \frac{\Delta}{3}\right\} = \frac{D}{2} + \frac{\Delta}{3}.$$

For $b \in \mathcal{J}_4 \cap Y$, the distance $\left|p_0 - (b + \Delta)\right|$ is maximum when b is one of the endpoints of the interval $\mathcal{J}_4$. So,

$$\left|p_0, (b + \Delta)\right| \leq \max\left\{\left|p_0 - (y + \Delta)\right|, \frac{D}{2}\right\} = \max\left\{\frac{D}{2} + \varepsilon - \Delta, \frac{D}{2}\right\} = \frac{D}{2} + \frac{\Delta}{3}.$$

Similarly, for $b \in \mathcal{J}_5 \cap Y$, an edge $(a, b) \in \mathcal{C}$ cannot cross (p_0, q_0) because of the distortion bound. Following the argument for $\mathbb{I}_1$, we conclude $\left|a - (b + \Delta)\right| \leq \frac{D}{2} + \frac{\Delta}{3}$.

Case 2 ($A = \emptyset, B \neq \emptyset$)**:** We denote $q_1 = \min B$ and $\eta = y - D - q_1$. We also let $p_1 \in Y \cap (x, \infty)$ such that $(p_1, q_1) \in \mathcal{C}$ and $\eta' = p_1 - x$. We show, in this case, that $d_H(X, Y + \Delta) \leq \frac{D}{2} + \frac{\Delta}{3}$ for $\Delta = \frac{3}{4}\eta$. In this case, we choose $\Delta = \frac{3}{4}\eta$.

We first observe that $(p_1 - x') \geq (q_1 - y')$. Therefore, from the distortion of the pair

(x', y') and (p_1, q_1) we get

$$\begin{aligned} D &\geq \left|(p_1 - x') - (q_1 - y')\right| = (p_1 - x') - (q_1 - y'), \text{ since } (p_1 - x') \geq (q_1 - y') \\ &= [(x - x') + \eta'] - \left[\frac{D}{2} + (x - x') - \frac{D}{2} - \eta\right] = \eta' + \eta. \end{aligned}$$

In particular, $\eta' \leq D$. Now from the distortion of the pair (x, y) and (p_1, q_1), we also get

$$D \geq \left|D + \eta - \eta'\right| = D + \eta - \eta'.$$

This implies that $\eta' \geq \eta$. Combining this with $\eta + \eta' \leq D$, we get $\eta \leq \frac{D}{2}$.

In order to show $\overrightarrow{d_H}(X, Y + \Delta) \leq \frac{D}{2} + \frac{\Delta}{3}$, we consider the following intervals of the real line:

$$\begin{aligned} \mathbb{I}_1 &= \left(-\infty, q_1 + \Delta - \frac{D}{2}\right], \mathbb{I}_2 = \left[q_1 + \Delta - \frac{D}{2}, x\right] \mathbb{I}_3 = \left[x, x + \frac{\eta}{2}\right] \\ \mathbb{I}_4 &= \left[x + \frac{\eta}{2}, y + \Delta - \frac{D}{2}\right], \text{ and } \mathbb{I}_5 = \left[y + \Delta - \frac{D}{2}, \infty\right) \end{aligned}$$

By the symmetry of the problem, we follow the arguments presented in Case (1) for $\mathcal{J}_5, \mathcal{J}_4, \mathcal{J}_3, \mathcal{J}_2$, and $\mathcal{J}_1$ to conclude the same about the nearest neighbor distances for $\mathbb{I}_1, \mathbb{I}_2, \mathbb{I}_3, \mathbb{I}_4$, and $\mathbb{I}_5$, respectively.

Now, in order to show $\overrightarrow{d_H}(Y + \Delta, X) \leq \frac{D}{2} + \frac{\Delta}{3}$, we consider the following intervals:

$$\begin{aligned} \mathcal{J}_1 &= (-\infty, q_1), \mathcal{J}_2 = \left[q_1, p_1 - \frac{D}{2} - \Delta\right], \\ \mathcal{J}_3 &= \left[p_1 - \frac{D}{2} - \Delta, p_1 + \frac{D}{2} - \Delta\right], \text{ and } \mathcal{J}_4 = \left[p_1 + \frac{D}{2} - \Delta, \infty\right). \end{aligned}$$

Again by the symmetry of the problem, we follow the arguments presented in Case (1) for $\mathbb{I}_4, \mathbb{I}_3, \mathbb{I}_2$, and $\mathbb{I}_1$ to conclude the same about the nearest neighbor distances for $\mathcal{J}_1, \mathcal{J}_2, \mathcal{J}_3$, and $\mathcal{J}_4$ respectively.

Case 3 ($A \neq \emptyset, B \neq \emptyset$)**:** In this case, we take $\Delta = \frac{3}{4}\max\{\varepsilon, \eta\}$ and consider all the intervals from Case (1) and Case (2) to conclude that $d_H(X, Y + \Delta) \leq \frac{D}{2} + \frac{\Delta}{3}$.

□

Now, we undertake the task of finding a suitable isometry/alignment when there is a double crossing in $\mathcal{C}$. In this case, we may have to consider flipping Y to construct such an isometry. We always flip Y about the midpoint of x and x' and denote the image by $\widetilde{Y}$. We first present two technical lemmas.

Lemma 7.4.6. *Let $(p, q) \in \mathcal{C}$ be a double crossing; see Figure 7.6. If we denote $h = (x - x')$, $\varepsilon_1 = (p - x)$, and $\varepsilon_2 = (y' - q)$, then we have the following:*

i) $\varepsilon_1 - \varepsilon_2 \geq h$,

ii) $\varepsilon_1 - \varepsilon_2 \leq D - h$,

iii) $h \leq \frac{D}{2}$, *and*

iv) $\left|p - \widetilde{q}\right| \leq \frac{D}{2} - h$, *where $\widetilde{q}$ denotes the reflection of q about the midpoint of x and x'.*

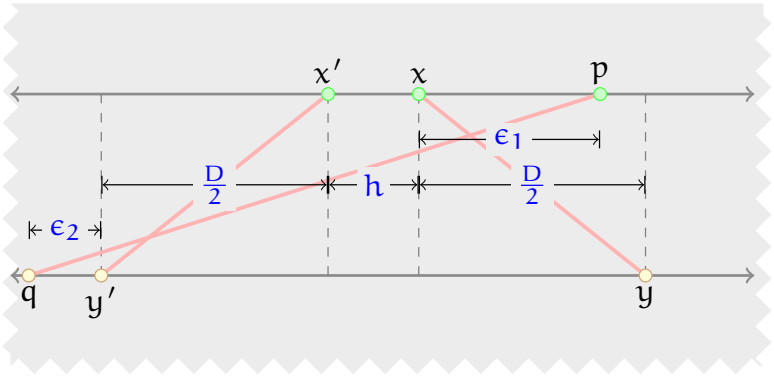

Figure 7.6: A double crossing (p, q) is shown.

Proof. i) Let us assume the contrary, i.e., $\varepsilon_1 < \varepsilon_2 + h$. Then, the distortion for the pairs (x, y) and (p, q) becomes

$$\left|\varepsilon_2 + D + h - \varepsilon_1\right| = \varepsilon_2 + h + D - \varepsilon_1 > D.$$

This contradicts the fact that the distortion of $\mathcal{C}$ is D. Therefore, we conclude that $\varepsilon_1 - \varepsilon_2 \geq h$.

ii) Since from (i) we have $\varepsilon_1 \geq \varepsilon_2$, from the distortion for the pairs (p, q) and (x', y'), we have

$$h + \varepsilon_1 - \varepsilon_2 \leq D \tag{7.2}$$

So, $\varepsilon_1 - \varepsilon_2 \leq D - h$.

iii) From (ii) we have $\varepsilon_2 + D \geq \varepsilon_1$. Hence, the distortion for the pairs (p, q) and (x, y) implies

$$\varepsilon_2 + D + h - \varepsilon_1 \leq D. \tag{7.3}$$

Adding (7.2) and (7.3), we get $2h \leq D$. Hence, $h \leq \frac{D}{2}$.

iv) If $p > \widetilde{q}$, then

$$p - \widetilde{q} = \varepsilon_1 - \frac{D}{2} - \varepsilon_2 \leq (D - h) - \frac{D}{2} - \varepsilon_2 \leq \frac{D}{2} - h.$$

Otherwise,

$$\widetilde{q} - p = \frac{D}{2} + \varepsilon_2 - \varepsilon_1 \leq \frac{D}{2} - (\varepsilon_1 - \varepsilon_2) \leq \frac{D}{2} - h.$$

Therefore, $\left|p - \widetilde{q}\right| \leq \frac{D}{2} - h$.

□

In our pursuit of constructing the right isometry, we first define a wide (double) crossing. We show in Theorem 7.4.9, that we need to flip Y in the presence of such a wide crossing.

Definition 7.4.7 (Wide Crossing)**.** A crossing edge $(p, q) \in \mathcal{C}$ is called a *wide crossing* if either p or q lie outside $(x' - D, x + D)$; see Figure 7.7.

Before presenting Theorem 7.4.9, we make an important observation first in the following technical lemma.

Lemma 7.4.8 (Wide Crossing)**.** *Let there be a wide crossing $(p, q) \in \mathcal{C}$ and an edge $(p_0, q_0) \in \mathcal{C}$ such that $p_0 > x + D$ and $y' < q_0 < y$. If we denote $\varepsilon = p_0 - x - D$, $\varepsilon' = y - q_0$ and $h = x - x'$, then we have $\varepsilon' \geq h$.*

Proof. We prove by contradiction. Let us assume that $\varepsilon' < h$. In Figure 7.7, we have shown two possible positions of p. In each of the following cases, we arrive at a contradiction.

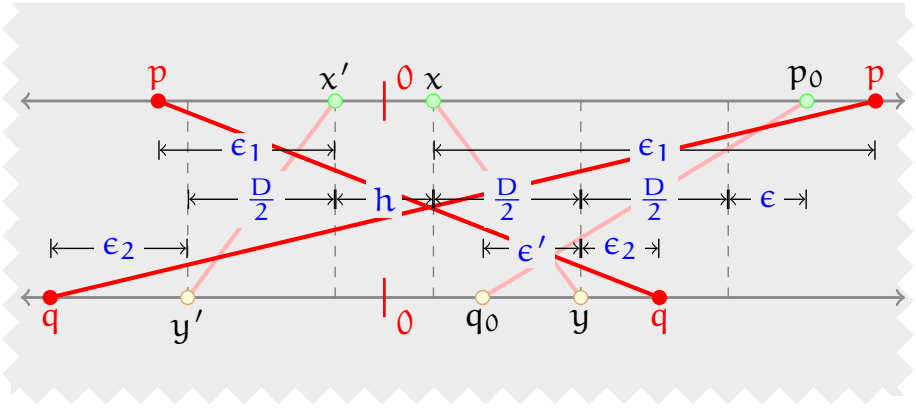

Figure 7.7: A wide crossing (p, q) is shown. Both the cases are shown in bright red.

Case 1 $(p < x' - D)$**:** From the distortion of the pair (p, q) and (p_0, q_0), we have

$$\left|(\varepsilon_1 + h + D + \varepsilon) - (\varepsilon' + \varepsilon_2)\right| \leq D.$$

Since by assumption $h > \varepsilon'$ and from Lemma 7.4.6 we have $\varepsilon_1 \geq \varepsilon_2$, we get

$$\varepsilon' \geq h + (\varepsilon_1 - \varepsilon_2) + \varepsilon \geq 2h + \varepsilon > h.$$

Case 2 ($p > p_0$)**:** From the distortion of the pair (p, q) and (p_0, q_0), we get

$$\left|(\varepsilon_2 + D + h - \varepsilon') - (\varepsilon_1 - D - \varepsilon)\right| \leq D.$$

Since $D - (\varepsilon_1 - \varepsilon_2) \geq h$ and $h > \varepsilon'$, we have

$$\varepsilon' \geq D + h - (\varepsilon_1 - \varepsilon_2) + \varepsilon \geq 2h + \varepsilon > h.$$

Case 3 ($x + D < p < p_0$)**:** Again from the distortion of the pair (p, q) and (p_0, q_0), we get

$$\varepsilon_2 + \frac{D}{2} + h + \left(\frac{D}{2} - h\right) - \varepsilon \leq D.$$

We get $\varepsilon_2 \leq \varepsilon$. So, $\varepsilon' \geq \varepsilon \geq \varepsilon_2 \geq \varepsilon_1 + h - D \geq h$.

Therefore, $\varepsilon' \geq h$. □

Theorem 7.4.9 (Wide Crossing)**.** *Let $\mathcal{C}$ be a correspondence between two compact sets $X, Y \subseteq \mathbb{R}^1$ with distortion D. If there is a wide crossing $(p, q) \in \mathcal{C}$, then there exists a value $\Delta \in \mathbb{R}$ such that*

$$d_H(X, \widetilde{Y} + \Delta) \leq \frac{5}{8}D,$$

where $\widetilde{Y}$ denotes the reflection of Y about the midpoint of x and x'.

Proof. We first note from Lemma 7.4.6 that $h = x - x' \leq \frac{D}{2}, \left|p - \widetilde{q}\right| \leq \left(\frac{D}{2} - h\right)$.

Let us define

$$A = \{p \in X \cap (x + D, \infty) \mid \text{ there exists } q \in Y \cap [y', y] \text{ with } (p, q) \in \mathcal{C}\},$$

and

$$A' = \{p \in X \cap (-\infty, x' - D) \mid \text{ there exists } q \in Y \cap [y', y] \text{ with } (p, q) \in \mathcal{C}\}.$$

Case 1 ($A \neq \emptyset$)**:** Let $p_0 = \max A$ and $\varepsilon = p_0 - x - D$. We now define

$$B = \{q \in Y \cap [y, \infty) \mid \text{ there exists } p \in X \cap [x, \infty) \text{ with } (p, q) \in \mathcal{C}\}.$$

Let us also define $q_1 = \max B$, $\eta = q_1 - y$, and let there exists edge $(p_1, q_1) \in \mathcal{C}$ with $\eta' = p_1 - x$. Comparing with the edge (x, y), we get $\eta' \geq \eta$. Because of the distortion bound with the wide crossing edge, we must have $\eta \leq \frac{D}{2}$. From Lemma 7.4.8, we also have $\varepsilon' = (y - q_0) \geq h$.

If we take $\Delta = \frac{3}{4}\max\{\varepsilon, \eta\}$, we argue that

$$d_H(X, \widetilde{Y} + \Delta) \leq \frac{D}{2} + \frac{\Delta}{3}.$$

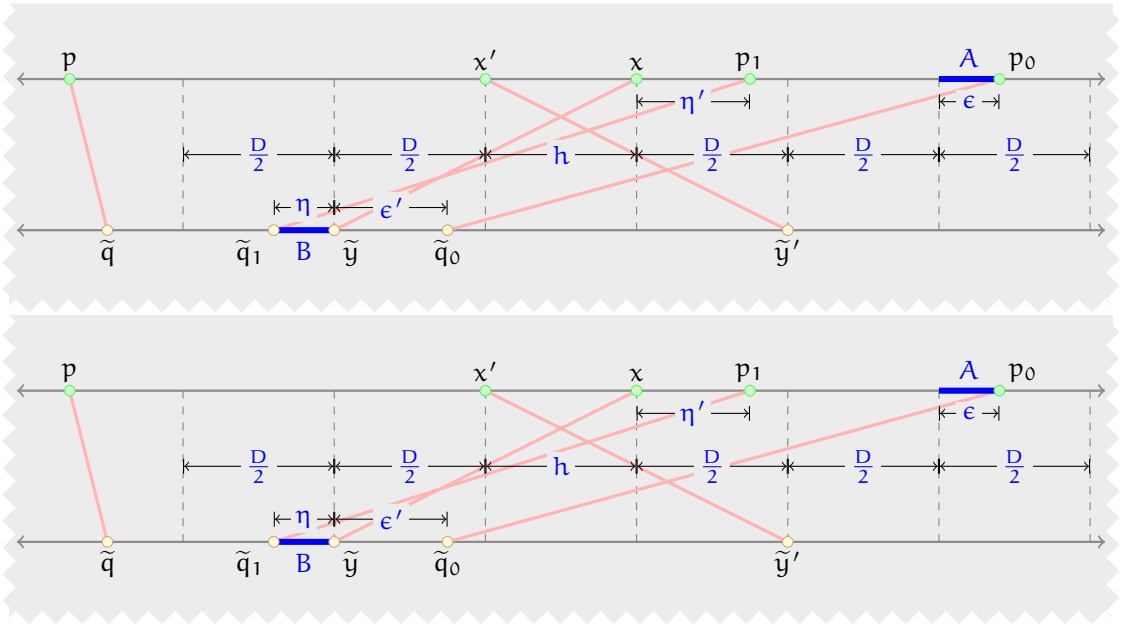

Figure 7.8: The correspondence with a wide crossing is shown. The sets A and B are subsets of the thick, dark blue regions on top and bottom respectively. In the bottom, we show the configuration when Y is flipped about the midpoint of x and x′.

In order to show that $\overrightarrow{d}_H(X, \widetilde{Y} + \Delta) \leq \frac{D}{2} + \frac{\Delta}{3}$, we define the following intervals:

$$\mathbb{I}_1 = \left(-\infty, \widetilde{q_1} + \Delta - \frac{D}{2}\right] \mathbb{I}_2 = \left[\widetilde{q_1} + \Delta - \frac{D}{2}, x'\right] \mathbb{I}_3 = \left[x', \widetilde{q_0} + \Delta + \frac{D}{2}\right],$$
$$\mathbb{I}_4 = \left[\widetilde{q_0} + \Delta + \frac{D}{2}, p_0\right], \text{ and } \mathbb{I}_5 = [p_0, \infty).$$

For $a \in (\mathbb{I}_1 \cup \mathbb{I}_5) \cap X$ and an edge $(a, b) \in \mathcal{C}$, the edge has to be a double crossing edge because of the distortion bound with the wide crossing edge. So after the flip, the edge $(a, \widetilde{b})$ does not cross $(p_0, \widetilde{q_0})$ or $(p_1, \widetilde{q_1})$. As a result, when $a \geq \widetilde{b}$, we have $(a - \widetilde{b}) \leq \left(\frac{D}{2} - h\right)$ as shown in Lemma 7.4.6 and $(\widetilde{b} - a) \leq \left(\frac{D}{2} - \max\{\varepsilon, \eta\}\right)$ otherwise. Therefore, $\left|a - (\widetilde{b} + \Delta)\right| \leq \frac{D}{2}$.

For $a \in \mathbb{I}_2 \cap X$ we have

$$\left|a - (\widetilde{q_1} + \Delta)\right| \leq \max\left\{\frac{D}{2}, \left|x' - \widetilde{q_1} - \Delta\right|\right\} = \max\left\{\frac{D}{2}, \left|\frac{D}{2} + \eta - \Delta\right|\right\} \leq \frac{D}{2} + \frac{\Delta}{3}.$$

For $a \in \mathbb{I}_3 \cap X$, we have

$$\left|a - (\widetilde{q_0} + \Delta)\right| \leq \max\left\{\left|x' - \widetilde{q_0} - \Delta\right|, \frac{D}{2}\right\} \leq \max\left\{\left|\varepsilon' - \frac{D}{2}\right|, \frac{D}{2}\right\} \leq \frac{D}{2}$$

For $a \in \mathbb{I}_4 \cap X$ we have

$$\begin{aligned}\left|a-(\widetilde{y}'+\Delta)\right| &\leq \max\left\{\left|\widetilde{q}_0+\frac{D}{2}-\widetilde{y}'\right|,\left|p_0-\widetilde{y}'-\Delta\right|\right\}\\ &= \max\left\{\left|\frac{D}{2}-(D+h-\varepsilon')\right|,\left|\frac{D}{2}+\varepsilon-\Delta\right|\right\}\\ &= \max\left\{\left|\frac{D}{2}-(\varepsilon'-h)\right|,\left|\frac{D}{2}+\frac{\Delta}{3}\right|\right\} \leq \frac{D}{2}+\frac{\Delta}{3}.\end{aligned}$$

In order to show that $\overrightarrow{d}_H(\widetilde{Y}+\Delta, X) \leq \frac{D}{2}+\frac{\Delta}{3}$, we define the following intervals:

$$\begin{aligned}&\mathcal{J}_1=(-\infty,\widetilde{q}_1]\,,\ \mathcal{J}_2=\left[\widetilde{q}_1,x'+\frac{D}{2}-\Delta\right]\,,\ \mathcal{J}_3=\left[x'+\frac{D}{2}-\Delta,\widetilde{y}'-\frac{2\Delta}{3}\right]\,,\\ &\mathcal{J}_4=\left[\widetilde{y}'-\frac{2\Delta}{3},\widetilde{y}'\right]\,,\ \mathcal{J}_5=\left[\widetilde{y}',p_0+\frac{D}{2}-\Delta\right]\,,\text{ and }\mathcal{J}_6=\left[p_0+\frac{D}{2}-\Delta,\infty\right)\,.\end{aligned}$$

For $\mathcal{J}_1$, $\mathcal{J}_2$, $\mathcal{J}_4$, $\mathcal{J}_5$, and $\mathcal{J}_6$ we use routine arguments used in Case (1) of Theorem 7.4.5. As a new situation, we only consider $\mathcal{J}_3$ here. For $b \in \mathcal{J}_3 \cap Y$ we have

$$\begin{aligned}\left|x-(b+\Delta)\right| &\leq \max\left\{\left|x-x'-\frac{D}{2}\right|,\left|x-\widetilde{y}'+\frac{2\Delta}{3}-\Delta\right|\right\}\\ &\leq \max\left\{\left|\frac{D}{2}-h\right|,\left|\frac{D}{2}+\frac{\Delta}{3}\right|\right\} \leq \frac{D}{2}+\frac{\Delta}{3}.\end{aligned}$$

Case 2 ($A=\emptyset$)**:** In this case, we assume, without loss of generality, that $\eta_1 \leq \eta_2$; see Figure 7.9. When considering $\widetilde{Y}$, we first note from the distortion bound with $(p,\widetilde{q})$ that $\eta_1,\eta_2 \leq \left(\frac{D}{2}-h\right)$.

If $h > \frac{3D}{8}$, then $\eta_1 > \frac{D}{8}$. We take $\Delta = \left(\eta_1-\eta_2'-\frac{D}{8}\right)$, and we argue that

$$d_H(X,\widetilde{Y}+\Delta) \leq \frac{D}{2}+\frac{D}{8}.$$

In order to show that $\overrightarrow{d}_H(X,\widetilde{Y}+\Delta) \leq \frac{D}{2}+\frac{D}{8}$, we define the following intervals:

$$\begin{aligned}&\mathbb{I}_1=\left(-\infty,\widetilde{q}_1+\Delta-\frac{D}{2}\right]\,,\mathbb{I}_2=\left[\widetilde{q}_1+\Delta-\frac{D}{2},x'\right]\,,\mathbb{I}_3=\left[x',x'+\frac{D}{8}+\Delta\right]\,,\\ &\mathbb{I}_4=\left[x'+\frac{D}{8}+\Delta,x-\frac{D}{8}+\Delta\right]\,,\mathbb{I}_5=\left[x-\frac{D}{8}+\Delta,\widetilde{y}'-\frac{5D}{8}+\Delta\right]\,,\text{ and}\\ &\mathbb{I}_5=\left[\widetilde{y}'+\Delta+\frac{D}{2},\infty\right)\,.\end{aligned}$$

For $\mathbb{I}_1$ and $\mathbb{I}_5$, we use the arguments from Case (1).

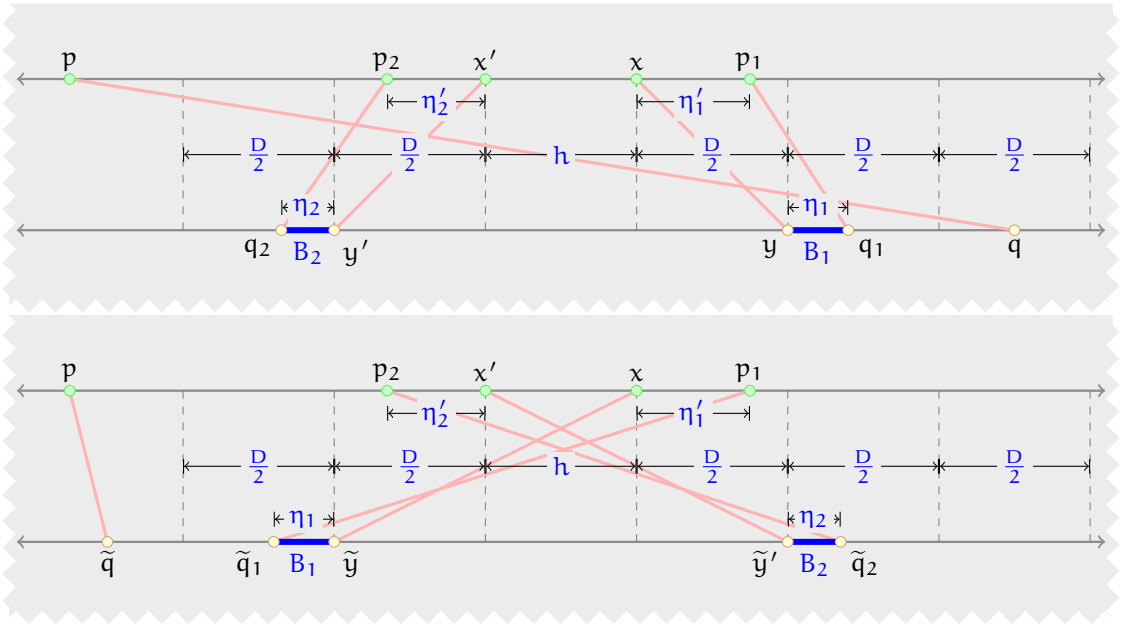

Figure 7.9: Wide crossing exists, and both $A = \emptyset$, $A' = \emptyset$

For $a \in \mathbb{I}_2 \cap X$, we get

$$\begin{aligned}\left|a - (\widetilde{q_1} + \Delta)\right| &\le \max\left\{\frac{D}{2}, x' - \widetilde{q_1} - \Delta\right\} = \max\left\{\frac{D}{2}, \frac{D}{2} + \eta_1 - \Delta\right\} \\ &= \max\left\{\frac{D}{2}, \frac{D}{2} + \eta_1 - \eta_1 + \frac{D}{8}\right\} = \frac{D}{2} + \frac{D}{8}.\end{aligned}$$

A similar argument holds also for $\mathbb{I}_3, \mathbb{I}_5$.

For $a \in \mathbb{I}_4 \cap X$, let $b \in [y', y] \cap Y$ such that $(a, b) \in \mathcal{C}$. If $a \ge b$, then by the distortion bound with (x, y) we have $(a - x') \le (b - y')$. So,

$$\begin{aligned}\left|(\widetilde{b} + \Delta) - a\right| &= \Delta + \frac{D}{2} + h - (a - x') - (b - y') \le \Delta + \frac{D}{2} + h - 2(a - x') \\ &\le \Delta + \frac{D}{2} + h - 2\left(\frac{D}{8} + \Delta\right) = \frac{D}{2} + h - \frac{D}{4} - \Delta = \frac{D}{2} + h - \frac{D}{4} \\ &\le \frac{D}{2} + \frac{3D}{8} - \frac{D}{4} = \frac{D}{2} + \frac{D}{8}.\end{aligned}$$

If $a \le b$, we argue by symmetry that $\left|(\widetilde{b} + \Delta) - a\right| \le \frac{D}{2} + \frac{D}{8}$.

In order to show that $\overrightarrow{d}_H(\widetilde{Y}+\Delta, X) \leq \frac{D}{2}+\frac{D}{8}$, we define the following intervals:

$$\mathcal{J}_1 = (-\infty, \widetilde{q_1}], \mathcal{J}_2 = [\widetilde{q_1}, x'], \mathcal{J}_3 = \left[x', x'+\frac{D}{2}-\Delta\right]$$
$$\mathcal{J}_4 = \left[x'+\frac{D}{2}-\Delta, x+\frac{D}{2}-\Delta\right], \mathcal{J}_5 = \left[x+\frac{D}{2}-\Delta, \widetilde{q_2}\right], \text{ and } \mathcal{J}_6 = [\widetilde{q_2}, \infty).$$

The analysis for $\mathbb{I}_1, \mathbb{I}_2, \mathbb{I}_3, \mathbb{I}_4$ are similar to Case (1). We note for $\mathcal{J}_5$ that $\left|(\widetilde{q_2}+\Delta) - p_1\right| = \frac{D}{2}+\eta_2-\eta_1'+\Delta \leq \frac{D}{2}+\eta_2'-\eta_1+\Delta = \frac{D}{2}+\eta_2'-\eta_1+\left(\eta_1-\eta_2'-\frac{D}{8}\right) \leq \frac{D}{2}$.

If $h \leq \frac{3D}{8}$, then $\eta_1 \geq \frac{D}{8}$. We take $\Delta = \left(\frac{D}{8}-\eta_1\right)$, and we argue that

$$d_H(X, \widetilde{Y}+\Delta) \leq \frac{D}{2}+\frac{D}{8}.$$

We use the same intervals as Case (1). With this new Δ, the only changes in the calculations appear in $\mathbb{I}_3$. We show $\mathbb{I}_3$ here.

$$\begin{aligned}\left|(\widetilde{b}+\Delta)-a\right| &= \Delta+\frac{D}{2}+h-(a-x')-(b-y') \leq \Delta+\frac{D}{2}+h-2(a-x') \\ &\leq \Delta+\frac{D}{2}+h-2\left(\frac{D}{8}+\Delta\right) = \frac{D}{2}+h-\frac{D}{4}-\Delta \\ &= \frac{D}{2}+h-\frac{D}{4}-\left(\frac{D}{8}-\eta_1\right) \\ &\leq \frac{D}{2}+h-\frac{3D}{8}+\eta_1 \leq \frac{D}{2}+h-\frac{3D}{8}+\left(\frac{D}{2}-h\right) = \frac{D}{2}+\frac{D}{8}.\end{aligned}$$

This completes the proof for wide crossing. □

In order to complete our analysis of various types of correspondences, we show now that a flip is not required if there is no wide crossing in $\mathcal{C}$.

Theorem 7.4.10 (No Wide Crossing)**.** *Let $\mathcal{C}$ be a correspondence between two compact sets $X, Y \subset \mathbb{R}^1$ with distortion D. If there are double crossings but not wide, then there exists a value $\Delta \in \mathbb{R}$ such that*

$$d_H(X, Y+\Delta) \leq \frac{D}{2}+\frac{D}{8}.$$

Proof. We assume that there are double crossings in $\mathcal{C}$, but none of them are wide; see Figure 7.10.

Case 1 ($A \neq \emptyset, B_2 = \emptyset$)**:** This case is similar to Case (1) and Case (3) of Theorem 7.4.5.

Case 2 ($A \neq \emptyset, B_2 \neq \emptyset$)**:** If $\eta_1 \geq \varepsilon$, then we note that $d_H(X, Y) \leq \frac{D}{2}$. This is the trivial case. So, we assume that $\eta_1 < \varepsilon$.

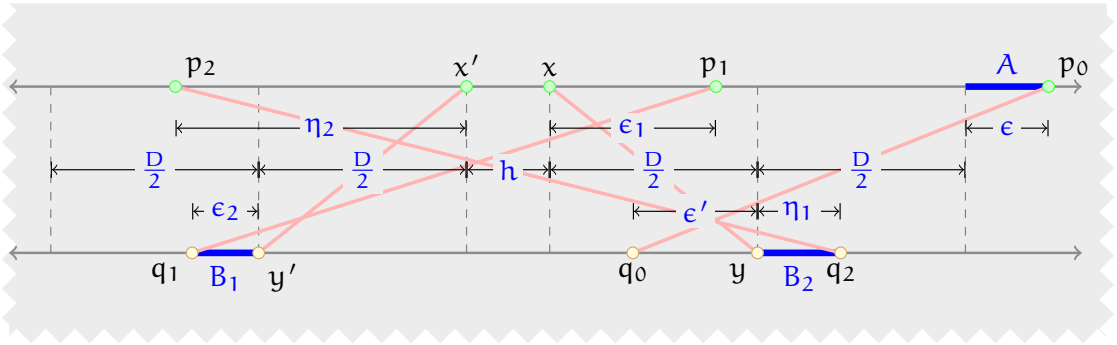

Figure 7.10: No wide crossing exists

From the distortion of the pair (p_0, q_0) and (p_2, q_2), we have

$$D \geq (\eta_2 + h + D + \varepsilon) - (\eta_1 + \varepsilon').$$

So, we get $\eta_2 + \varepsilon + h \leq \eta_1 + \varepsilon'$.

We take $\Delta = \varepsilon - \eta_1$. We first consider the following intervals:

$$\mathbb{I}_1 = \left(-\infty, y' + \Delta - \frac{D}{2}\right], \mathbb{I}_2 = \left[y' + \Delta - \frac{D}{2}, x'\right] \mathbb{I}_3 = [x', x],$$
$$\mathbb{I}_4 = \left[x, q_0 + \frac{D}{2} + \Delta\right], \mathbb{I}_5 = \left[q_0 + \frac{D}{2} + \Delta, p_0\right], \text{ and } \mathbb{I}_6 = [p_0, \infty).$$

The intervals similar to $\mathbb{I}_2, \mathbb{I}_3, \mathbb{I}_4, \mathbb{I}_5$ are considered already in Theorem 7.4.5. We show that if $p_2 \in \mathbb{I}_1 \cap X$, then any edge $(p_2, q_2) \in \mathcal{C}$ cannot cross (x', y'), consequently $\left|p_2 - (q_2 + \Delta)\right| \leq \frac{D}{2}$. If we assume the contrary, then the edge has to be a double crossing; see Figure 7.10. Since p_2 is assumed to be in $\mathbb{I}_1$, we have $\left(\eta_2 - \frac{D}{2}\right) > \left(\frac{D}{2} - \Delta\right)$. This would imply

$$\eta_2 > D - \Delta = D - (\eta_1 - \varepsilon) \geq D + \eta_2 + h - \varepsilon' = h + \eta_2 + (D - \varepsilon') \geq h + \eta_2.$$

This is a contradiction. Therefore, $\overrightarrow{d}_H(X, Y + \Delta) \leq \frac{D}{2}$.

For $\overrightarrow{d}_H(Y + \Delta, X)$, the arguments are similar to Theorem 7.4.5.

Case 3 ($A = \emptyset$)**:** In this case, we choose $\Delta = \frac{3}{4}\max\{\eta_1, \varepsilon_2\}$ and conclude the result using arguments similar to Case (2) in Theorem 7.4.9.

This concludes the proof. □

We conclude this section by showing in Theorem 7.4.11 that the bound of Theorem 7.4.3 is a tight upper bound in the following sense:

Theorem 7.4.11 (Tightness of the Bound)**.** *For any $0 < \varepsilon < \frac{1}{4}$ and $\delta > 0$, there exist compact $X, Y \subset \mathbb{R}$ with $d_{GH}(X, Y) = \delta$ and*

$$d_{H,iso}(X, Y) = \left(\frac{5}{4} - \varepsilon\right)\delta.$$

Proof. It suffices to assume that $\varepsilon = \frac{1}{4(2k+1)}$ for some $k \in \mathbb{N}$. We now take (sorted)

$$X = \{x', x, x_k, x_{k-1}, \cdots, x_1, x_0\} \text{ and } Y = \{y', y_0, y_1, \cdots, y_{k-1}, y_k, y\},$$

with distances as shown in Figure 7.11. As a result, we also have $(y_i - x) = 4i\varepsilon\delta$ and $(x_k - y_i) = 2\delta + 4(k-i+1)\varepsilon\delta$, $\forall i \in \{0, 1, 2, \cdots, k\}$.

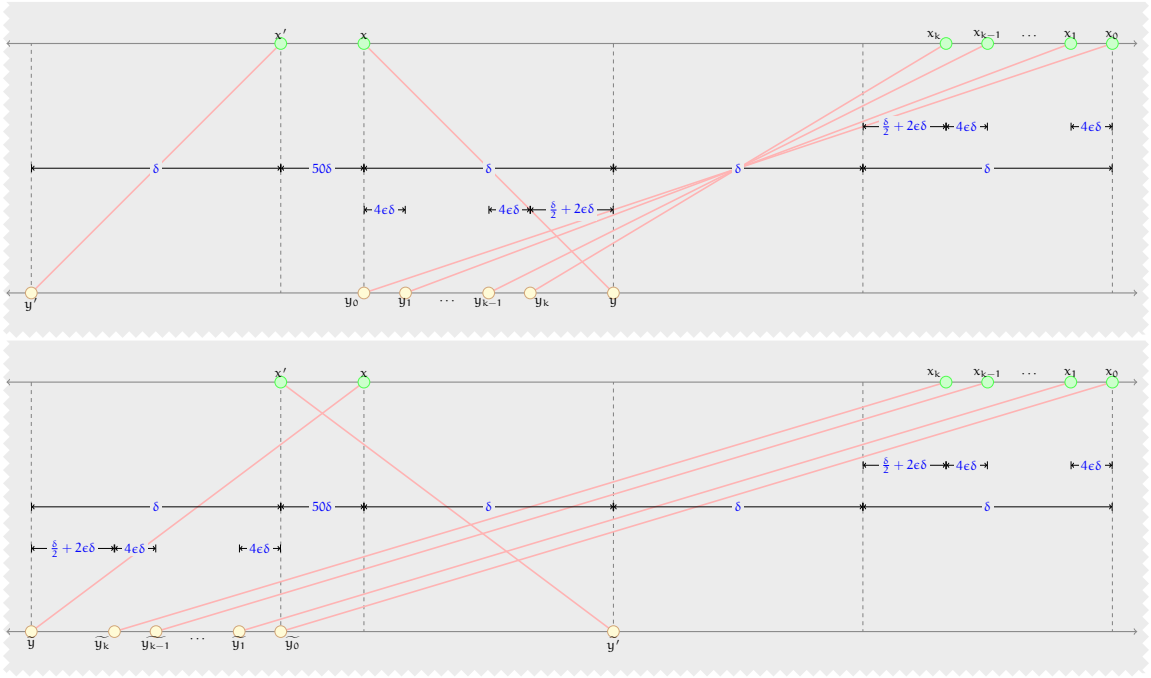

Figure 7.11: This picture demonstrates the configuration of X and Y. The correspondence $\mathcal{C}$ is shown using the red edges. In the bottom, X and $\widetilde{Y}$, the reflection of Y about the midpoint of x and x', are shown, along with the correspondence $\mathcal{C}$ by the red edges.

To prove our claim that $d_{H,iso}(X, Y) = \left(\frac{5}{4} - \varepsilon\right)\delta$, we consider translating both Y and $\widetilde{Y}$, the reflection of Y about the midpoint of x and x'.

When translating $\widetilde{Y}$, we note that the smallest Hausdorff distance of $\frac{3\delta}{2}$ is achieved for a translation of $\widetilde{Y}$ by an amount of $\frac{\delta}{2}$ to the right. For this amount of translation, $\widetilde{y}'$ becomes the midpoint of x and x_0, where $\widetilde{y}'$ is the reflection of y' about the midpoint of x and x'. And all the other points of $\widetilde{Y}$ are at distance at least 50δ from x.

Now, we consider translating Y by an amount $\Delta \in \mathbb{R}$. We first observe that $d_H(X, Y) = 2\delta$, and the distance is attained by x_0 and y. Now, a translation of Y to the left is only going to increase the Hausdorff distance $d_H(X, Y + \Delta)$. Taking this argument one step further we get the following analysis as we vary Δ:

If $\Delta \in \left(-\infty, \frac{3\delta}{4} + \varepsilon\delta\right)$, then the pair (x_0, y) gives

$$d_H(X, Y + \Delta) = 2\delta - \Delta > 2\delta - \frac{3\delta}{4} - \varepsilon\delta = \left(\frac{5}{4} - \varepsilon\right)\delta.$$

For $\Delta = \frac{3\delta}{4} + \varepsilon\delta$, we get $x_0 - (y + \Delta) = \left(\frac{5}{4} - \varepsilon\right)\delta$. Also, $y_k + \Delta - x = \left(\frac{5}{4} - \varepsilon\right)\delta$ and $x_k - (y_k + \Delta) = \left(\frac{5}{4} - \varepsilon\right)\delta + 4\varepsilon\delta$. So, $d_H(X, Y + \Delta) = \left(\frac{5}{4} - \varepsilon\right)\delta$, which is attained by $|x_0 - y_k|$.

Following this pattern, we conclude that $d_H(X, Y + \Delta) > \left(\frac{5}{4} - \varepsilon\right)\delta$, except for $\Delta = \frac{3\delta}{4} + \varepsilon\delta + 4i\varepsilon\delta$ for $i \in \{0, 1, 2, \cdots, k\}$. Therefore, $d_{H,iso}(X, Y) = \left(\frac{5}{4} - \varepsilon\right)\delta$. We summarize our analysis in Table 7.2.

Δ	$\overrightarrow{d}_H(X, Y+\Delta)$	$\overrightarrow{d}_H(Y+\Delta, X)$	$d_H(X, Y+\Delta)$
$(-\infty, \frac{3\delta}{4} + \varepsilon\delta)$	(x_0, y)	–	$> \left(\frac{5}{4} - \varepsilon\right)\delta$
$\frac{3\delta}{4} + \varepsilon\delta$	(x_0, y)	$(y_k, x), (y, x_k)$	$\left(\frac{5}{4} - \varepsilon\right)\delta$
$\left(\frac{3\delta}{4} + \varepsilon\delta, \frac{3\delta}{4} + \varepsilon\delta + 4\varepsilon\delta\right)$	–	$(y_k, x), (y_k, x_k)$	$> \left(\frac{5}{4} - \varepsilon\right)\delta$
$\frac{3\delta}{4} + \varepsilon\delta + 4\varepsilon\delta$	–	$(y_{k-1}, x), (y_k, x_k)$	$\left(\frac{5}{4} - \varepsilon\right)\delta$
$\cdots$	$\cdots$	$\cdots$	$\cdots$
$\left(\frac{3\delta}{4} + \varepsilon\delta + 4i\varepsilon\delta, \frac{3\delta}{4} + \varepsilon\delta + 4(i+1)\varepsilon\delta\right)$	–	$(y_{k-i}, x), (y_{k-i}, x_k)$	$> \left(\frac{5}{4} - \varepsilon\right)\delta$
$\frac{3\delta}{4} + \varepsilon\delta + 4(i+1)\varepsilon\delta$	–	(y_{k-i-1}, x), (y_{k-i}, x_k)	$\left(\frac{5}{4} - \varepsilon\right)\delta$
$\cdots$	$\cdots$	$\cdots$	$\cdots$
$\frac{3\delta}{4} + \varepsilon\delta + 4k\varepsilon\delta$	(x, y_0)	(y_0, x)	$(\frac{5}{4} - \varepsilon)\delta$
$\left(\frac{3\delta}{4} + \varepsilon\delta + 4k\varepsilon\delta, \infty\right)$	(x, y_0)	–	$> \left(\frac{5}{4} - \varepsilon\right)\delta$

Table 7.2: A summary of $d_H(X, Y + \Delta)$ is recorded for $\Delta \in \mathbb{R}$. In the second and third columns, the directed Hausdorff distances are achieved for the shown pairs of points. The other columns are self-explanatory.

With the $d_{H,iso}(X, Y)$ computed, we now define the following correspondence $\mathcal{C}$ between X and Y:

$$\mathcal{C} = \left\{(x_i, y_i) \mid i \in \{0, 1, \cdots, k\}\right\} \cup \left\{(x', y'), (x, y)\right\}.$$

The distortion of $\mathcal{C}$ is evidently 2δ. Moreover, we observe that $\mathcal{C}$ is an optimal correspondence. Therefore, $d_{GH}(X, Y) = \delta$. □

7.5 Discussions

In our investigation, we focus on approximating Gromov-Hausdorff distance by the Hausdorff distance for subsets of $\mathbb{R}^1$. The use of $d_{H,iso}$ yields an approximation algorithm with a tight factor. We do not know, however, if other algorithms can be devised with a better approximation factor. We believe that the problem of computing the Gromov-Hausdorff distance or even approximating it by a factor less

than $\frac{5}{4}$ in $\mathbb{R}^1$ is NP-hard. The question of a polynomial-time approximation algorithm for subsets of $\mathbb{R}^d$ is still open for $d \geq 2$.

I travel not to go anywhere, but to go. I travel for travel's sake. The great affair is to move.

—Robert Louis Stevenson, Travels with a Donkey in the Cévennes

Bibliography

[1] Sushovan Majhi, Jeffrey Vitter, and Carola Wenk. Approximating Gromov-Hausdorff Distance in Euclidean Space. *arXiv:1912.13008 [math.MG]*, 2019.

[2] Brittany Terese Fasy, Sushovan Majhi, and Carola Wenk. Threshold-based graph reconstruction using discrete Morse theory. In *Fall Workshop on Computational Geometry*, New York, NY, November 2018.

[3] Brittany Terese Fasy, Rafal Komendarczyk, Sushovan Majhi, and Carola Wenk. On the Reconstruction of Geodesic Subspaces of $\mathbb{R}^n$. *arXiv:1810.10144 [math.AT]*, 2018.

[4] Brittany Terese Fasy, Rafal Komendaczyk, Sushovan Majhi, and Carola Wenk. Topological reconstruction of metric graphs in $\mathbb{R}^n$. In *Fall Workshop on Computational Geometry*, New York, NY, October 2017.

[5] Partha Niyogi, Stephen Smale, and Shmuel Weinberger. Finding the homology of submanifolds with high confidence from random samples. *Discrete And Computational Geometry*, 39. 1-3:419–441, 2008.

[6] Frédéric Chazal and André Lieutier. Smooth manifold reconstruction from noisy and non-uniform approximation with guarantees. *Computational Geometry*, 40(2):156–170, 2008.

[7] Frédéric Chazal and S. Y. Oudot. Towards persistence-based reconstruction in Euclidean spaces. In *Proc. 24th ACM Sympos. Comput. Geom.*, pages 232–241, 2008.

[8] Frédéric Chazal, David Cohen-Steiner, and André Lieutier. A sampling theory for compact sets in Euclidean space. *Discrete & Computational Geometry*, 41(3):461–479, 2009.

[9] Frédéric Chazal and André Lieutier. Stability and computation of topological invariants of solids in $\mathbb{R}^n$. *Discrete & Computational Geometry*, 37(4):601–617, 2007.

[10] Frédéric Chazal, Ruqi Huang, and Jian Sun. Gromov-Hausdorff approximation of filamentary structures using reeb-type graphs. *Discrete & Computational Geometry*, 53(3):621–649, Apr 2015.

[11] Mridul Aanjaneya, Frédéric Chazal, Daniel Chen, Marc Glisse, Leonidas Guibas, and Dmitriy Morozov. Metric graph reconstruction from noisy data. *International Journal of Computational Geometry & Applications*, 22(04):305–325, 2012.

[12] Fabrizio Lecci, Alessandro Rinaldo, and Larry Wasserman. Statistical analysis of metric graph reconstruction. *J. Mach. Learn. Res.*, 15(1):3425–3446, January 2014.

[13] Facundo Mémoli and Guillermo Sapiro. A Theoretical and Computational Framework for Isometry Invariant Recognition of Point Cloud Data. *Foundations of Computational Mathematics*, 5(3):313–347, July 2005.

[14] Alexander Hall and Christos Papadimitriou. Approximating the Distortion. In *Approximation, Randomization and Combinatorial Optimization. Algorithms and Techniques*, volume 3624, pages 111–122. Springer Berlin Heidelberg, Berlin, Heidelberg, 2005.

[15] Tamal K. Dey, Jiayuan Wang, and Yusu Wang. Graph reconstruction by discrete Morse theory. In *34th International Symposium on Computational Geometry*, pages 31:1–31:15, 2018.

[16] Robin Forman. A user's guide to discrete Morse theory. *Séminaire Lotharingien de Combinatiore*, (48):Art. B48c, 2002.

[17] Günter Rote. Computing the minimum Hausdorff distance between two point sets on a line under translation. *Information Processing Letters*, 38(3):123 – 127, 1991.

[18] D. N. Kozlov. *Combinatorial algebraic topology*. Number v. 21 in Algorithms and computation in mathematics. Springer.

[19] James R. Munkres. *Elements Of Algebraic Topology*. Addison-Wesley Publishing Company, Second edition, 1996.

[20] Edwin H Spanier. *Algebraic topology*, volume 55. Springer Science & Business Media, 1994.

[21] Allen Hatcher. *Algebraic Topology*. Cambridge University Press, First edition, 2002.

[22] Paul Alexandroff. Über den allgemeinen Dimensionsbegriff und seine Beziehungen zur elementaren geometrischen Anschauung. *Mathematische Annalen*, 98(1):617–635, March 1928.

[23] Nina Amenta, Marshall Bern, and David Eppstein. The crust and the β-skeleton: Combinatorial curve reconstruction. *Graphical models and image processing*, 60(2):125–135, 1998.

[24] Tamal K. Dey. *Curve and Surface Reconstruction: Algorithms with Mathematical Analysis (Cambridge Monographs on Applied and Computational Mathematics)*. Cambridge University Press, New York, NY, USA, 2006.

[25] Jean-Claude Hausmann. On the Vietoris-Rips Complexes and a Cohomology Theory for Metric Spaces. In Frank Quinn, editor, *Prospects in Topology (AM-138)*, Proceedings of a Conference in Honor of William Browder. (AM-138), pages 175–188. Princeton University Press, 1995.

[26] J. Latschev. Vietoris-Rips complexes of metric spaces near a closed Riemannian manifold. *Archiv der Mathematik*, 77(6):522–528, December 2001.

[27] Dominique Attali, André Lieutier, and David Salinas. Vietoris-Rips complexes also provide topologically correct reconstructions of sampled shapes. *Computational Geometry*, 46(4):448 – 465, 2013. 27th Annual Symposium on Computational Geometry (SoCG 2011).

[28] Fabrizio Lecci, Alessandro Rinaldo, and Larry A Wasserman. Statistical analysis of metric graph reconstruction. *Journal of Machine Learning Research*, 15(1):3425–3446, 2014.

[29] André Lieutier. Any open bounded subset of $\mathbb{R}^n$ has the same homotopy type as its medial axis. *Computer-Aided Design*, 36(11):1029–1046, 2004.

[30] Vin De Silva and Gunnar Carlsson. Topological estimation using witness complexes. In *Proceedings of the First Eurographics Conference on Point-Based Graphics*, SPBG'04, pages 157–166, Aire-la-Ville, Switzerland, Switzerland, 2004. Eurographics Association.

[31] Henry Adams and Joshua Mirth. Metric thickenings of Euclidean submanifolds. *Topology and its Applications*, 254:69–84, Mar 2019.

[32] Mikhael Gromov. Homotopical effects of dilatation. *J. Differential Geom.*, 13(3):303–310, 1978.

[33] Mikhael Gromov. Filling Riemannian manifolds. *J. Differential Geom.*, 18(1):1–147, 1983.

[34] M. Gromov, J. Lafontaine, and P. Pansu. *Metric Structures for Riemannian and Non-Riemannian Spaces*. Progress in Mathematics - Birkhäuser. Birkhäuser, 1999.

[35] John M. Sullivan. *Curves of Finite Total Curvature*, pages 137–161. Birkhäuser Basel, Basel, 2008.

[36] D. Burago, I.U.D. Burago, I.U.D. Burago, J.D. Burago, Y. Burago, I.U.D. Burago, S. Ivanov, S. Ivanov, and American Mathematical Society. *A Course in Metric Geometry*. Crm Proceedings & Lecture Notes. American Mathematical Society, 2001.

[37] James R. Munkres. *Topology*. Featured Titles for Topology Series. Prentice Hall, Incorporated, 2000.

[38] Erin W. Chambers, Vin de Silva, Jeff Erickson, and Robert Ghrist. Vietoris–Rips complexes of planar point sets. *Discrete & Computational Geometry*, 44(1):75–90, Jul 2010.

[39] Michał Adamaszek, Florian Frick, and Adrien Vakili. On homotopy types of Euclidean Rips complexes. *Discrete Comput. Geom.*, 58(3):526–542, October 2017.

[40] Xiaoyin Ge, Issam Safa, Mikhail Belkin, and Yusu Wang. Data skeletonization via reeb graphs. In *Proceedings of the 24th International Conference on Neural Information Processing Systems*, NIPS'11, pages 837–845, USA, 2011. Curran Associates Inc.

[41] Suyi Wang, Yusu Wang, and Yanjie Li. Efficient map reconstruction and augmentation via topological methods. In *Proceedings of the 23rd SIGSPATIAL International Conference on Advances in Geographic Information Systems - GIS '15*, pages 1–10. ACM Press, 2015.

[42] Mahmuda Ahmed, Brittany Terese Fasy, Matt Gibson, and Carola Wenk. Choosing thresholds for density-based map construction algorithms. In *Proceedings of the 23rd SIGSPATIAL International Conference on Advances in Geographic Information Systems*, SIGSPATIAL '15, pages 24:1–24:10, New York, NY, USA, 2015. ACM.

[43] Larry Wasserman. *All of Nonparametric Statistics (Springer Texts in Statistics)*. Springer-Verlag, Berlin, Heidelberg, 2006.

[44] J. Milnor, M. SPIVAK, and R. WELLS. *Morse Theory. (AM-51), Volume 51*. Princeton University Press, 1969.

[45] Kevin P Knudson. *Morse theory*. Annals of mathematics studies. Princeton Univ. Press, Princeton, NJ, 5. printin edition, jul 1973.

[46] Konstantin Mischaikow and Vidit Nanda. Morse theory for filtrations and efficient computation of persistent homology. *Discrete Comput. Geom.*, 50(2):330–353, September 2013.

[47] Ulrich Bauer, Carsten Lange, and Max Wardetzky. Optimal topological simplification of discrete functions on surfaces. *Discrete and Computational Geometry*, 47:347–377, 2012.

[48] V. Robins, P. J. Wood, and A. P. Sheppard. Theory and algorithms for constructing discrete morse complexes from grayscale digital images. *IEEE Transactions on Pattern Analysis and Machine Intelligence*, 33(8):1646–1658, 2011.

[49] O. Delgado-Friedrichs, V. Robins, and A. Sheppard. Skeletonization and partitioning of digital images using discrete morse theory. *IEEE Transactions on Pattern Analysis and Machine Intelligence*, 37(3):654–666, 2015.

[50] Nicholas Scofille. Discrete Morse Theory. In *Lecture Notes in Mathematics*, volume 1928, pages 51–66. 2008.

[51] David Cohen-Steiner, Herbert Edelsbrunner, and John Harer. Stability of persistence diagrams. *Discrete & Computational Geometry*, 37(1):103–120, 2007.

[52] T. Sousbie. The persistent cosmic web and its filamentary structure - I. Theory and implementation. *Monthly Notices of the Royal Astronomical Society*, 414(1):350–383, jun 2011.

[53] Ulrich Bauer, Carsten Lange, and Max Wardetzky. Optimal Topological Simplification of Discrete Functions on Surfaces. *Discrete and Computational Geometry*, 47(2):347–377, mar 2012.

[54] Facundo Memoli. On the use of Gromov-Hausdorff distances for shape comparison. In M. Botsch, R. Pajarola, B. Chen, and M. Zwicker, editors, *Eurographics Symposium on Point-Based Graphics*. The Eurographics Association, 2007.

[55] Marcel Berger. Encounter with a Geometer, Part I. 47(2):12, 2000.

[56] Facundo Mémoli. Gromov-Hausdorff distances in Euclidean spaces. In *2008 IEEE Computer Society Conference on Computer Vision and Pattern Recognition Workshops*, pages 1–8, Anchorage, AK, USA, June 2008. IEEE.

[57] Facundo Mémoli. Some Properties of Gromov-Hausdorff Distances. *Discrete & Computational Geometry*, 48(2):416–440, September 2012.

[58] Christos Papadimitriou and Shmuel Safra. The complexity of low-distortion embeddings between point sets. In *Proceedings of the Sixteenth Annual ACM-SIAM Symposium on Discrete Algorithms*, SODA '05, pages 112–118, USA, 2005. Society for Industrial and Applied Mathematics.

[59] Pankaj K. Agarwal, Kyle Fox, Abhinandan Nath, Anastasios Sidiropoulos, and Yusu Wang. Computing the Gromov-Hausdorff distance for metric trees. *ACM Trans. Algorithms*, 14(2):24:1–24:20, April 2018.

[60] Claire Kenyon, Yuval Rabani, and Alistair Sinclair. Low Distortion Maps Between Point Sets. *SIAM Journal on Computing*, 39(4):1617–1636, January 2010.

[61] Mikhael Gromov. *Metric structures for Riemannian and non-Riemannian spaces*. Modern Birkhäuser classics. Birkhäuser, Boston, 2007.

[62] Dmitri Burago, Yuri Burago, and Sergei Ivanov. *A Course in Metric Geometry*, volume 33 of *Graduate Studies in Mathematics*. American Mathematical Society, Providence, Rhode Island, June 2001.

[63] M. Artin. *Algebra*. Pearson Prentice Hall, 2011.

Index

The author was born at Gangadharpur, a small village near Calcutta, India in 1988. He finished his college in 2009, and received a bachelor's degree in mathematics from Calcutta University. The author then received a master's degree in applicable mathematics from Tata Institute of Fundamental Research, Bangalore in 2012. He co-founded a startup in Bangalore, India and continued to make profit until he joined Tulane University as a graduate student in the fall of 2014. In the fall of 2020, the author received his PhD in mathematics.